Continuous Ultrasonic Welding of Thermoplastic Composites
An experimental study towards understanding factors influencing weld quality

Jongbloed, B.C.P.

DOI
10.4233/uuid:9e47e2cc-97f2-4482-8d46-96371c2c3d06

Publication date
2022

Document Version
Final published version

Citation (APA)
Jongbloed, B. C. P. (2022). *Continuous Ultrasonic Welding of Thermoplastic Composites: An experimental study towards understanding factors influencing weld quality*. [Dissertation (TU Delft), Delft University of Technology]. https://doi.org/10.4233/uuid:9e47e2cc-97f2-4482-8d46-96371c2c3d06

Continuous Ultrasonic Welding of Thermoplastic Composites

Bram Jongbloed

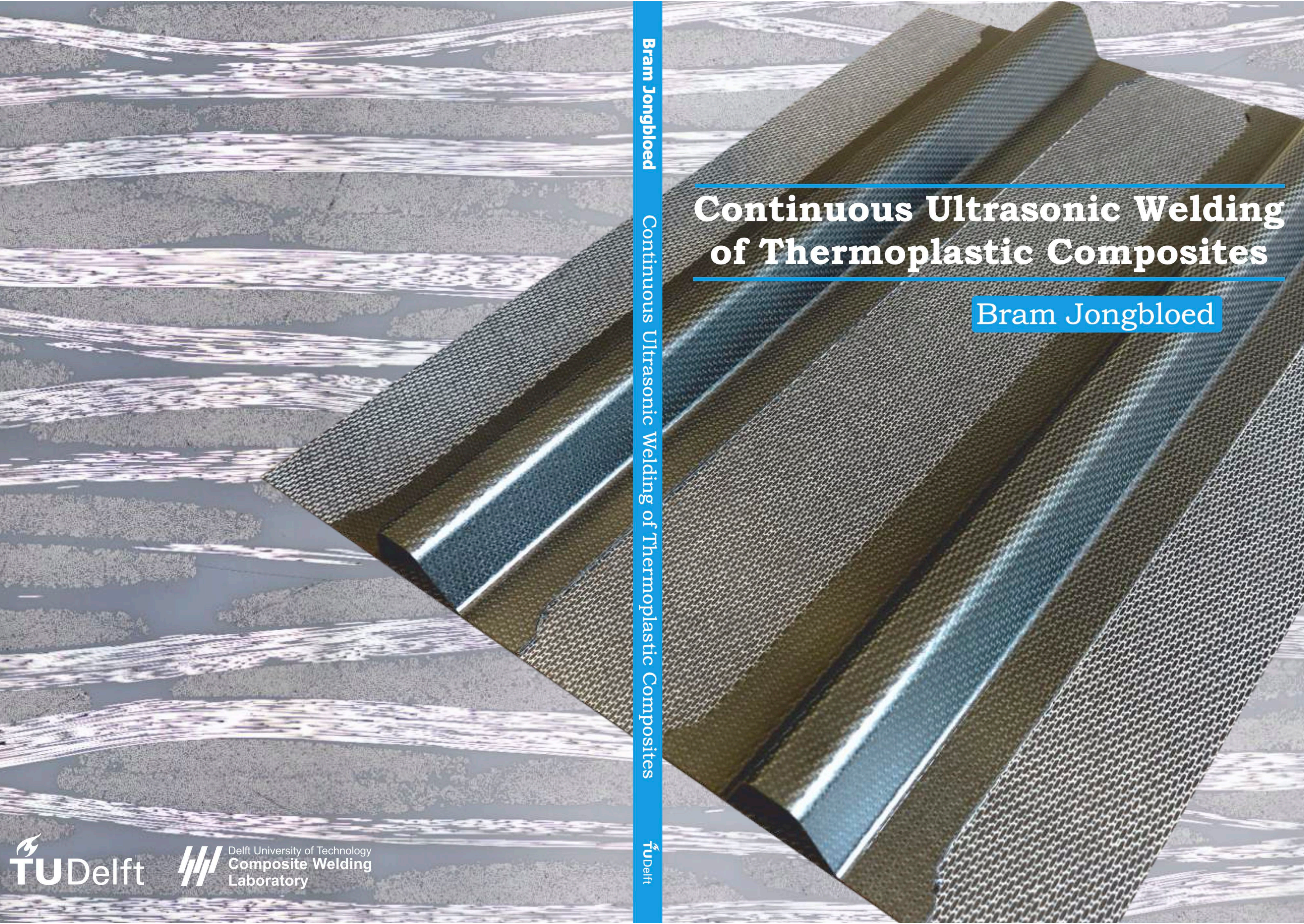

Bram Jongbloed Continuous Ultrasonic Welding of Thermoplastic Composites

TU Delft

Delft University of Technology
Composite Welding Laboratory

Continuous Ultrasonic Welding of Thermoplastic Composites

An experimental study towards understanding factors influencing weld quality

Continuous Ultrasonic Welding of Thermoplastic Composites

An experimental study towards understanding factors influencing weld quality

Dissertation

for the purpose of obtaining the degree of doctor
at Delft University of Technology
by the authority of the Rector Magnificus, Prof.dr.ir. T.H.J.J. van der Hagen,
Chair of the Board for Doctorates
to be defended publicly on
Tuesday 11 January 2022 at 12:30h

by

Bram Cornelius Petrus JONGBLOED

Master of Science in Aerospace Engineering,
Delft University of Technology, the Netherlands,
born in Breda, the Netherlands.

This dissertation has been approved by the (co)promotors.

Composition of the doctoral committee:

Rector Magnificus,	chairperson
Dr. I. Fernandez Villegas,	Delft University of Technology, promotor
Prof.dr.ir. R. Benedictus,	Delft University of Technology, promotor
Dr.ir. J.J.E. Teuwen,	Delft University of Technology, copromotor
Independent members:	
Prof.dr.-ing. P. Mitschang,	Technische Universität Kaiserslautern, Germany
Prof.dr.-ing. F. Balle,	Albert-Ludwigs-Universität Freiburg, Germany
Prof.dr. A.R. Balkenende,	Delft University of Technology
Dr.ir. K. van Rijswijk,	SAM|XL
Prof.dr. C. Bisagni,	Delft University of Technology, reserve member

This research was part of the ecoTECH project and has received funding from the European Union's Horizon 2020 Clean Sky 2 Joint Undertaking under the AIRFRAME ITD grant agreement numbers 807083 and 945521.

Keywords: Ultrasonic welding, fusion bonding, thermoplastic composites, energy director, CF/PPS

Printed by: Ipskamp Printing

Front & Back: The background shows a part of a cross-sectional micrograph of continuously welded CF/PPS adherends. On the front, the photo shows the 400 mm by 500 mm stiffened demonstrator panel made for the ecoTECH project. Two CF/PPS omega stiffeners were continuously welded to a CF/PPS skin.

ISBN 978-94-6421-596-0

An electronic version of this dissertation is available at
http://repository.tudelft.nl/.

Contents

Summary

To increase fuel efficiency of aircraft, there is a need for more efficient engines, better aerodynamic designs, and lighter aircraft structures. The latter can be achieved by using fibre-reinforced composite materials. The use of composite materials in commercial aviation requires the use of cost-effective manufacturing methods. Exactly this is why the interest and application of thermoplastic composites is increasing. They soften and ultimately melt upon heating which can be utilized to shape structures through stamp forming processes and to join them by means of welding techniques. One of the most promising welding techniques for thermoplastic composites is ultrasonic welding. It is mainly known as a static technique to make spot welds. However, the relatively new technology continuous ultrasonic welding of thermoplastic composites makes it possible to obtain large fully welded seams with higher load carrying capabilities. However, at the start of the research conducted for this dissertation very little knowledge on the process was available. The weld quality in the state-of-the-art research was significantly lower than the weld quality of the statically welded counterpart in terms weld uniformity as unwelded and overwelded areas were present simultaneously, the single-lap strength, and the presence of voids. Additionally, damage to the adherends was observed as a likely result of through-the-thickness heating. Hence, before continuous ultrasonic welding can be industrially applied the weld quality needs to be improved. Consequently, the main objective of this dissertation was to acquire a deeper understanding of the continuous ultrasonic welding process of thermoplastic composites to promote its development for future industrial applications. The main research question that needs to be answered to meet the objective is: how can high-quality continuous ultrasonic welds be obtained for thermoplastic composites?

First how to improve the weld uniformity was researched. It was investigated whether increasing the energy director compliance would improve the weld uniformity in continuous ultrasonic welding by more efficiently heating up the energy director. A woven polymer mesh energy director was introduced and compared to the current state-of-the-art thin film energy director. It was found that the mesh energy director significantly improved the weld uniformity and single-lap shear strength. To understand how the mesh improved the weld quality, the static welding process was utilized. It was found that the filament crossings of the mesh energy director, uniformly present all over the joint, directly come in contact with the adherends from the start of the welding process. The filaments flatten and the contact between the mesh and the adherends gradually improves during the welding process by deforming the filaments and filling up the open areas within the mesh. This resulted in full contact between the energy director and the adherends, and the wetting of the welding interface, which ultimately led to a more uniformly welded joint. However, the continuous joint still contained a significant number of voids.

Now that more uniform joints were obtained, the second focus was on what are optimal welding parameters for continuous ultrasonic welding with the mesh energy director and to understand to which extent the continuous process could benefit from the available knowledge on the static process. This was done by identifying differences and similarities between the static and continuous welding processes. The two processes were experimentally compared for three combinations of welding force and vibration amplitude. An interesting finding is that the optimum vibration times and welding speeds (i.e. conditions that result in the highest singe-lap shear strength) in both processes were similar for the three combinations of welding force and vibration amplitude. However, the weld quality of the continuous welded joints was still significantly lower than the weld quality of the statically welded joints: significantly lower single-lap shear strength values were measured for the continuous welded joints, which was expected to be related to the presence of voids at the continuous welded interface caused by a lack of consolidation during cooling.

To improve the weld quality further, a consolidator was introduced to the welding setup. To determine the required consolidation pressure, the size of the consolidator, and its distance from the sonotrode a stepwise approach was taken based on the static process. High-quality continuously welded joints with virtually no porosity and high strength were obtained when the consolidator was placed relatively far (86.4 mm) from the sonotrode. The closest consolidation distance (18.4 mm), best representing the static welding conditions, did not improve the weld quality as the observed porosity seems to be caused by squeeze flow of molten matrix in the adherends by the consolidator.

Since porosity seemed to be caused by through-the-thickness heating, the last part of this research focused on understanding what causes higher through-the-thickness heating in continuous ultrasonic welding of thermoplastic composites as compared to the static process. To this end, thermocouples were used to measure the temperature evolution within the adherends and at the weld interface for different welding configurations and combinations of welding parameters. The results were compared to temperature measurements from an equivalent static welding process and to the predictions from a simplified numerical heat transfer model. Viscoelastic bulk heat generation was identified as the main cause for the higher through-the-thickness heating in the top adherend during the continuous process. The top adherend seemed to absorb most of the vibrational energy in the continuous process as opposed to a more balanced energy share between top and bottom adherend in the static process. Reducing the total vibration energy associated to the process was found to have a substantial effect on through-the-thickness heating and the corresponding matrix and fibre squeeze flow in the top adherend.

In conclusion, the research presented in this dissertation aided in better understanding the continuous ultrasonic welding process of thermoplastic composites, and demonstrated how high-quality continuous welds can be obtained. The presented research takes the process a significant step forward towards its readiness for future industrial applications.

Samenvatting

Om brandstofefficiëntie van vliegtuigen te verhogen, is er behoefte aan efficiëntere motoren, betere aerodynamische vormgeving en lichtere vliegtuigconstructies. Dit laatste kan worden bereikt door gebruik te maken van vezelversterkte composietmaterialen. Het gebruik van kosteneffectieve fabricagemethoden kan het gebruik hiervan versnellen in de commerciële luchtvaart. Precies daarom neemt de interesse en toepassing van thermoplastische composieten toe. Zij verzachten en smelten uiteindelijk bij verhitting. Dit kan worden benut om onderdelen te maken door middel van persvormprocessen en om ze aan elkaar te verbinden door middel van lastechnieken. Eén van de meest belovende lastechnieken voor thermoplastische composieten is ultrasoon lassen. Deze is vooral gekend als een statische puntlastechniek. Echter, de relatief nieuwe technologie continu ultrasoon lassen maakt het mogelijk om lange, volledig gelaste naden te verkrijgen die een hogere belasting kunnen weerstaan. Bij de aanvang van het onderzoek voor dit proefschrift was er nog weinig kennis over dit continue lasproces. De laskwaliteit was significant lager dan de laskwaliteit van de statisch gelaste tegenhanger door de niet-uniformiteit van de las, waarbij niet gelaste en te veel gelaste gebieden tegelijkertijd aanwezig waren, de lagere afschuifsterkte van de las en de aanwezigheid van porositeit. Bovendien werd degradatie van het materiaal waargenomen in de gelaste laminaten, mogelijk als gevolg van verhitting door de dikte. Het was daarom noodzakelijk om de laskwaliteit te verbeteren voordat continu ultrasoon lassen industrieel kan worden toegepast. Het hoofddoel van dit proefschrift is dan ook om een dieper inzicht te verkrijgen in het continu ultrasoon lasproces van thermoplastische composieten om de ontwikkeling ervan voor toekomstige industriële toepassingen te bevorderen. De belangrijkste onderzoeksvraag die beantwoord dient te worden om de doelstelling te bereiken, is: hoe kunnen hoogwaardige continu ultrasone lassen worden verkregen voor thermoplastische composieten?

Eerst werd onderzocht hoe de uniformiteit van de las kon worden verbeterd door het verhogen van de flexibiliteit van de energierichter waardoor deze efficiënter opwarmt. Een weefsel van polymeer filamenten werd hiervoor gebruikt en vergeleken met de voorheen gebruikte dunne film energierichter. Deze geweven energierichter verbeterde de lasuniformiteit en de afschuifsterkte van de las aanzienlijk. Om te begrijpen hoe het weefsel de laskwaliteit verbeterde, werd het statische lasproces gebruikt. Er werd gevonden dat de filamentkruisingen in het weefsel, uniform aanwezig over de hele overlap, direct vanaf het begin van het lasproces in contact komen met de laminaten. Het contact tussen de geweven energierichter en de laminaten verbetert tijdens het lasproces doordat de filamenten afplatten en vervormen en de open ruimtes in het weefsel worden opgevuld. Dit resulteerde in een volledig contact tussen de energierichter en de laminaten en het bevochtigen van het lasoppervlak, wat uiteindelijk leidde tot een meer uniforme lasverbinding. De

continue lasverbinding bevatte echter nog aanzienlijke porositeit.

Nu er uniformere lasverbindingen werden verkregen, lag de tweede focus op wat optimale lasparameters zijn voor het continu ultrasoon lassen en om te begrijpen in hoeverre het continue proces kan gebruik maken van de huidige kennis over het statische lasproces. Dit werd gedaan door het identificeren van verschillen en overeenkomsten tussen het statische en continue lasproces. De twee processen werden experimenteel vergeleken voor drie combinaties van laskracht en trillingsamplitude. Een interessante bevinding was dat de optimale trillingstijden en lassnelheden (d.w.z. parameters die resulteren in de hoogste afschuifsterkte) in beide processen vergelijkbaar waren voor deze drie combinaties. Echter werden er voor de continu gelaste verbindingen significant lagere afschuifsterktes van de las gemeten. Dit was naar verwachting gerelateerd aan de aanwezigheid van porositeit veroorzaakt door een gebrek aan consolidatie tijdens het afkoelen.

Om de laskwaliteit verder te verbeteren, werd een consolidator in de lasopstelling geïntroduceerd. Om de vereiste consolidatiedruk, de grootte van de consolidator en de plaatsing ten opzichte van de sonotrode te bepalen, werd een stapsgewijze aanpak gevolgd gebaseerd op het statische lasproces. Continu gelaste verbindingen van hoge kwaliteit vrijwel zonder porositeit en hoge afschuifsterkte werden verkregen wanneer de consolidator relatief ver (86,4 mm) van de sonotrode werd geplaatst. De kortste consolidatie-afstand (18,4 mm), die het beste de statische lasomstandigheden representeerde, verbeterde de laskwaliteit niet aangezien porositeit werd waargenomen die veroorzaakt lijkt te zijn door het uitpersen van gesmolten hars uit de laminaten door de consolidator.

Aangezien de porositeit veroorzaakt leek te worden door verhitting van de laminaten door de dikte, was het laatste deel van het onderzoek gericht op het begrijpen van de oorzaak hiervan bij het continu ultrasoon lassen in vergelijking met het statische lasproces. Visco-elastische bulk-warmteontwikkeling werd geïdentificeerd als de belangrijkste oorzaak voor de hogere door de dikte verwarming in het bovenste laminaat tijdens het continu lasproces. Het bovenste laminaat leek de meeste trillingsenergie in het continue proces te absorberen, in tegenstelling tot een meer gebalanceerde energieverdeling tussen het bovenste en onderste laminaat tijdens het statische lasproces. Het verminderen van de totale ingebrachte trillingsenergie, bleek een positief effect te hebben op de door de dikte verwarming en bijbehorende vezel- en harsuitpersing.

Tot slot kan er worden geconcludeerd dat het onderzoek in dit proefschrift heeft bijgedragen aan een beter begrip van het continue ultrasone lasproces van thermoplastische composieten en heeft aangetoond hoe hoogwaardige continue ultrasone lassen kunnen worden verkregen. Met dit onderzoek is er een belangrijke stap voorwaarts gezet voor de toekomstige toepassing van dit proces in de industrie.

1 Introduction

1.1. Background

Increasing the fuel efficiency has been the main driver behind the development and introduction of new technologies in the commercial aviation industry [1]. Mainly because it reduces the operating cost for airlines, but also because it reduces the green house emissions responsible for climate change. To increase fuel efficiency, there is a need for more efficient engines, better aerodynamic designs, and lighter aircraft structures. The latter can be achieved by using fibre-reinforced composite materials. These composites typically have a high specific stiffness (stiffness to density ratio) and strength (strength to density ratio), and the material properties can be tailored for the intended application, which makes them more suitable for weight savings than their metallic counterparts. Current examples of the latest commercial aircraft containing composite materials are the Boeing 787 dreamliner (Figure 1.1) with 50% structural composite weight [2], and the Airbus A350 XWB with 53% structural composite weight [3]. These new generation aircraft have an improved fuel efficiency up to 25% [4, 5] compared to similarly sized previous generation aircraft.

Figure 1.1: Boeing 787-8 Dreamliner.

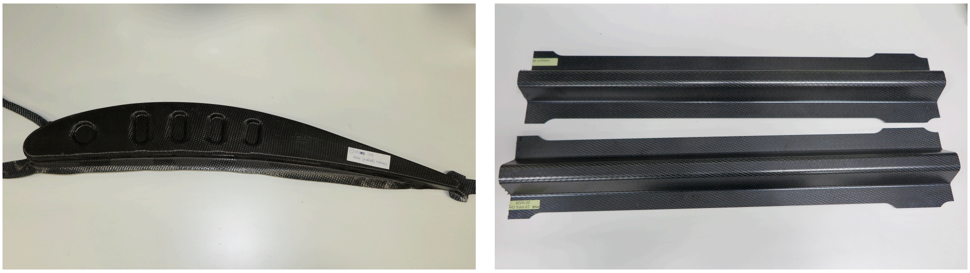

(a) (b)

Figure 1.2: Examples of press formed aerospace parts. (a) CF/PPS rib, and (b) CF/PPS omega stiffeners.

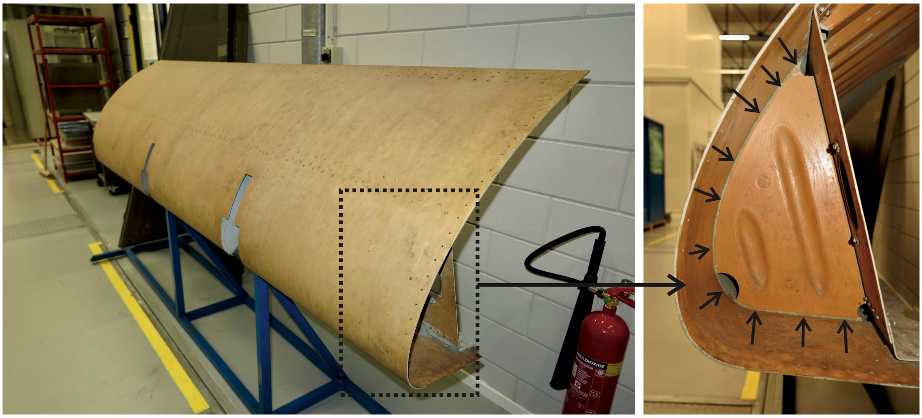

Figure 1.3: GF/PPS leading edge of A340 showing press formed rib that is resistance welded onto the skin. Arrows indicate the welded area.

A composite material consists of two or more individual materials on a macroscopic scale, whose combined properties are better than those of the materials individually [6]. Composite materials used in aircraft are fibre-reinforced composites, typically stiff and strong continuous carbon or glass fibres are used to reinforce a plastic called the matrix. These plastics can be either thermosets or thermoplastics. Thermoplastics, in contrast to thermosets, do not form a cross-linked network, they rely on the entanglement of long linear polymer chains to form a solid structure. Thermoplastics are gaining popularity because they have multiple advantages over thermosets such as a higher toughness, fire retardant, more chemically resistant, no shelf life, and recyclable. Additionally, thermoplastics soften and melt upon the application of heat, allows the use of fast and cost effective manufacturing and joining methods like press forming (examples shown in Figure 1.2) and welding. Current examples of thermoplastic composite applications are the rudder and elevator of the Gulfstream G650 that have been welded together via induction welding [7], and the fixed leading edge of the A340 and A380 consists of press formed ribs resistance welded to the skin (shown in Figure 1.3) [8].

1.2. Joining techniques for thermoplastic composites

Aircraft consist of many thousands or even millions of parts [9, 10] that have to be joined together. Building an aircraft from just a couple of parts is impossible due to the inherent complexity and size. Traditional joining methods currently used for metallic and composite structures are mechanical fastening (e.g. riveting) and adhesive bonding. Mechanical fastening has the following characteristics: it allows for assembly of dissimilar materials, does not need surface treatments, the process is relatively insensitive to the environment, the joints are not sensitive to peel stresses, and a big advantage is the ease with which they can be removed for inspection or repair purposes. When mechanical fastening is used on composite structures the stress concentrations are higher compared to metallic structures, because composite structures do not yield and thus stress concentrations remain high when heavily loaded [11]. Additionally, when joining composite structures together by means of mechanical fastening holes must be drilled disrupting the fibres and thus intentionally damaging the structure. To compensate for this damage changes must be made to ensure a proper load introduction into the composite structures, which is typically done by increasing the number of plies increasing the weight. Additionally drilling holes in composites requires proper procedures to avoid delaminations. Adhesive bonding, on the other hand, results in lower stress concentrations compared to mechanical fastening [11]. However, adhesive bonds are more sensitive to peel stresses, they are susceptible to the environmental influences (i.e. moisture uptake, degradation due to UV, etc.), need to be cured which increases the cycle time and thus the cost, and require extensive surface treatments using chemicals [11]. Additionally, adhesive bonding of thermoplastic composites is challenging because of the low surface energy of thermoplastics.

Welding has significant advantages over mechanical fastening and adhesive bonding. Drilling of holes and intensive surface treatments are not needed. Welding processes can easily be automated resulting in short cycle times and cost-efficient processes without being labour intensive. Additionally, welding minimizes stress concentrations compared to mechanic fastening, and the interface is as insensitive to environmental influences as the adherend material itself. A disadvantage however is that disassembly of welded parts is not possible yet. Welding, also known as fusion bonding, uses the fact that thermoplastics soften and eventually melt upon heating. Fusion bonding techniques are based on the following principles [12–14] illustrated in Figure 1.4: intimate contact between the to-be-welded adherends is promoted by the application of heat and pressure which results in flattening of surface asperities and wetting of the surfaces forming an interface. Now molecular inter-diffusion takes place as the thermoplastic polymer chains can freely cross the interface. Upon cooling down under pressure the polymer chains are being frozen (i.e. solidified) in their new location, making the weld line indistinguishable from the rest of the adherend material since the two adherends now form one integral whole.

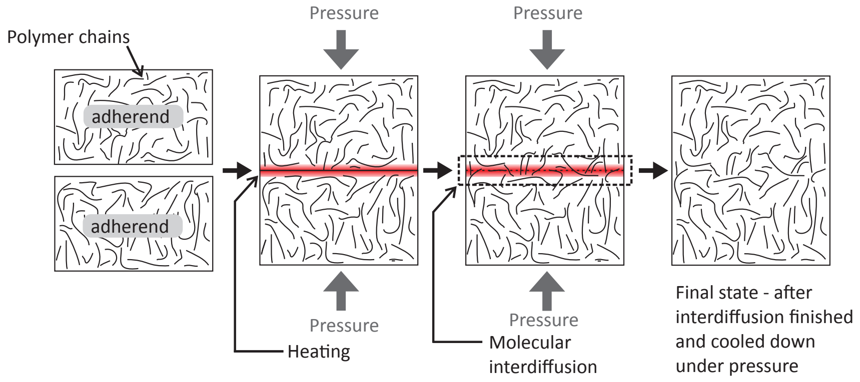

Figure 1.4: Schematic of fusion bonding principles based on [14, 15].

The different welding techniques can be categorized based on their heating mechanism as shown in Figure 1.5, electromagnetic welding, friction welding, and thermal welding. Electromagnetic welding relies on a electrically conductive susceptor at the interface (e.g. stainless steel, carbon fabric) and applying an electromagnetic field or a high-current. Friction welding relies on frictional work at the weld interface during the application of pressure to create a joint. Lastly, thermal welding relies on the external application of heat to melt the weld interface. Thermal welding techniques typically rely on two steps, in the first step heat is directly applied to the two separate interfaces and in the second step the two surfaces are brought together under pressure [16]. The most promising welding techniques for fibre-reinforced thermoplastic composites are induction, resistance and ultrasonic welding [16–18] thanks to their potential to be applied on large structures, high joint strength, automation potential, and limited heat affected zone. From these techniques, ultrasonic welding emerges generally as the fastest and most energy-efficient process [19] among the three. Consequently, the research conducted in this dissertation uses ultrasonic welding.

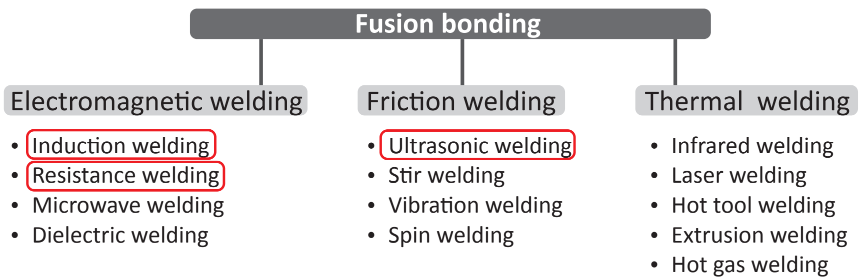

Figure 1.5: Classification of welding techniques [16]. The three most promising welding techniques for fibre-reinforced thermoplastic composites have been high-lighted [16, 17, 20].

1.3. Basics of ultrasonic welding of thermoplastic composites

During the ultrasonic welding process high frequency (10-70 kHz) low amplitude (typically 10 µm - 250 µm peak-to-peak) transverse mechanical vibrations are exerted to the to-be-welded adherends while applying pressure [21]. Heat is generated because of surface friction and intermolecular friction as a result of the cyclic deformation of asperities at the adherends' interface. To focus the heat generation to the interface artificial asperities called energy directors (EDs) are placed at the interface. These energy directors are made from the same polymer matrix and either consist of one or more protrusions moulded on the adherends surface [22–24] or a resin rich layer such as a film (also called flat ED) [25, 26]. Due to the lower compressive stiffness the energy director experiences a higher cyclic strain compared to the adherends, subsequently producing more heat [21, 24, 27]. As a result, the energy director melts and flows to form a connection between the adherends as described in Section 1.2.

A schematic of an ultrasonic welding setup is shown in Figure 1.6. The welding parameters can be defined in the computer prior to welding. The ultrasonic generator linked to the computer converts line voltage to high voltage at ultrasonic frequency to operate the ultrasonic transducer in the converter [21]. The operating frequency of the welder is fixed as the vibrating components, the ultrasonic assemblage of converter, booster, and sonotrode vibrate at their specifically designed resonance frequency. The converter amplitude is amplified by the booster and the sonotrode. Ultimately, the amplitude is transmitted into the adherends. A transverse displacement sensor measures the transverse displacement of the ultrasonic assemblage. A controller in the generator continuously monitors and controls the amplitude, power, maximum power, energy consumption, force, vertical displacement, and time. The force and vertical displacement are sometimes controlled by an external controller, which allows for more flexible automation solutions.

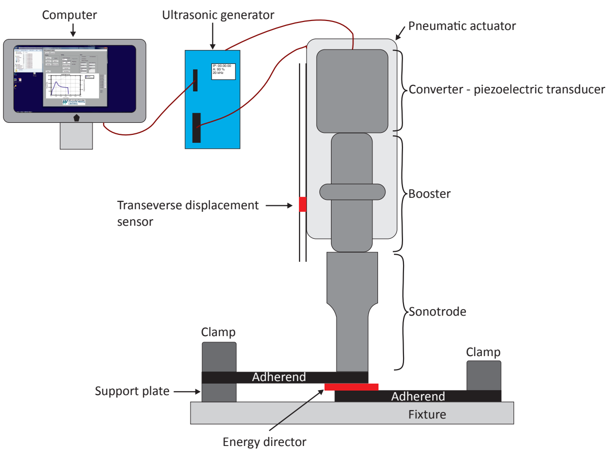

Figure 1.6: Schematic of ultrasonic welding setup for thermoplastic composites.

1.4. Motivation for the research

Ultrasonic welding is mainly known as a static welding technique to make for example spot welds. Most studies up to now focused on understanding and developing a robust static welding process for thermoplastic composites [22, 25–34], which led to the development of sequential ultrasonic spot welding by Zhao et al. [29, 32, 35] as illustrated in Figure 1.7a. During this process one spot is welded after another, which allows joining of large structural parts and is therefore promising for large scale industrial applications. However, the resulting joint has non-welded sections in between adjacent spots that generally lowers the load transferring capabilities compared to a fully welded overlap and makes the joint permeable for air and liquid, which is often undesirable for aerospace applications.

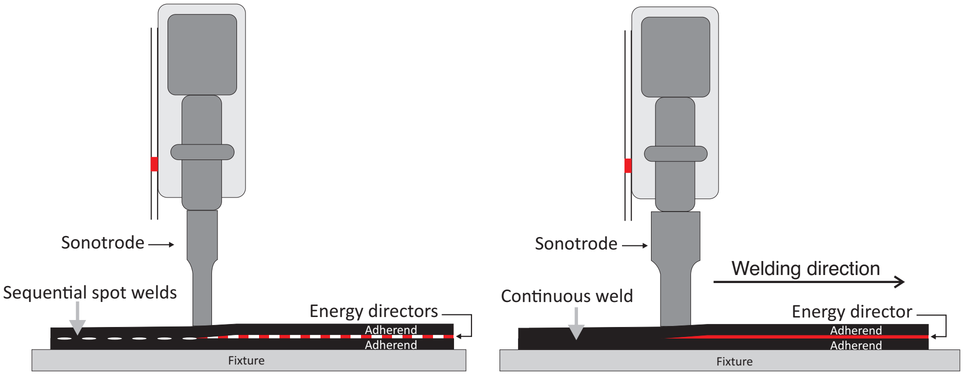

(a) Sequential spot welding

(b) Continuous welding

Figure 1.7: Schematics of ultrasonic welding processes for thermoplastic composites.

Continuous ultrasonic welding of thermoplastic composites, on the the other hand, enables large fully welded seams. During the process the sonotrode moves relative to the to-be-welded adherends, as illustrated in 1.7b, while applying the welding force and ultrasonic vibrations. The larger welded area means a higher load carrying capability for the continuously welded joints. Additionally, they are as fluid tight as the thermoplastic composite material itself. However, continuous ultrasonic welding of thermoplastic composites is a relatively new technology and very little knowledge on the process is available. At the start of this research the state-of-the-art of the process originates from one study by Senders et al. [36] in which the concept and feasibility of the process was successfully demonstrated. They proposed zero-flow welding in which a 0.08 mm-thin film energy director was used to avoid squeeze flow of the energy director. For thick energy directors in the static welding process squeeze flow was found necessary to obtain high-quality welds [25, 28]. But when utilizing a thick energy director for the continuous process they expected "the cold energy director ahead of the sonotrode to stop or slow down the required squeeze flow, and have an undesirable effect on the welding process and weld quality" (Senders et al. [36]). The weld quality obtained with the zero-flow welding process was, however, significantly lower than the weld quality of the statically welded counterpart [22, 37] in terms of single-lap strength, presence of voids, and weld uniformity as unwelded and overwelded areas were present simultaneously. Additionally, damage to the adherends was observed as a likely result of through-the-thickness heating. Hence, before continuous ultrasonic welding can be industrially applied it needs to be better understood to improve the weld quality.

1.5. Research objective and dissertation outline

The main objective of this research is to acquire a deeper understanding of the continuous ultrasonic welding process of thermoplastic composites to promote its development for future industrial applications. As mentioned in the previous section, the weld quality of the state-of-the-art continuous welds [36] was significantly lower than the weld quality obtained for the static process [22, 37]. Hence, the main research question that needs to be answered to meet the objective is: How can high-quality continuous ultrasonic welds be obtained for thermoplastic composites? 'High-quality' in this research is defined as follows: an uniformly welded interface (e.g. no unwelded or overwelded areas), single-lap shear strength values similar to that of joints obtained with the static ultrasonic welding process for optimum welding parameters for the same material (i.e. approximately 37 MPa [22, 37]), and the lowest possible porosity. The following core chapters of this dissertation contribute to answering the research question with their research areas:

- **Chapter 2 - Continuous ultrasonic welding of thermoplastic composites: enhancing the weld uniformity by changing the energy director**. The objective of this chapter is to investigate whether increasing the compliance of the energy director would improve the weld uniformity in continuous ultrasonic welding of thermoplastic composites. In the first part of this chapter an energy director with an higher compliance than the state-of-the-art thin film energy director [36] was selected. In the second part the changes that the use of such an energy director introduced in the ultrasonic welding process were investigated.

- **Chapter 3 - On Differences and Similarities between Static and Continuous Ultrasonic Welding of Thermoplastic Composites**. With the aim of identifying how to benefit from existing knowledge on static ultrasonic welding of thermoplastic composite parts to boost the development of the continuous version of the process, this chapter focuses on identifying and understanding differences and similarities between both processes. To this end, the melting of the interface, the consumed power, temperature at the weld interface, and the optimum welding conditions were experimentally compared.

- **Chapter 4 - Improving the quality of continuous ultrasonically welded thermoplastic composite joints by adding a consolidator to the welding setup**. The aim of this study is to investigate how the quality of continuous ultrasonically welded joints can be improved by adding a consolidation shoe to the welding setup. To determine the required consolidation pressure,

1

the size of the consolidator, and its distance from the sonotrode a stepwise approach was taken based on the static process.

- **Chapter 5 - A study on through-the-thickness heating in continuous ultrasonic welding of thermoplastic composites**. Through-the-thickness heating may lead to excessive fibre and resin squeeze out from the adherends accompanied by porosity, and a knock-down in strength. The objective of this chapter is to gain insight into what causes higher through-the-thickness heating in continuous ultrasonic welding of thermoplastic composites as compared to the static process. To this end, thermocouples were used to measure the temperature evolution within the adherends and at the weld interface for different welding configurations and combinations of welding parameters. The results were compared to temperature measurements from an equivalent static welding process and to the predictions from a simplified numerical heat transfer model.

References

[1] R. Slayton and G. Spinardi, "Radical innovation in scaling up: Boeing's dreamliner and the challenge of socio-technical transitions," *Technovation*, vol. 47, pp. 47 – 58, 2016.

[2] Boeing, "Boeing 787 from the ground up." https://www.boeing.com/commercial/aeromagazine/articles/qtr_4_06/article_04_2.html, (accessed: 09.12.2020).

[3] Airbus, "A350 xwb family." https://www.airbus.com/aircraft/passenger-aircraft/a350xwb-family.html, (accessed: 09.12.2020).

[4] Airbus, "Airbus family figures booklet," June 2020.

[5] Boeing, "Environmental report," 2014.

[6] I. Daniel and O. Ishai, *Engineering Mechanics of Composite Materials*. No. v. 13 in Engineering mechanics of composite materials, Oxford University Press, 2006.

[7] A. Offringa, "New thermoplastic composite design concepts and their automated manufacture," *JEC composites magazine*, vol. 58, pp. 45–49, 2010.

[8] G. Gardiner, "Thermoplastic composites gain leading edge on the A380." https://www.compositesworld.com/articles/thermoplastic-composites-gain-leading-edge-on-the-a380, (accessed: 09.12.2020).

[9] A. Linn, "Hundreds of suppliers, one boeing 737 airplane." https://www.nbcnews.com/id/wbna36507420, (accessed: 21.09.2021).

[10] Boeing, "Boeing celebrates delivery of 50th 747-8." https://boeing.mediaroom.com/2013-05-29-Boeing-Celebrates-Delivery-of-50th-747-8, (accessed: 21.09.2021).

[11] F. Campbell. ASM International, 2010.

[12] R. P. Wool and K. M. O'Connor, "A theory crack healing in polymers," *Journal of Applied Physics*, vol. 52, no. 10, pp. 5953–5963, 1981.

[13] R. P. Wool, B.-L. Yuan, and O. J. McGarel, "Welding of polymer interfaces," *Polymer Engineering & Science*, vol. 29, no. 19, pp. 1340–1367, 1989.

[14] Y. H. Kim and R. P. Wool, "A theory of healing at a polymer-polymer interface," *Macromolecules*, vol. 16, no. 7, pp. 1115–1120, 1983.

[15] A. C. Loos and M.-C. Li, "Non-isothermal autohesion model for amorphous thermoplastic composites," *Journal of Thermoplastic Composite Materials*, vol. 7, no. 4, pp. 280–310, 1994.

[16] A. Yousefpour, M. Hojjati, and J. Immarigeon, "Fusion Bonding/Welding of Thermoplastic Composites," *Journal of Thermoplastic Composite Materials*, vol. 17, no. 4, pp. 303–341, 2004.

[17] A. Benatar and T. G. Gutowski, "Method for fusion bonding thermoplastic composites," *SAMPE Q.; (United States)*.

[18] C. Ageorges, L. Ye, and M. Hou, "Advances in fusion bonding techniques for joining thermoplastic matrix composites: A review," *Composites - Part A: Applied Science and Manufacturing*, vol. 32, no. 6, pp. 839–857, 2001.

[19] I. F. Villegas, L. Moser, A. Yousefpour, P. Mitschang, and H. E. Bersee, "Process and performance evaluation of ultrasonic, induction and resistance welding of advanced thermoplastic composites," *Journal of Thermoplastic Composite Materials*, vol. 26, no. 8, pp. 1007–1024, 2013.

[20] C. Ageorges, L. Ye, and M. Hou, "Experimental investigation of the resistance welding of thermoplastic-matrix composites. part ii: optimum processing window and mechanical performance," *Composites Science and Technology*, vol. 60, no. 8, pp. 1191 – 1202, 2000.

[21] D. Grewell, A. Benatar, and J. Park, *Plastics and Composites Welding Handbook*. No. 10 in Plastics and composites welding handbook, Hanser Gardener, 2003.

[22] I. Villegas, B. Valle Grande, H. Bersee, and R. Benedictus, "A comparative evaluation between flat and traditional energy directors for ultrasonic welding of cf/pps thermoplastic composites," *Composite Interfaces*, vol. 22, no. 8, pp. 717–729, 2015.

[23] I. Villegas and G. Palardy, "Ultrasonic welding of cf/pps composites with integrated triangular energy directors: melting, flow and weld strength development," *Composite Interfaces*, vol. 24, no. 5, pp. 515–528, 2017.

[24] A. Benatar, R. V. Eswaran, and S. K. Nayar, "Ultrasonic welding of thermoplastics in the near-field," *Polymer Engineering & Science*, vol. 29, no. 23, pp. 1689–1698, 1989.

[25] I. Villegas, "In situ monitoring of ultrasonic welding of thermoplastic composites through power and displacement data," *Journal of Thermoplastic Composite Materials*, vol. 28, no. 1, pp. 66–85, 2015.

[26] G. Palardy and I. Villegas, "On the effect of flat energy directors thickness on heat generation during ultrasonic welding of thermoplastic composites," *Composite Interfaces*, vol. 24, no. 2, pp. 203–214, 2017.

[27] A. Levy, S. Le Corre, and I. Villegas, "Modeling of the heating phenomena in ultrasonic welding of thermoplastic composites with flat energy directors," *Journal of Materials Processing Technology*, vol. 214, no. 7, pp. 1361–1371, 2014.

[28] I. Villegas, "Strength development versus process data in ultrasonic welding of thermoplastic composites with flat energy directors and its application to the definition of optimum processing parameters," *Composites Part A: Applied Science and Manufacturing*, vol. 65, pp. 27–37, 2014.

[29] T. Zhao, G. Palardy, I. Villegas, C. Rans, M. Martinez, and R. Benedictus, "Mechanical behaviour of thermoplastic composites spot-welded and mechanically fastened joints: A preliminary comparison," *Composites Part B: Engineering*, vol. 112, pp. 224–234, 2017.

[30] I. Villegas and P. Rubio, "On avoiding thermal degradation during welding of high-performance thermoplastic composites to thermoset composites," *Composites Part A: Applied Science and Manufacturing*, vol. 77, no. Supplement C, pp. 172 – 180, 2015.

[31] I. Villegas and H. Bersee, "Ultrasonic welding of advanced thermoplastic composites: An investigation on energy-directing surfaces," *Advances in Polymer Technology*, vol. 29, no. 2, pp. 112–121, 2010.

[32] T. Zhao, C. Broek, G. Palardy, I. Villegas, and R. Benedictus, "Towards robust sequential ultrasonic spot welding of thermoplastic composites: Welding process control strategy for consistent weld quality," *Composites Part A: Applied Science and Manufacturing*, vol. 109, pp. 355–367, 2018.

[33] N. Koutras, J. Amirdine, N. Boyard, I. F. Villegas, and R. Benedictus, "Characterisation of crystallinity at the interface of ultrasonically welded carbon fibre pps joints," *Composites Part A: Applied Science and Manufacturing*, vol. 125, p. 105574, 2019.

[34] W. Tao, X. Su, H. Wang, Z. Zhang, H. Li, and J. Chen, "Influence mechanism of welding time and energy director to the thermoplastic composite joints by ultrasonic welding," *Journal of Manufacturing Processes*, vol. 37, pp. 196–202, 2019.

[35] T. Zhao, C. Rans, I. Fernandez Villegas, and R. Benedictus, "On sequential ultrasonic spot welding as an alternative to mechanical fastening in thermoplastic composite assemblies: A study on single-column multi-row single-lap shear joints," *Composites Part A: Applied Science and Manufacturing*, vol. 120, pp. 1 – 11, 2019.

[36] F. Senders, M. van Beurden, G. Palardy, and I. Villegas, "Zero-flow: A novel approach to continuous ultrasonic welding of CF/PPS thermoplastic composite plates," *Advanced Manufacturing: Polymer & Composites Science*, vol. 0340, no. September 2017, pp. 1–10, 2016.

[37] N. Koutras, R. Benedictus, and I. F. Villegas, "Thermal effects on the performance of ultrasonically welded cf/pps joints and its correlation to the degree of crystallinity at the weldline," *Composites Part C: Open Access*, vol. 4, p. 100093, 2021.

2

Enhancing the weld uniformity by changing the energy director

This chapter is based on the journal article: B. Jongbloed, J. Teuwen, G. Palardy, I.F. Villegas, and R. Benedictus, *Continuous ultrasonic welding of thermoplastic composites: Enhancing the weld uniformity by changing the energy director*, Journal of Composite Materials **54**, 14 (2020).

2.1. Introduction

Thermoplastic composites are gaining interest in the aerospace industry, because low-cost manufacturing and welding techniques can be applied on them [1–4]. They can be re-shaped, making the use of low-cost forming techniques possible. Locally re-melting the thermoplastic composites makes it possible to weld individual parts together. Already industrially applied welding techniques are resistance welding and induction welding. For example, the inboard leading edge of the A340-500/600, and two-third of the fixed leading edge of the A380 are assembled using resistance welding [3, 4], and the rudder and elevators for the Gulfstream G650 are assembled using induction welding [3].

Another promising welding technique is ultrasonic welding, which is a fast and efficient welding technique that does not require foreign material at the interface [5–13]. During the welding process a sonotrode (metal horn) applies high-frequency (i.e. 20 kHz), low amplitude (i.e. 50 to 100 µm peak-to-peak) vibrations to the weld interface, while simultaneously applying a constant static pressure. The interface generates heat through surface friction and viscoelastic heating. An energy director, i.e. a resin rich layer, is placed at the interface to focus the heat generation. Higher cyclic strains in the energy director ensure higher viscoelastic heating of the energy director as compared to the fibre reinforced adherends [14–16].

2

Continuous ultrasonic welding (CUW) has been shown to be a fast and feasible welding technique [17]. Senders et al. demonstrated the feasibility of continuous ultrasonic welding by joining 100 mm-long carbon fibre-reinforced polyphenylene sulfide (CF/PPS) plates with a continuously welded seam. A thin (0.08 mm-thick) PPS film energy director was used to minimise squeeze flow at the weld interface ("zero-flow" welding) [17]. However, these state-of-the-art joints are non-uniformly welded, and contain areas with intact energy director material. Our follow-up experiments on longer plates (220 mm) of the same material confirmed the previous observations, which can be observed from the fracture surfaces shown in Figure 2.1.

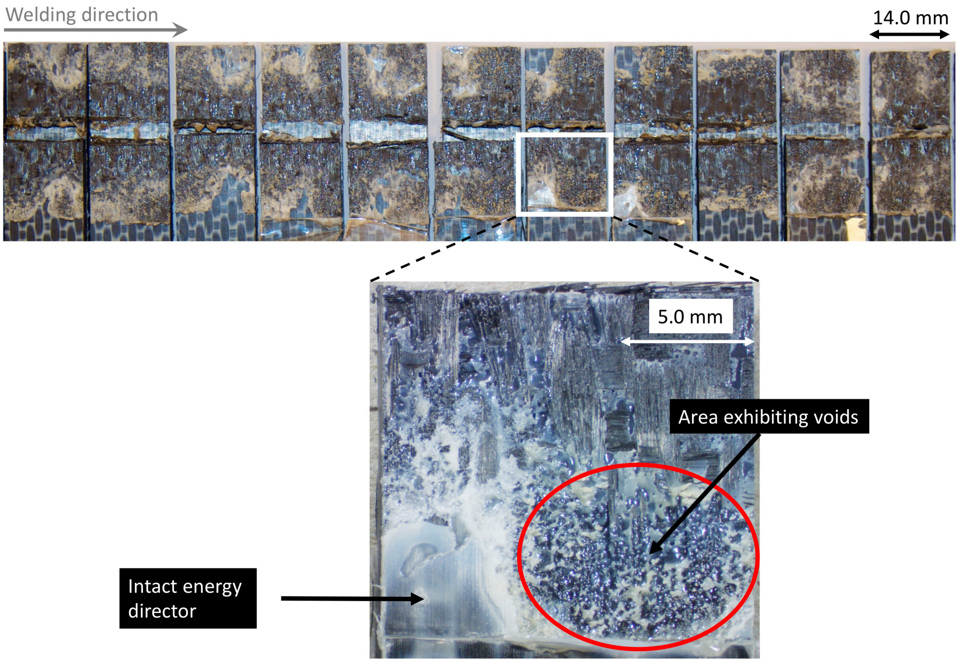

Figure 2.1: Representative fracture surfaces of 220 mm-long CF/PPS plates continuously welded with a thin film energy director, and a single overlap of 12.7 mm. The welding parameters were weld speed of 40 mm/s, welding force 500 N, and vibrational amplitude 82.5 µm.

At the moment it is not known how to improve the weld uniformity in continuous ultrasonic welding. We believe that the presence of areas with intact energy director in the weld originates from the fact that a thin energy director was used, given that a similar issue was also observed in the work done by Palardy et al. in static ultrasonic welding with thin energy directors [8]. The presence of areas with intact energy director could be an indication of either insufficient heat for the energy director to melt or poor contact between the energy director and the adherends at those locations. It should be noted that in any thermoplastic composite welding process, lack of intimate contact or "wetting" at the welding interface (between the energy director and the adherends in the case of ultrasonic welding) would preclude the formation of the welded joint. Given that the viscoelastic heat generation rate in ultrasonic welding is proportional to the square of the cyclic strain experienced by the energy director [14, 18], a way to increase overall heat generation during the process would be to increase the compliance of the energy director [16]. A more compliant energy director would as well undergo a bigger deformation under the force applied by the sonotrode, which would promote a better contact with the adherends and hence improved wetting of the interface [14]. However, the increased local deformation of a more compliant energy director might interfere with the continuous ultrasonic welding process in a similar fashion as the squeeze flow [17].

Therefore, the objective of this study is to investigate whether increasing the compliance of the energy director would improve the weld uniformity in continuous ultrasonic welding of thermoplastic composite plates. In the first part of this study we selected an energy director with an higher compliance than the thin film energy director used so far. In the second part we investigated the changes that the use of such an energy director introduced in the ultrasonic welding process.

2.2. Materials & experimental procedures

The materials used in this paper are thermoplastic fibre reinforced composite adherends and the energy directors that make it possible to focus the heat generation at the weld interface.

2.2.1. Adherends

Thermoplastic composite laminates were made out of carbon fibre-reinforced polyphenylene sulfide (CF/PPS) fabric (five harness satin weave). The laminates were made from six powder-coated prepreg plies with product code: CF 0286 127 Tef4 43% (TenCate Advanced Composites, the Netherlands). The carbon fibre in the prepreg was of the type T300JB, and the prepreg had a nominal fibre volume content of 50%. The six CF/PPS prepreg plies were stacked in a $[0/90]_{3s}$ sequence, and consolidated in a hydraulic hot plate Joos press between stainless steel plates for 20 min at 320 °C and 1 MPa pressure. The nominal laminate thickness was approximately 1.85 mm. The consolidated laminates were cut into plates with dimensions 220 mm by 101.6 mm for the continuous ultrasonic welding process, and for the static process into adherends with dimensions of 25.4 mm by 101.6 mm.

2.2.2. Energy directors

Two types of PPS energy directors were used: flat film energy directors, and a 0.20 mm-thick plain woven PPS mesh energy director (referred to as mesh energy director). Table 2.1 gives an overview of the energy directors together with their product name, thickness, material volume as a percentage of the thin energy director, the compliance, and the glass transition and melting temperature. The PPS100 mesh was supplied by PVF GmbH, Germany. The 0.08 mm-thick film energy director (referred to as thin film energy director) was supplied by TenCate with product name

Rayotec S 080 PPS film. The glass transition temperature (T_g), and the melting temperature (T_m) for the energy directors were determined using a Perkin Elmer DSC 8000 in order to ensure that we had similar grades of PPS. Both mesh and the film energy directors had a similar T_g, and T_m, which can be seen from the values presented in Table 2.1.

As explained in the introduction, increasing the energy director compliance increases the overall heat generation [16]. Additionally, a more compliant energy director would undergo a larger deformation under the force applied by the sonotrode promoting better contact with the adherends and therefore improving the wetting of the interface [14].

In order to find the energy director with the highest compliance and to quantify the compliance, it was assumed that, under the static welding force, the energy director behaves like a spring with stiffness, k. This simplified assumption is based on the work of Benatar and Gutowski [14]. The compliance, C, is proportional to the energy director thickness and inversely proportional to the contact area and modulus of the material through the following equation:

$$C = k^{-1} = \frac{t}{A \cdot E} \tag{2.1}$$

with t equal to the thickness of the energy director, A area of contact of the energy director (top view) with the adherends compressed by the sonotrode over an area of 12.7 mm (overlap) by 14.9 mm (sonotrode width), and E the compressive modulus of the material of the energy director (2.9 GPa for PPS [19]). Thus, in order to increase the compliance for a fixed material type we can either increase the thickness, t, or reduce the contact area, A. Table 2.1 shows the energy directors considered in this study: the current state-of-the-art thin film (0.08 mm-thick) for CUW [17], a thick film (0.24 mm-thick) with higher compliance which resulted in high-quality static welds in previous studies [6–8], and an energy directing mesh with an even higher compliance, because the area A is reduced and the thickness t is increased in equation 2.1 compared to the state-of-the-art energy director.

To calculate the compliance of the mesh equation 2.1 is used. However, in order to estimate the contact area, A, of the mesh, it can be noted that the mesh only has contact points with the adherends at the filament crossings as shown in Figure 2.2. Hence, it can be assumed that the contact area is equal to the sum of the contact areas of all filament crossings at the interface. The contact area of one filament crossing can be estimated by representing it as a square with sides equal to the diameter of the filaments. This estimation then results in approximately 15.2 % of contact of the total area covered by the mesh. Table 2.1 shows that the mesh energy director has a compliance that is approximately 17 times higher than the thin film energy director and approximately 5.5 times higher than the thick film.

Another benefit of the mesh is that it has a similar material volume as the thin film energy director. This would eliminate the potential influence of the amount of energy directing material at the interface. The thick film energy director on the other hand has three times more material compared to the thin film energy director. The material volume [mm^3] of the 0.20 mm-thick mesh for a unit area (top view) was estimated according to the following equation:

$$V_m = 2 \cdot \left[\left(\frac{1}{MO + TD} \right)^2 \cdot \sqrt{(MO + TD)^2 + TD^2} \right] \cdot \pi \cdot \left(\frac{TD}{2} \right)^2 , \tag{2.2}$$

in which MO is the mesh opening (154 μm), and TD, the thread diameter (100 μm) (see Figure 2.2). The mesh open area (top view) is 37% and the mesh count is 39 per cm according to the data sheet of the manufacturer.

Table 2.1: Overview of energy directors with their product name, thickness, corresponding material volume as a percentage of the material volume of the thin film energy director, the compliance, and the T_g and T_m.

ED type	**Product name**	**Thickness** $[mm]$	**Compliance** $[mm/N] \cdot 10^{-7}$	**Material volume** $[\%]$	**T_g / T_m** $[°C]$
Thin film	PPS film	0.08	1.4	100	97/280
Thick film	PPS film	0.24	4.3	300	97/281
Mesh	PPS100	0.20	23.4	83	97/283

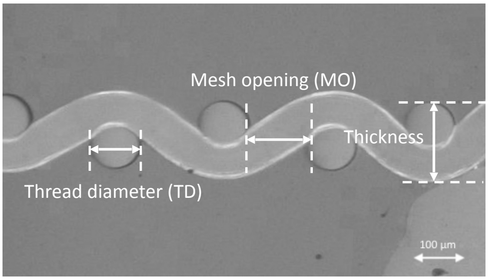

Figure 2.2: Cross-sectional micrograph of mesh energy director. The definitions of mesh opening (MO=154 μm), thread diameter (TD=100 μm) and mesh thickness are indicated. The cross-section open area in this figure when this pristine mesh is placed in between two adherends is approximately 22%.

We will study the 0.20 mm-thick mesh energy director and compare it with the thin film state-of-the-art energy director. The 0.20 mm-thick mesh energy director is a good choice for the experiments in this study since it has a much higher compliance than the thin film energy director and it has a similar amount of energy directing material at the weld interface. The thick film energy director is discarded, since it only has a slightly higher compliance than the thin film energy director, but it also has more material, which is expected to interfere with the welding process [17].

2.2.3. Continuous ultrasonic welding

The continuous ultrasonic welding machine, shown in Figure 2.3, was used for the continuous ultrasonic welding process. A ultrasonic welder from Rinco Ultrasonics (C20-10) was used that operated at 20 kHz. For each welded seam, two CF/PPS plates were welded together in a single lap shear configuration with a 12.7 mm overlap.

The CF/PPS plates were kept in place by the two aluminium bar clamps shown in Figure 2.3b with a spacing of 70 mm. During the welding process, the welding train (converter, booster, and sonotrode) was pneumatically pressed against the welding stack (stack of materials at the overlap directly underneath the sonotrode), and moved along the overlap area indicated in Figures 2.3b, and 2.3c. A rectangular sonotrode with a width of 14.9 mm, and a length of 30 mm was used. The orientation of the sonotrode with respect to its translational movement can be seen in Figures 2.3b and 2.3c. At the start and end of the continuous welding process, the welding train accelerated and decelerated at a rate of $0.6 m/s^2$. Hence the welding speed was not constant at the start and end of the welded seam, and therefore one sample at the start and one sample at the end of the welded seam was discarded for mechanical testing. After the welding process, 14.0 mm-wide lap shear samples were cut from the welded plates, resulting in 11 samples per continuous weld (after discarding the samples at the two edges and the cut losses). The process parameters for continuous ultrasonic welding were the welding force, the vibrational amplitude, and the welding speed. A constant welding force of 500 N, a vibrational peak-to-peak amplitude of 82.5 μm, and welding speeds of 40 mm/s (for the thin film energy director), and 45 mm/s (mesh energy director) were used during the process. Note that for the thin film energy director the actual welding force was 60 N lower than the set welding force of 500 N due to the accuracy of setting the pneumatic piston.

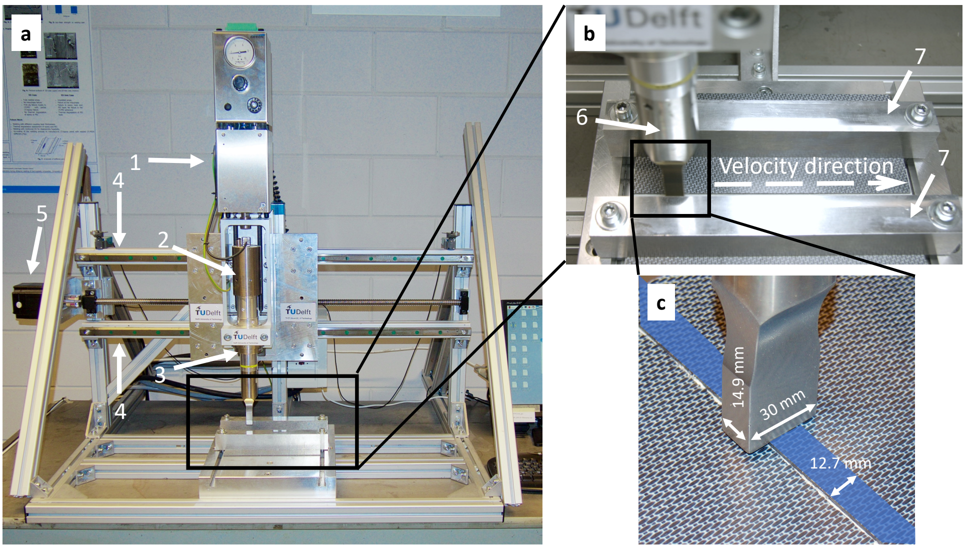

Figure 2.3: (a) Overview of setup used for continuous ultrasonic welding (1. pneumatic press, 2. converter, 3. booster, 4. rails for moving the stack, and 5. stepper motor). (b) 6. Sonotrode with indicated welding direction, and 7. bar clamps. (c) Close-up of weld seam (blue area) and sonotrode with indicated dimensions.

2.2.4. Static ultrasonic welding

To understand the welding behaviour of the energy directors, static ultrasonic welding was used in the second part of this study. For this part of the study a Rinco Dynamic 3000 static ultrasonic welding machine with a cylindrical (40 mm-diameter) sonotrode was utilized. Adherends with dimensions of 25.4 mm-width by 101.6 mm-length were used. The custom-built welding jig (Figure 2.4a) kept the adherends (Figure 2.4b) in place assuring an overlap of 12.7 mm. The welding jig allowed the upper adherend to move vertically during the welding process to avoid potential bending caused by the downward displacement of the sonotrode due to the squeeze out of the polymer from the energy director at the weld overlap. A welding force of 500 N and a peak-to-peak vibrational amplitude of 86.2 μm were used. Additionally, a consolidation force of 1000 N was used for a period of 4000 ms directly after the ultrasonic vibrations stopped.

Samples were welded at four different moments of the welding process to understand the behaviour of the energy director during the welding process. The ultrasonic welding machine provides feedback data during the welding process. In this study, the power and transverse sonotrode displacement data during the welding processes were collected and studied to understand the phenomena happening at the interface.

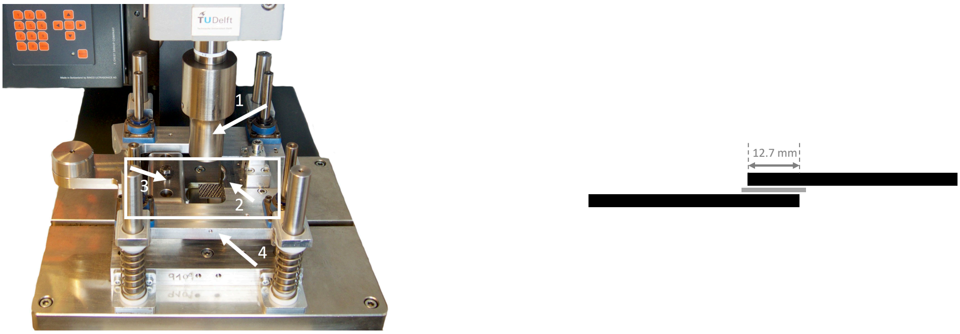

(a) (b)

Figure 2.4: (a) Custom-built welding jig and ultrasonic welding machine, (1) sonotrode, (2) upper adherend clamp, (3) lower adherend clamp, and (4) spring-supported platform for the upper clamp. The white box shows the location and orientation of the single lap shear adherends schematically shown in (b). (b) CF/PPS adherends (black) and ED (grey).

2.2.5. Mechanical testing and microscopy characterisation

After the continuous welding process, the welded plates were cut into 14.0 mm-wide single lap shear samples, which were mechanically tested to obtain the lap shear strength. For the cutting, a Proth water-cooled grinding machine with a diamond-coated blade was used.

The single lap shear samples were mechanically tested with a Zwick/Roell 250 kN universal testing machine with a cross-head speed of 1.3 mm/min. The grips were given the necessary offset to ensure parallelism between the load introduction and the overlap as an alternative to tabs. After testing, the fracture surfaces were analysed using a ZEISS Discovery.V8 SteREO microscope.

Specimens were cut from the overlaps of the welded samples in such a way that a cross-sectional view from the adherends and the weld line could be obtained. The specimens were embedded in epoxy resin. The embedded specimens were grinded and polished with a Struers Tegramin-20 polisher. A Keyence VH-Z100UR digital microscope was used to observe the polished cross sections. The Keyence software was used to measure the weld line thickness. In order to measure the cross-sectional open areas the software ImageJ version 1.52a was used.

2.3. Results

2.3.1. Part 1: a woven PPS mesh as an energy director in CUW

Figure 2.5 shows the fracture surfaces after single lap shear testing of the individual samples cut from the welded seam obtained with the mesh energy director. The entire welded seam is more uniformly welded as compared to the weld made with a thin film energy director (shown in Figure 2.1). No intact energy director can be found in the fracture surfaces, but at numerous locations voids can be observed.

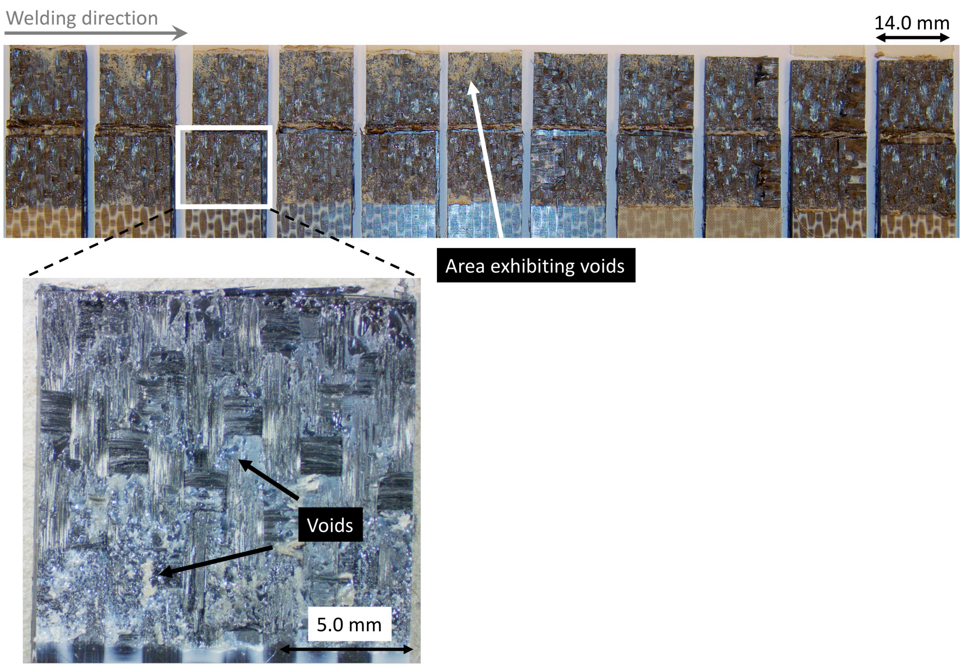

Figure 2.5: Representative fracture surfaces of 220 mm-long CF/PPS plates continuously welded with the mesh energy director and a single overlap of 12.7 mm. Weld speed was 45 mm/s, welding force 500 N, and vibrational amplitude 82.5 µm.

The lap shear strengths over the length of the welded seam made with the mesh energy director and the thin film reference energy director are shown in

Figure 2.6. For the seam made with the mesh the strength is relatively constant with an average strength of 33.4 MPa and a coefficient of variation of 7.2 %. In the case of the reference thin film energy director the average strength is 18.8 MPa with a coefficient of variation of 33.0 %. The obtained average lap shear strength values for the two energy directors are consistent with the corresponding fracture surfaces. Table 2.2 shows an overview of the lap shear strength values for the two investigated energy directors. Since the mesh energy director improved the weld uniformity and lab shear strength, the next section will focus on how the weld behaviour of the mesh improved the weld uniformity compared to the thin film energy director.

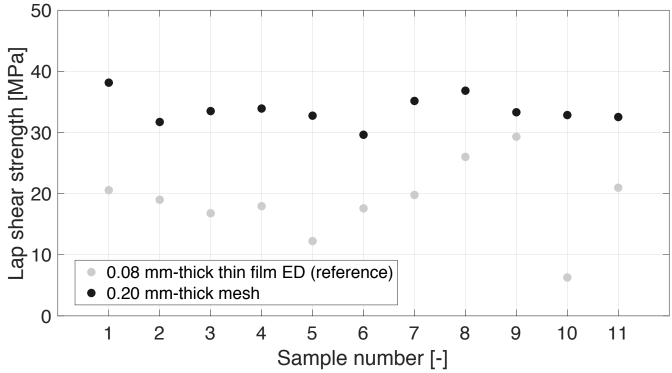

Figure 2.6: Lap shear strength visualised over length of the welded seam. Each dot represents one lap shear sample. Welding force of 500 N, and peak-to-peak vibrational amplitude was 82.5 µm. Weld speeds: 40 mm/s (thin film energy director) and 45 mm/s (mesh energy director).

Table 2.2: Lap shear strength (LSS) results, standard deviation (SD), and coefficient of variation (CoV) for continuously welded plates for the two energy directors. One plate per energy director type was welded. Amount of lap shear samples per energy director case is 11.

Energy director	**LSS [MPa]**	**SD [MPa]**	**CoV [%]**
Thin film	18.8	6.2	33.0
Mesh	33.7	2.4	7.2

2.3.2. Part 2: melting, flow, and strength generation of the mesh studied in static ultrasonic welding

To understand why the mesh improves the weld uniformity, the melting and flow behaviour of the mesh energy director is analysed using static welding and compared to the behaviour of the thin film energy director. Figure 2.7 shows representative power and displacement curves for the mesh and the thin film energy director. For the mesh, the displacement curve (shown in Figure 2.7a) increases significantly at the beginning of the welding process from 0.00 mm to 0.06 mm, where it plateaus.

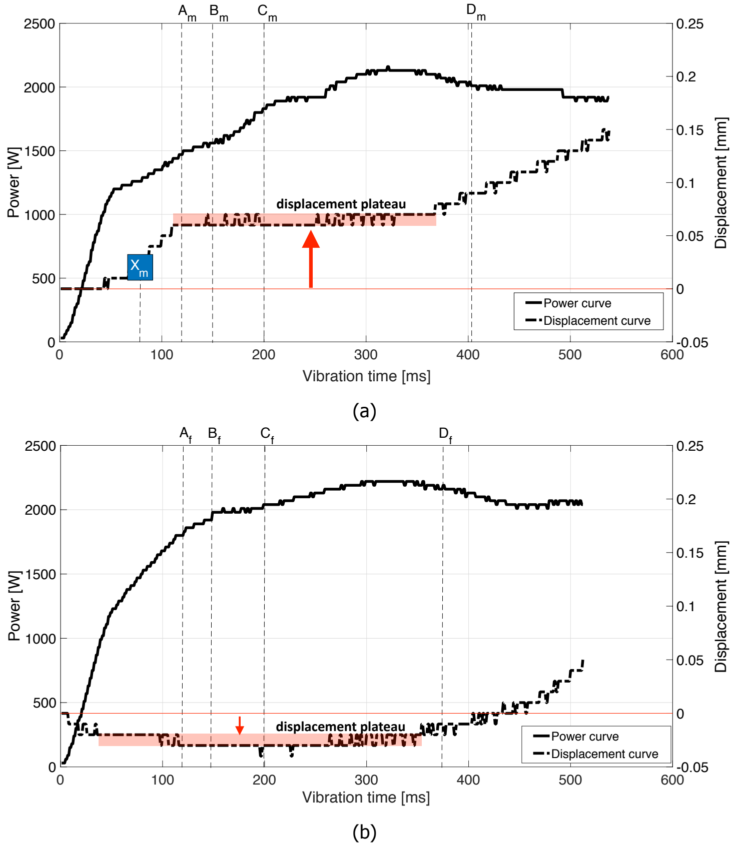

Figure 2.7: Representative power and displacement curves for the ultrasonic welding with (a) the mesh energy director and (b) a thin film energy director. For the mesh, X_m defines a moment before the displacement plateau. For both the mesh energy director (m) and the thin film energy director (f), A_x (x is either m or f) defines the beginning of the displacement plateau, B_x and C_x are different moments within the displacement plateau, and D_x defines the end of the displacement plateau.

The plateau is followed by another increase in displacement. The power increases significantly at the beginning of the welding process for 50 ms. Afterwards the power continues to increase during the displacement plateau at a lower rate until a maximum is reached towards the end of the plateau.

For the thin film energy director in Figure 2.7b, the displacement starts with a small decrease of 0.02 - 0.03 mm (upward sonotrode displacement) after which it plateaus. The end of the plateau is followed by an increase in displacement. Similarly to the mesh energy director, the power for the thin film energy director increases significantly from the start of the welding process for 50 ms and keeps increasing at a lower rate until a maximum is reached. This maximum in power is found to coincide with the end of the displacement plateau. After the maximum power is reached, the power slowly decreases. When comparing the displacement curves for the mesh energy director in Figure 2.7a and the thin film energy director in Figure 2.7b, the main difference can be found at the beginning of the welding process: the displacement of the mesh steeply increased whereas the displacement of the thin film energy director decreased. From the start of the displacement plateau of the mesh energy director, the displacement curves for both mesh energy director and thin film energy director exhibit a very similar behaviour as seen in Figure 2.7.

Figure 2.8 shows the top view of a mesh on top of the bottom adherend after the welding process is stopped at moment X_m indicated in Figure 2.7a. On the left, the initial state of the mesh is shown as a reference. Mesh flattening is observed at the locations where the filament crossings come into contact with the adherends, forming oval-shaped contact areas uniformly distributed over the entire weld. Due to the flattening, the mesh filaments widen, decreasing the open areas within the mesh.

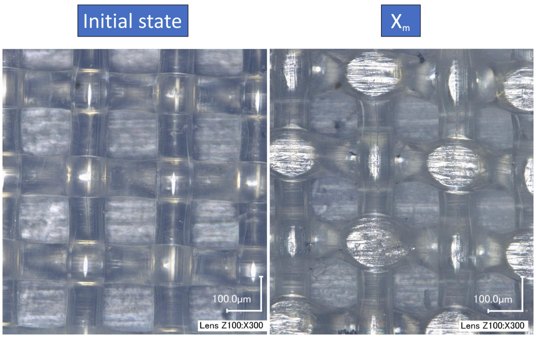

Figure 2.8: Top view of mesh demonstrating flattening of the mesh at the filament crossings. Pristine mesh outside of the joint (Initial state) and partially welded mesh within the weld before reaching the plateau in displacement (X_m).

Figures 2.9 and 2.10 show cross-sectional micrographs of adherends welded until moments A_x, B_x, C_x, and D_x of the welding process for the mesh energy director and the thin film energy director respectively, as indicated in Figures 2.7a and 2.7b. Moment A_x (x being either m for mesh or f for thin film energy director) defines the beginning of the displacement plateau at 120 ms. Moment B_x at 150 ms, and moment C_x at 200 ms are moments within the first half of the displacement plateau, moment D_x approximately defines the end of the displacement plateau.

In Figure 2.9, it can be seen that at moment A_m the mesh filaments are partially filling up the open areas within the mesh. A small separation between the compressed mesh and the surfaces of the adherends is visible. At moment B_m the separation between the mesh and the adherends is less obvious compared to moment A_m, and the open areas filled up further. At moment C_m the open areas in the mesh have almost completely been filled up by the filaments. The separation between the mesh and adherends' surfaces are almost indistinguishable. The cross-sectional micrograph at moment D_m shows that all open areas within the mesh have been filled with the polymer from the filaments, and the weld line thickness is close

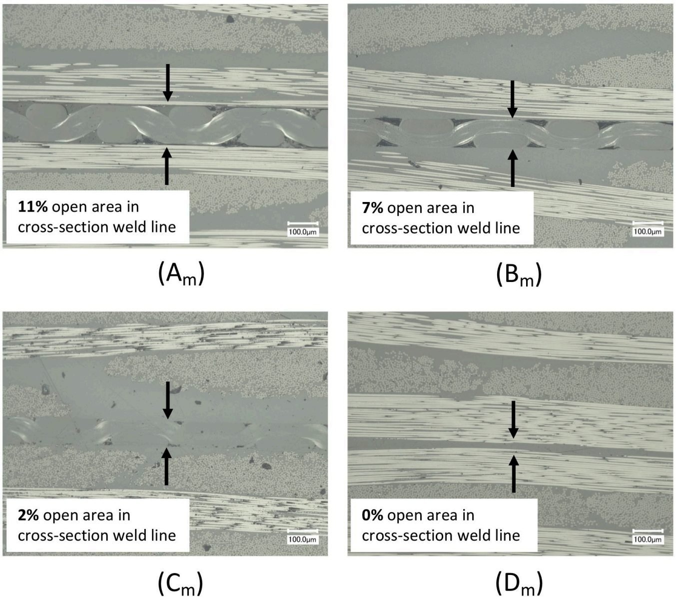

Figure 2.9: Representative micrographs of weld line made with the mesh. The micrographs have been taken during the welding process at moments A_m, B_m, C_m, and D_m, indicated in Figure 2.7a. The black arrows indicate the location of the weld line.

to zero.

From the micrographs at moments A_f, B_f, and C_f as shown in Figure 2.10 it is observed that areas of contact and areas with separations between the thin film energy director and the adherends are present next to each other. The weld line thickness at moments A_f, B_f, and C_f also remains approximately constant at 85 µm, which is approximately the same thickness as the pristine energy director. In the micrograph obtained at moment D_f no clear separations are observed between the energy director and the adherends. However, voids can be observed in the weld line and in between the first and second composite layers.

Figure 2.11 shows the lap shear strength of samples welded at the different moments defined in Figure 2.7 of the welding process for the mesh and thin film energy director. Samples welded with the mesh energy director at moment A_m have a strength of 1.0 MPa. The strength increases to 5.9 MPa for samples welded at moment B_m, and to 16.2 MPa at moment C_m until the strength of 35.4 MPa is reached at moment D_m.

For the thin film energy director a strength of 6.1 MPa is obtained for samples welded at moment A_f. The strength stays approximately the same at moment B_f. At moment C_f the strength increases again to 24 MPa, until a strength of 33.3 MPa is reached at moment D_f at the end of the displacement plateau.

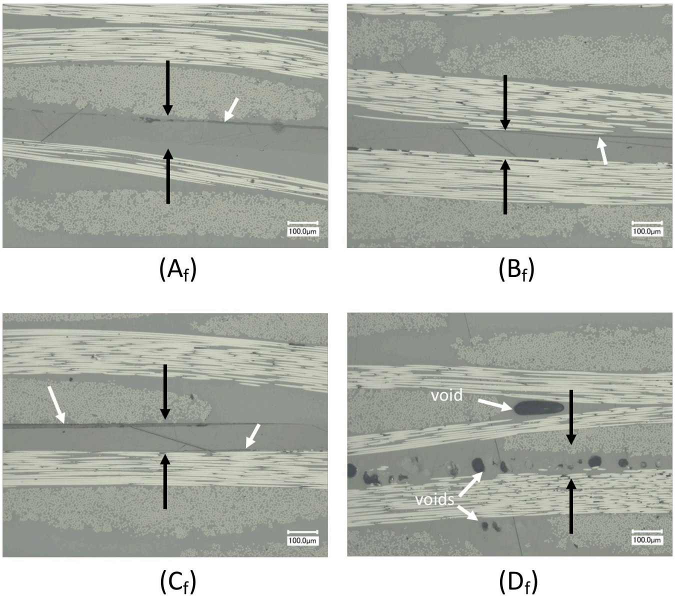

Figure 2.10: Representative micrographs of weld line made with a thin film energy director. The micrographs have been taken during the welding process at moments A_f, B_f, C_f, and D_f, indicated in Figure 2.7b. The black arrows indicate the location of the weld line. The white arrows in C_f highlight separations between the energy director and the adherends. The two white arrows in D_f indicate voids.

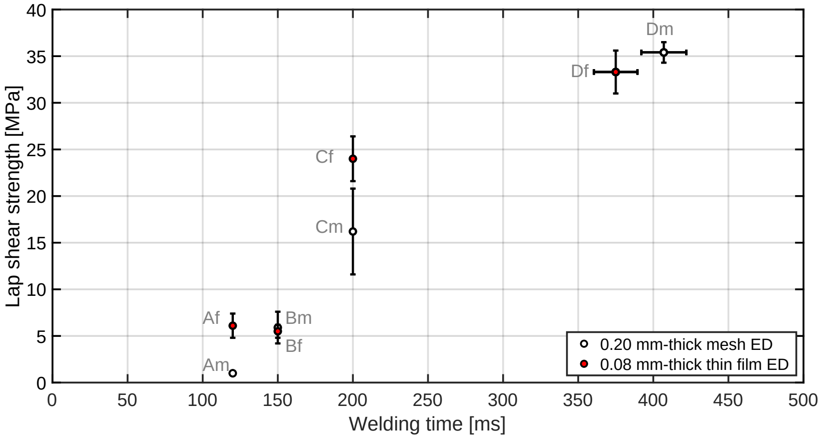

Figure 2.11: Lap shear strength at moments A_x, B_x, and C_x as defined in Figures 2.7a and 2.7b, and at the end of the displacement plateau at an energy control value of 600 J, (D_m and D_f) for the mesh and thin film energy director. Each bar gives the average LSS and standard deviation of three samples.

In Figure 2.12 two representative fracture surfaces are shown after single lap shear testing of samples welded with the mesh energy director (Figure 2.12a) and the thin film energy director (Figure 2.12b). They are welded at the end of the displacement plateau (at D_x). The fracture surface obtained with the mesh energy director is very uniform in quality without any intact energy director. The fracture surface obtained with the thin film energy director contains an area with intact energy director.

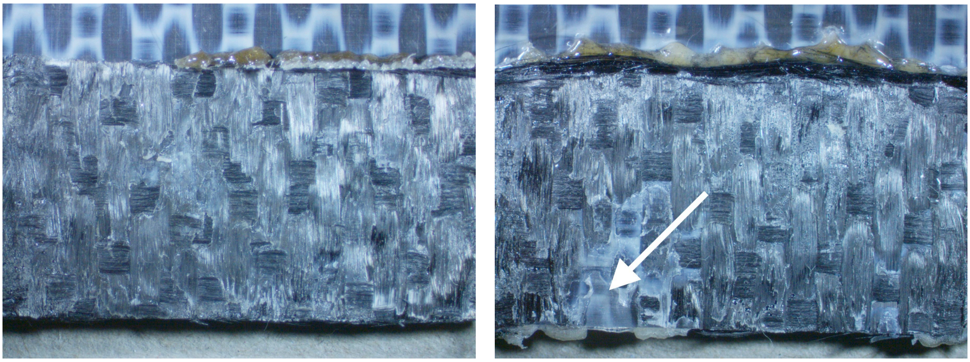

(a) (b)

Figure 2.12: Representative fracture surfaces of CF/PPS samples welded at the conditions for the highest strength with 600 J for the mesh energy director (a), and for the thin film energy director (b). The white arrow in (b) indicates a part of intact energy director.

2.4. Discussion

To understand how the more compliant mesh energy director improves the weld uniformity compared to the thin film energy director, the evolution of contact between the energy directors and the adherends, and the strength development is studied. Understanding the evolution of contact between the energy director and adherends is important, because it is not possible to establish a weld at the locations where the energy director and the adherends do not come in contact with each other. As mentioned in the introduction, a more compliant energy director would undergo a bigger deformation under the force applied by the sonotrode, which would promote a better contact with the adherends and hence improved wetting of the interface [14]. For the mesh energy director, it is found that first the filament crossings of the mesh come in contact with the adherends, establishing multiple small areas of contact that are uniformly distributed across the entire overlap. These small areas of contact experience a relatively high static and dynamic pressure. The deformation of the mesh is therefore initially targeted at the areas of contact as shown in Figure 2.8, flattening the mesh filaments, which can be seen in Figure 2.7a as the initial increase in displacement before the displacement plateau. The mesh filaments then expand within the open areas as shown in Figure 2.9, further increasing the contact area between the energy director and the adherends, wetting the entire interface. It is also believed that due to the uniform deformation of the mesh, the air present in the mesh can pass through the mesh openings, and hence would not contribute to the void content in the interface.

Contrarily, for the thin film energy director, the contact between the energy director and the adherends does not seem to improve during the welding process. The absence of a downward sonotrode displacement during the welding process until moment D_f indicates that no flattening of the thin film energy director occurs, which prevents improvement in contact between the energy director and the adherends or prevents full wetting of the adherend surfaces. Additionally, the contact between the energy director and the adherends in Figure 2.10 seems to be more random.

The strength development of the lap shear samples statically welded with the mesh and the thin film energy director is also found to be different. At the start of the displacement plateau (moment A_m) only a strength of 1.0 MPa is found for the samples welded with the mesh energy director, while at the same moment (A_f) the samples welded with the thin film energy director already exhibit a strength of 6.1 MPa. The absence of strength at the start of the displacement plateau for the mesh energy director indicates that not sufficient heat has been generated in the adherends and transferred to the adherends to melt them, which most likely means that the heat generation is mainly focused at the energy director itself. This is supported by the fact that the filaments of the mesh at the start of the displacement plateau are clearly deformed.

The explanation why some strength is already generated early in the welding process for the thin film energy director has been explained by Palardy et al [8]. They discussed that for thin energy directors, the energy director and the adherends generate heat faster and simultaneously. The hotter adherends reduce the heat transfer from the interface to the adherends, which in our case most likely causes the generation of voids observed between the 1st and 2nd layers of the adherends in Figure 2.10 at moment D_f.

The lap shear strength values of the samples welded with both energy directors increase during the welding process towards moment D. The 6% higher strength obtained with the mesh energy director as compared to the thin film energy director can be explained by the fact that no unwelded areas were present for the mesh energy director as shown in Figure 2.12a, while in the case where the thin film energy director is used, still unwelded areas with intact energy director are present as shown in Figure 2.12b. The cross-sectional micrograph of the weld made with the thin film energy director in Figure 2.10 also displayed porosity at moment D_f, which most likely indicates overheating of the adherends and the interface. The unwelded areas and the porosity are also most likely responsible for the increase in scatter at the maximum obtained lap shear strength (D_f) as can be seen in Figure 2.11.

2.5. Conclusions

The goal of this study was to improve the weld uniformity in continuous ultrasonically welded joints of thermoplastic composites by using a more compliant energy director. A woven polymer mesh energy director was introduced and compared to the current state-of-the-art thin film energy director. It was found that the mesh energy director significantly improved the weld uniformity and lap shear strength. An average lap shear strength of 33.7 $\pm$ 2.4 MPa was obtained for the mesh energy director, compared to 18.8 $\pm$ 6.2 MPa for the thin film energy director. To understand the behaviour of the mesh during the welding process, static welding was used. The main observations on the welding process with the mesh energy director compared to the thin film energy director are the following:

1. The filament crossings of the mesh energy director, uniformly present all over the joint, directly come in contact with the adherends. While for the thin low-compliant film energy director the contact with the adherends seems to be more random.

2. The filaments flatten early in the process and the contact between the mesh and the adherends gradually improves during the welding process by deforming the filaments and filling up the open areas within the mesh. This resulted in full contact between the energy director and the adherends and wetting of the interface. For the thin film energy director, on the other hand, no flattening takes place during the welding process and the absence of downward sonotrode displacement prevents improvement in contact and wetting.

In conclusion, the flattening of the mesh filaments initiated at the uniformly distributed filament crossings early in the welding process, and the gradual increase in contact between the mesh energy director and the adherends during the displacement plateau ensure a full contact between the energy director and the adherends over the entire interface. This contact leads to a fully wetted and uniformly welded area. Since the mesh energy director improved the quality of continuous ultrasonically welded joints significantly, it can be expected that energy directors in the form of woven polymer meshes will play an important role in the development of continuous ultrasonic welding. We believe that this study is a first step towards new studies to optimize the geometry of energy directors to improve the wetting of the surface and to further understand the heat transfer from the energy director to the adherends.

References

[1] A. Yousefpour, M. Hojjati, and J. Immarigeon, "Fusion Bonding/Welding of Thermoplastic Composites," *Journal of Thermoplastic Composite Materials*, vol. 17, no. 4, pp. 303–341, 2004.

[2] C. Ageorges, L. Ye, and M. Hou, "Advances in fusion bonding techniques for joining thermoplastic matrix composites: A review," *Composites - Part A: Applied Science and Manufacturing*, vol. 32, no. 6, pp. 839–857, 2001.

[3] A. Offringa, "New thermoplastic composite design concepts and their automated manufacture," *JEC composites magazine*, vol. 58, pp. 45–49, 2010.

[4] G. Gardiner, "Thermoplastic composites gain leading edge on the A380." https://www.compositesworld.com/articles/

thermoplastic-composites-gain-leading-edge-on-the-a380, (accessed: 09.12.2020).

[5] I. Villegas, B. Valle Grande, H. Bersee, and R. Benedictus, "A comparative evaluation between flat and traditional energy directors for ultrasonic welding of cf/pps thermoplastic composites," *Composite Interfaces*, vol. 22, no. 8, pp. 717–729, 2015.

[6] I. Villegas, "In situ monitoring of ultrasonic welding of thermoplastic composites through power and displacement data," *Journal of Thermoplastic Composite Materials*, vol. 28, no. 1, pp. 66–85, 2015.

[7] I. Villegas, "Strength development versus process data in ultrasonic welding of thermoplastic composites with flat energy directors and its application to the definition of optimum processing parameters," *Composites Part A: Applied Science and Manufacturing*, vol. 65, pp. 27–37, 2014.

[8] G. Palardy and I. Villegas, "On the effect of flat energy directors thickness on heat generation during ultrasonic welding of thermoplastic composites," *Composite Interfaces*, vol. 24, no. 2, pp. 203–214, 2017.

[9] T. Zhao, G. Palardy, I. Villegas, C. Rans, M. Martinez, and R. Benedictus, "Mechanical behaviour of thermoplastic composites spot-welded and mechanically fastened joints: A preliminary comparison," *Composites Part B: Engineering*, vol. 112, pp. 224–234, 2017.

[10] I. Villegas and P. Rubio, "On avoiding thermal degradation during welding of high-performance thermoplastic composites to thermoset composites," *Composites Part A: Applied Science and Manufacturing*, vol. 77, no. Supplement C, pp. 172 – 180, 2015.

[11] A. Levy, S. Le Corre, and I. Villegas, "Modeling of the heating phenomena in ultrasonic welding of thermoplastic composites with flat energy directors," *Journal of Materials Processing Technology*, vol. 214, no. 7, pp. 1361–1371, 2014.

[12] I. Villegas and H. Bersee, "Ultrasonic welding of advanced thermoplastic composites: An investigation on energy-directing surfaces," *Advances in Polymer Technology*, vol. 29, no. 2, pp. 112–121, 2010.

[13] T. Zhao, C. Broek, G. Palardy, I. Villegas, and R. Benedictus, "Towards robust sequential ultrasonic spot welding of thermoplastic composites: Welding process control strategy for consistent weld quality," *Composites Part A: Applied Science and Manufacturing*, vol. 109, pp. 355–367, 2018.

[14] A. Benatar and T. Gutowski, "Ultrasonic welding of PEEK graphite APC-2 composites," *Polymer Engineering & Science*, vol. 29, no. 23, pp. 1705–1721, 1989.

2

[15] M. Tolunay, P. Dawson, and K. Wang, "Heating and bonding mechanisms in ultrasonic welding of thermoplastics," *Polymer Engineering & Science*, vol. 23, no. 13, pp. 726–733, 1983.

[16] N. Tateishi, T. H. North, and R. T. Woodhams, "Ultrasonic welding using tie-layer materials. part i: Analysis of process operation," *Polymer Engineering & Science*, vol. 32, pp. 600–611, 5 1992.

[17] F. Senders, M. van Beurden, G. Palardy, and I. Villegas, "Zero-flow: A novel approach to continuous ultrasonic welding of CF/PPS thermoplastic composite plates," *Advanced Manufacturing: Polymer & Composites Science*, vol. 0340, no. September 2017, pp. 1–10, 2016.

[18] Zongbo Zhang, Xiaodong Wang, Yi Luo, Zhenqiang Zhang, and Liding Wang, "Study on Heating Process of Ultrasonic Welding for Thermoplastics," *Journal of Thermoplastic Composite Materials*, vol. 23, no. 5, pp. 647–664, 2010.

[19] TenCate, *TenCate Cetex TC1100 PPS resin system*. CETEX TC1100 V4 DS 090116, 9 2016.

3

On differences and similarities between static and continuous ultrasonic welding of thermoplastic composites

This chapter is based on the journal article: B. Jongbloed, J. Teuwen, R. Benedictus, and I.F. Villegas, *On differences and similarities between static and continuous ultrasonic welding of thermoplastic composites*, Composites Part B: Engineering **203**, (2020).

3.1. Introduction

Aircraft manufacturers are constantly aiming to reduce manufacturing and operational cost. Therefore, aircraft manufacturers are increasing their interest in fibre-reinforced polymer matrix composites. They allow tailoring of the mechanical properties, and they can have a higher specific strength and stiffness compared to metals. This makes it possible to reduce the weight of the aircraft structure. The lower structural weight typically reduces the operational cost of aircraft by for example a lower fuel consumption.

The matrix of the composites consists of either a thermoplastic or a thermosetting polymer. Especially fibre-reinforced polymer matrix composites with a thermoplastic matrix system can significantly reduce cost during part manufacturing and assembly as compared to fibre-reinforced thermosetting composites. The main contributing factors are the ease of manufacturing (e.g. hot press forming), the reduction in the cycle time, the high material toughness, the recyclability of entire components and scraps produced during manufacturing, and the possibility to weld the thermoplastic composite components together.

The use of resistance welding to assemble the fixed leading edge of the A380 [1], and the use of induction welding to assemble the rudder and elevators of the Gulfstream G650 [2], demonstrate the applicability of welding techniques in the aerospace industry. Another promising welding technique is ultrasonic welding. This technique is fast, energy efficient, and can potentially be monitored and controlled in situ. Especially with the expectation that for next generation aircraft large structural components will be made from carbon fibre-reinforced thermoplastic composites, the need for a high-speed, and low-cost welding technique increases.

During the ultrasonic welding process, a sonotrode exerts high frequency, low amplitude vibrations to the to be welded parts, while, at the same time, applying a static force. These vibrations heat up the interface through frictional and viscoelastic heating [3, 4]. Zhang et al. showed that the heating of the interface is initiated by surface friction, after the glass transition temperature of the thermoplastic material has been reached at the interface, the main heating mechanism becomes viscoelastic heating [4]. To focus heat generation at the interface a relatively thin resin-rich layer, called energy director is used [5, 6]. The relatively low-stiffness energy director experiences a higher cyclic strain due to the vibrations and therefore heats up faster than the stiff adherends.

Most research in the field of ultrasonic welding of thermoplastic composites so far has focused on static welding of simple single lap shear samples [5–15]. Villegas at al. showed that during the static welding process different stages can be identified corresponding to heating up and melting of the interface [8]. Feedback data from the welder, more specifically power and vertical sonotrode displacement, could be used to identify these stages and in situ monitor and control the welding process [5, 7]. Villegas et al. showed that by identifying stages in the welding process, it is possible to find combinations of parameters that consistently result in high strength joints [5, 7].

Recently, continuous ultrasonic welding has shown to be a promising high-speed welding technique for carbon fibre-reinforced polyphenylene sulphide (CF/PPS) thermoplastic composites. For the continuous welding process the sonotrode moves over the to be welded overlap, while it applies the mechanical vibrations and static welding force [16]. Senders et al. demonstrated the possibility of welding two composite adherends together by using zero-flow welding with a 80 microns-thick flat energy director, i.e. a flat resin film, at the interface to focus the heat generation [16]. As a step forward, we continued to use the same composite material and experimental set-up and showed that the weld uniformity and quality could be improved by using a woven polymer mesh as energy director [17]. Additionally, continuous ultrasonic welding has been demonstrated as an efficient technique for tacking and, potentially, consolidating thermoplastic composite tapes during automated fibre placement (AFP) [18, 19] and filament winding (FW) [20, 21] processes. Such processes are however relatively different to the welding process subject of the present paper, since they deal with flexible pre-impregnated or semi-impregnated tapes instead of stiff composite adherends or parts.

In contrast to the static ultrasonic welding process of thermoplastic composite parts, the phenomena happening at the interface during the continuous ultrasonic welding process are not fully understood yet. As a result, the process of, for instance, finding an optimum welding speed (i.e. a speed that results in welded joints with the highest strength), is based on labour- and material-intensive trial-and-error procedures [16]. Contrarily, finding of optimum vibration times in static ultrasonic welding can be efficiently defined with the aid of in situ monitoring of the welding process [5]. Current understanding of the static ultrasonic welding process has been attained by studying a number of aspects of the process, among others:

- the melting phenomena of the interface. Fractography and cross-sectional microscopy were used by Villegas et al. to visualize the melt fronts to get insight into the melting of triangular energy directors [7, 22] and to understand the melting process for film energy directors [5].
- the feedback data of the welder, e.g. time, power, energy and vertical sonotrode displacement. The welding energy and the vertical sonotrode displacement have been related to the weld quality [5, 8, 23].
- the effect of the welding parameters, i.e. among others welding force, vibrational amplitude, and vibration time, on the welding process. In the static welding process, changing the welding parameters force and vibrational amplitude was found to influence the optimum weld duration significantly [5, 8, 23]. The welding force affects the degree of hammering of the sonotrode on the top adherend [11, 24]. A high welding force reduces the hammering, which makes the process more energy efficient en hence faster. The vibrational amplitude is directly linked to the viscoelastic heat generation $\dot{Q}_v$ through the following equation 3.1 [25],

$$\dot{Q}_v = \frac{\omega E"\varepsilon^2}{2} \tag{3.1}$$

  where ω is the frequency of the vibrations, $E"$ the loss modulus of the material, and ϵ the cyclic strain imposed on the material due to the mechanical vibration. Therefore, the amplitude has a major impact on duration of the welding process.

With the aim of identifying how to benefit from existing knowledge on static ultrasonic welding of thermoplastic composite parts to boost the development of the continuous version of the process, the present paper focuses on identifying and understanding differences and similarities between both processes. To this end, we experimentally compared melting of the interface, the consumed power, temperature at the weld interface, and the optimum welding conditions. This was done for three combinations of welding force and vibrational amplitude which are known to have a significant effect in both welding processes.

3.2. Experimental procedures

3.2.1. Materials

The thermoplastic composite laminates used for the welding experiments in this study were made out of carbon fibre fabric (five harness satin weave) impregnated with polyphenylene sulfide powder (CF/PPS semipreg), CF 0286 127 Tef4 43% from Toray Advanced Composites, the Netherlands. The laminates were stacked according to a $[0/90]_{3s}$ sequence and subjected to a consolidation process in a hot press for 20 min at 320 °C and 1 MPa pressure, which based on previous experience results in defect- and void-free laminates. The consolidated laminates had a size of 580 mm by 580 mm, and a thickness of approximately 1.85 mm. Adherends measuring 220 mm by 101.6 mm were cut from the consolidated laminates for the continuous welding experiments. For the static welding process 15.0 mm by 101.6 mm adherends were cut from the laminates. For both adherend sizes the main apparent fibre orientation was in the 101.6 mm direction. A 0.20 mm-thick woven PPS mesh energy director with 37% open area was used for all experiments to focus heat generation at the welding interface [17]. The PPS woven mesh (product name PPS100) was supplied by PVF GmbH, Germany.

3.2.2. Ultrasonic welding

The continuous ultrasonic welding machine, shown in Figure 3.1a, was developed in-house. This machine was used for all the static and continuous ultrasonic welding experiments. It consists of a stiff frame with a x-y table on a guiding system allowing automatic translation in its x-direction and an off-the-shelf ultrasonic welder from Herrmann Ultrasonics of the type VE20 SLIMLINE DIALOG 6200. The operating frequency of the welder is 20 kHz. The welding train consists of the converter, booster and sonotrode. The maximum operational amplitude of the sonotrode was defined to be 80 μm by the manufacturer. A rectangular sonotrode was used. The contact surface of the sonotrode was 15 mm-wide and 27 mm-long. In all the experiments carried out in this research, the sonotrode was oriented with its shorter side parallel to the direction in which the X-Y table automatically moved during the welding process (x-direction in Figure 3.1a). The ultrasonic welder records feedback data (such as time, power consumption, energy, vertical sonotrode displacement, and amplitude) at a 1 kHz frequency.

Figure 3.1b shows a close-up of the continuous ultrasonic welding set-up during the welding process. The CF/PPS top and bottom adherends were kept in place by two aluminium bar clamps placed 70 mm apart from each other. The mesh energy director was placed in between the two adherends. In order to consistently ensure a fixed overlap width of 12.7 mm between the two adherends, alignment pins were used. During the welding process the X-Y table moved underneath the sonotrode in x-direction over a welding distance of 205 mm as shown in Figure 3.2, while the sonotrode applied the static welding force and the high-frequency vibrations. The resulting relative movement of the sonotrode with respect to the adherends is indicated in Figure 3.1b. The parameters of the continuous welding process were force, amplitude and translational speed.

Figure 3.3 shows how the top and bottom adherends for the static welding process were clamped. The same welding machine and clamps were used as in the continuous welding set-up (see Figure 3.1). Note that for some samples the overlap was slightly (≈0.9 mm) smaller than the intended 12.7 mm. For the static welding process, the adherends had the same width as the sonotrode (15 mm). The parameters of the vibration phase for the static welding process were force, amplitude and vibration time. The vibration time was used to control the process i.e. the welder was set to vibrate for a set amount of time. After the vibration phase a consolidation force equal to the welding force was kept on the adherends by the sonotrode for 4000 ms.

Three combinations of welding force and vibrational amplitude were used for both static and continuous welding processes, shown in Table 3.1. For each combination of force and vibrational amplitude several welding speeds (continuous process) and several vibration times (static process) were used as listed in Table 3.1.

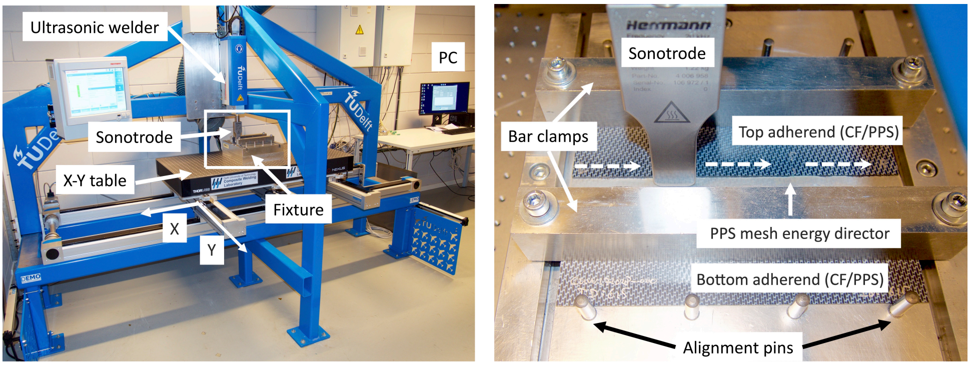

(a) (b)

Figure 3.1: (a) In-house developed continuous ultrasonic welding machine and (b) a close-up of the to be welded parts together with the sonotrode and the bar clamps.

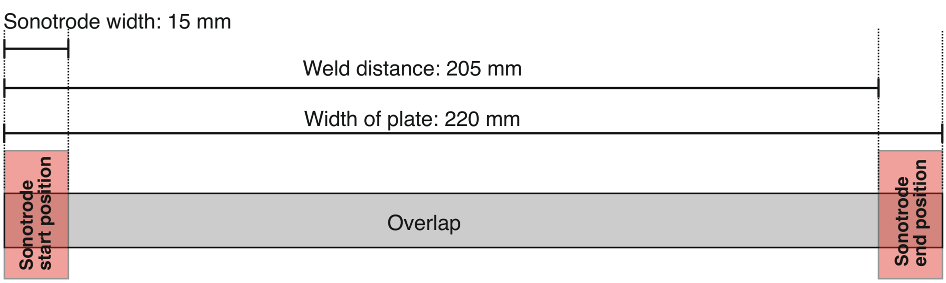

Figure 3.2: Schematic overview of start and end position of the sonotrode with respect to the to be welded overlap together with the welding distance.

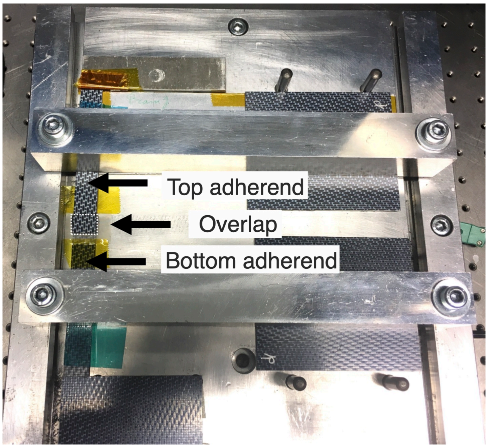

Figure 3.3: Clamping situation of adherends in static ultrasonic welding set-up.

Table 3.1: Test matrix for the static and continuous ultrasonic welding experiments for the three parameters with different welding forces (F) and vibrational amplitudes (A).

Parameters combination		Continuous welding	Static welding
F [N]	**A [μm]**	**Speed [mm/s]**	**Vibration time [ms]**
500	80	25	160, 200, 240, 290, 315, 340, 365, 390, 415, 440, 465, 515, 565
		35	
		45	
1500	80	35	110, 135, 160, 185, 210, 235, 260, 285, 310, 335, 385, 435
		45	
		55	
500	60	15	500, 600, 675, 800, 865, 915, 940, 965, 1000
		19	
		25	

3.2.3. Melt front analysis

To understand how the interface melts and to identify the location of the melt front for the continuous welding process a fractographic analysis was performed around the melt front. The location of the melt front was defined as the location from where the melted ED connected to the adherends. The continuous welding process was stopped prematurely at three different weld distances of 56 mm, 100 mm and 144 mm of the leftmost end of the overlap to check for consistency over the length of the plate (see Figure 3.2 for reference). For each weld distance one continuous weld was made on an individual set of (top and bottom) adherends until that weld distance was reached. This was done for each combination of welding force and vibrational amplitude (see Table 3.1) at the optimum welding speed. The welding speed used was defined as optimum from the results of regular single lap shear tests, as explained later on in Section 3.3.1. For each weld distance a 50 mm-wide sample was cut from the location were the process was stopped. Each of these samples were mechanically separated, and the resulting fracture surfaces were analysed using a ZEISS Discovery.V8 SteREO microscope. For the close-up image of the mesh a Keyence VR one-shot 3D (VR-5000) microscope was used.

To visualize the melting process during the static ultrasonic welding, four welds in a single lap shear configuration were welded for each combination of welding force, vibrational amplitude, and vibration time indicated in Table 3.1. These welds were then mechanically tested, and their fracture surfaces were analysed using the ZEISS Discovery.V8 SteREO microscope.

3.2.4. Energy and power consumption

The areal energy density and average consumed power were determined based on the feedback data from the welder. For the continuous process the optimum welding speed was used, and for the static welding process the optimum vibration time was used. For both processes the power curve was integrated with respect to time in order to obtain the consumed energy. The energy density per unit area was determined by dividing the total consumed energy by the total welded area. For the static welding process an average was taken over four welds. For the continuous process the consumed energy and the average power were determined based on the entire welded seam minus the first and last 15 mm since this area contained non-welded ED.

3.2.5. Temperature measurements

Figure 3.4 shows where the thermocouples were placed for (a) the continuous and (b) the static welding process. The thermocouples were placed in between the bottom adherend and energy director. The temperature at the weld interface was measured using K-type thermocouples supplied by Tempco (product number 2-2200-0004 and description GG220-2K-0). An analog output K-type thermocouple amplifier was used from Adafruit with product number AD8495 sampling the temperature at 1 kHz. The thermocouples had a wire diameter of 0.10 mm. A 25 moving average filter (using the filter function in matlab) was applied to the measured temperature data in order to filter high frequency fluctuations.

For the continuous process 5 evenly spaced thermocouples were placed along the overlap as indicated in Figure 3.4a. The same welded adherends were used for mechanical testing. For the static welding process, 5 additional welds with thermocouples were made for each combination of force and vibrational amplitude, on top of the welds used for mechanical testing. Per weld two thermocouples were placed at the weld interface, one (TC1) in the middle of the overlap and a second one (TC2) approximately 3 mm from the edge as shown in Figure 3.4b.

3.2.6. Mechanical testing

The continuously welded 220 mm-long adherends were cut into six 25.4 mm-wide single lap shear samples for mechanical testing to obtain their LSS (lap shear strength), after discarding the two edges (28.8 mm-wide each). For the static welding process four welds were made per vibration time for LSS-testing. The obtained single-lap shear samples from both the continuous and static welding processes were mechanically tested with a Zwick/Roell 250 kN universal testing machine with a cross-head speed of 1.3 mm/min. The grips were given the necessary offset to ensure parallelism between the load introduction and the overlap. The LSS was calculated by dividing the maximum load by the overlap area.

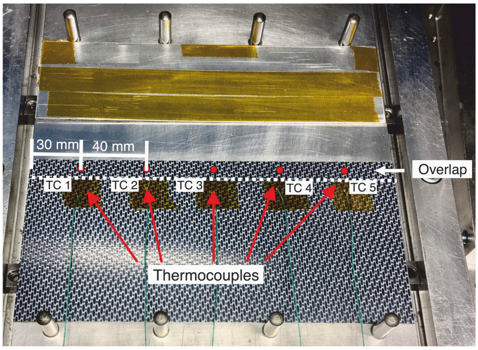

(a)

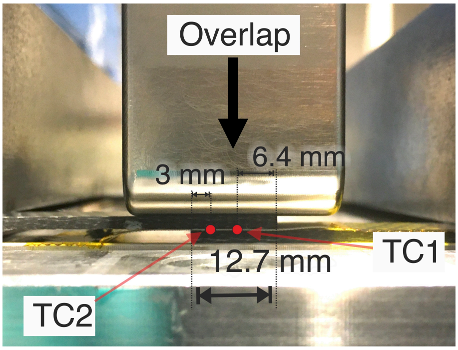

(b)

Figure 3.4: (a) Bottom adherend in the continuous ultrasonic welding set-up together with five thermocouples. (b) Side view of adherends for static welding with thermocouple locations.

3.3. Results

3.3.1. Mechanical tests

Figure 3.5 shows the results of the single lap shear tests of the welded joints obtained by means of the continuous welding process. It should be noted that each point in the graph represents the average strength of six samples cut from a panel welded under a specific combination of force, amplitude and welding speed values. It can be seen that the highest strength values obtained were around 28 MPa for all three force and amplitude combinations. It can also be seen that the optimum welding speed for the 500 N and 80 μm combination was approximately 35 mm/s, which was hence considered as the optimum welding speed for these conditions. A significant drop in strength occurred at either 25 mm/s and 45 mm/s. Increasing the welding force to 1500 N, while maintaining the same amplitude (80 μm) resulted in the highest lap shear strength being reached at both 35 and 45 mm/s. It should be noted that according to ANOVA statistical analysis the average lap shear strength values obtained for those two speeds are not statistically different (p-value = 0.0709 being not significant at $p < 0.05$, $F = 4.08$). However, since degradation of the top adherend was observed when welding at 35 mm/s, 45 mm/s was chosen as the optimum speed for this force and amplitude combination. When increasing the speed to 55 mm/s the strength decreased slightly. For the 500 N and 60 μm combination the optimum welding speed was approximately 15 mm/s. Above a welding speed of 15 mm/s the strength dropped. Below 15 mm/s severe thermal degradation of the top adherend was observed, and thus 15 mm/s was chosen as the lower limit for the speed in this case.

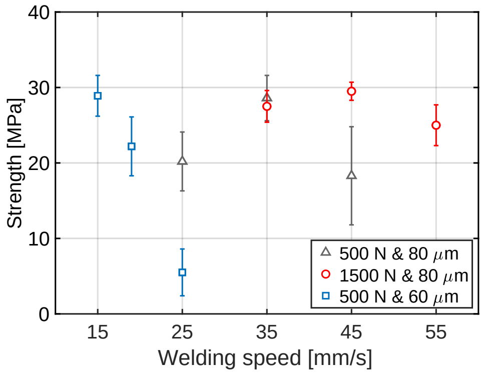

Figure 3.5: Average single lap shear strength values obtained after mechanical testing for the continuous ultrasonic welding process. The bars represent plus and minus the standard deviation around the average (n=6).

Figure 3.6 shows representative fracture surfaces of welds obtained at the optimum welding speed for each one of the three force and amplitude combinations. The fracture surfaces have a uniform appearance and no non-welded energy director was present for any of the welds. However, whitish resin-rich areas containing voids could be observed for all welds. Failure at the weld interface was the most frequent failure type for the 500 N and 80 μm and 1500 N and 80 μm combinations. However, some of the failure partially occurred in between the first and second layer of the bottom adherend. For the lowest vibrational amplitude (500 N and 60 μm combination), the failure most frequently occurred within the adherends with most of the first ply of the top adherend remaining adhered to the top adherend after failure.

Figure 3.7 shows the lap shear strength values corresponding to the static welding process. For the 500 N and 80 μm combination, the strength gradually increased to an interval of high strength values (around 36 MPa) for vibration times between 415 ms and 565 ms. When increasing the welding force to 1500 N and keeping the vibrational amplitude at 80 μm, the high strength interval (also around 36 MPa) was achieved within a shorter vibration time, between 260 ms and 435 ms. When lowering the vibrational amplitude to 60 μm while keeping the welding force at 500 N, the high strength interval (around 38 MPa) was reached significantly later, at vibration times between 860 ms and 960 ms. The optimum vibration times were determined within these high strength intervals based on fractographic analysis. The optimum vibration time was identified as the shortest vibration time within the said interval for which no non-welded energy director could be observed anymore: 440 ms for 500 N and 80 μm, 335 ms for 1500 N and 80 μm, and 940 ms for 500 N and 60 μm.

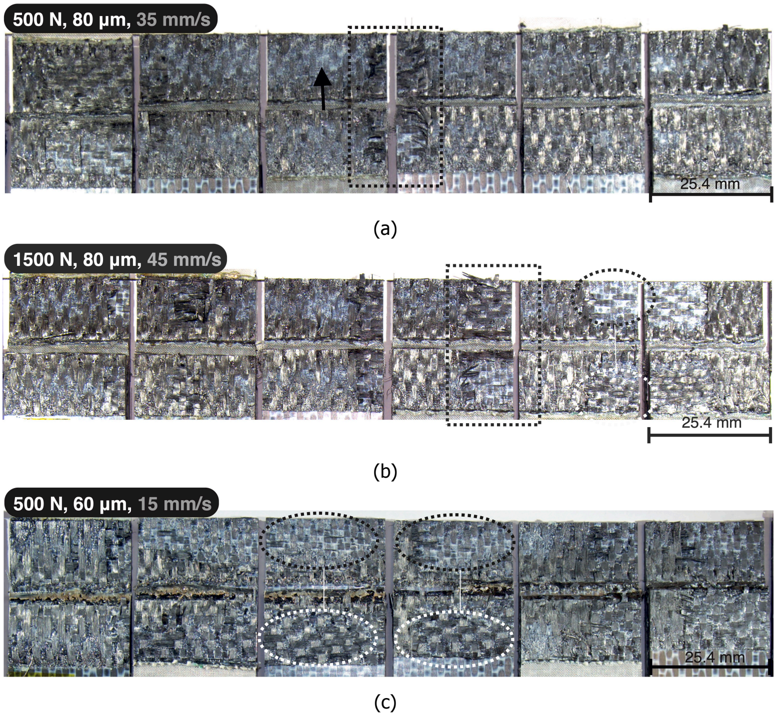

Figure 3.6: Fracture surfaces of adherends welded at the optimum welding speeds for the three combinations of welding force and vibrational amplitude. The arrow indicates a resin rich area containing voids. The dashed rectangular boxes indicate examples of failures that occurred in between the first and second layer of the bottom adherend. The circle combinations indicate where the first layer of the top adherend separated from the top adherend and remained adhered to the bottom adherend.

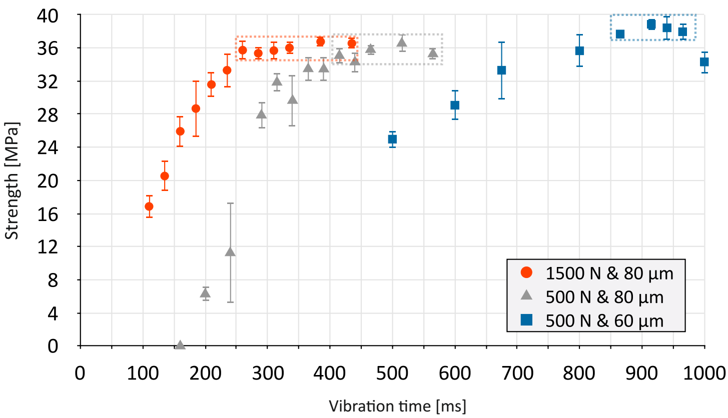

Figure 3.7: Average single lap shear strength obtained after mechanical testing of the samples statically welded at different vibration times. The bars represent plus and minus the standard deviation around the average (n=4).

3.3.2. Power and displacement curves

Figure 3.8 shows the power and displacement curves in the continuous ultrasonic welding process at the optimum welding speeds. For all combinations of welding force and vibrational amplitude the power quickly increased at the start of the welding process. Throughout the welding process the power fluctuated around an average power value of approximately 1600 W for 500 N & 80 µm (Figure 3.8a), 1900 W for 1500 N & 80 µm (Figure 3.8b), and 900 W for 500 N & 60 µm (Figure 3.8c). The power fluctuations near the start and end of the weld were bigger compared those in the middle. Overall, the power fluctuations were less pronounced for the 500 N & 60 µm case (Figure 3.8c). The vertical displacement of the sonotrode did not show a consistent behaviour.

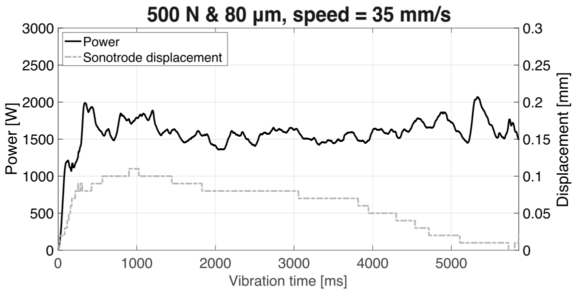

(a)

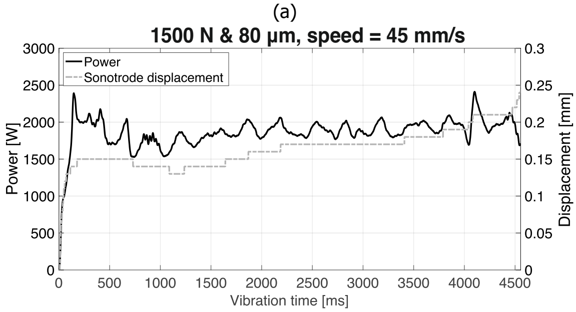

(b)

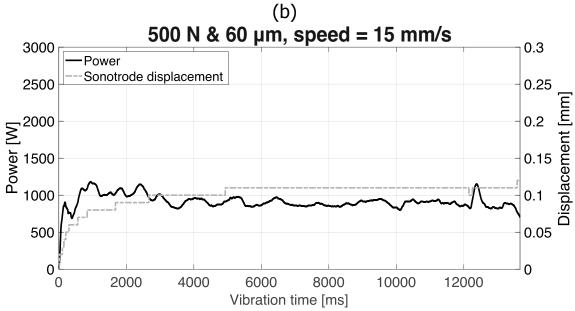

(c)

Figure 3.8: Power and vertical sonotrode displacement curves of the continuous ultrasonic welding process for the three combinations of force and vibrational amplitude welded at the optimum welding speed.

3

3

Figure 3.9 shows the power and displacement curves of the static ultrasonic welding process for the three different combinations of welding force and vibrational amplitude. As seen in Figures 3.9a, 3.9b, and 3.9c, in all cases the power steeply increased within the first 100 ms. The steepest power increase occurred for the 1500 N & 80 μm combination (Figure 3.9b), followed by the 500 N & 80 μm (Figure 3.9a) and the 500 N & 60 μm combinations (Figure 3.9c). After the initial increase the power remained between approximately 800 W and 1500 W for the 500 N & 80 μm combination (Figure 3.9a), between 1200 W and 1800 W for the 1500 N & 80 μm combination (Figure 3.9b), and between 500 W and 800 W for the 500 N & 60 μm combination (Figure 3.9c). The vertical displacement in Figures 3.9a, 3.9b, and 3.9c increased steeply within 130 ms (500 N & 80 μm), 50 ms (1500 N & 80 μm), and 220 ms (500 N & 60 μm) respectively. This initial steep increase was followed by a plateau in displacement, lasting approximately 80 ms for 500 N & 80 μm, 60 ms for 1500 N & 80 μm, and 240 ms for 500 N & 60 μm.

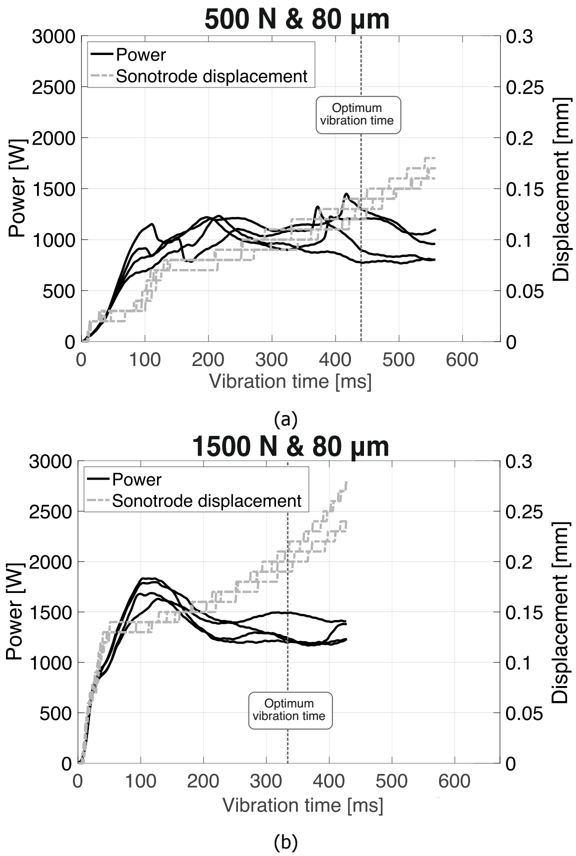

Figure 3.9: Power and vertical sonotrode displacement curves of the static ultrasonic welding process for the three combinations of force and vibrational amplitude.

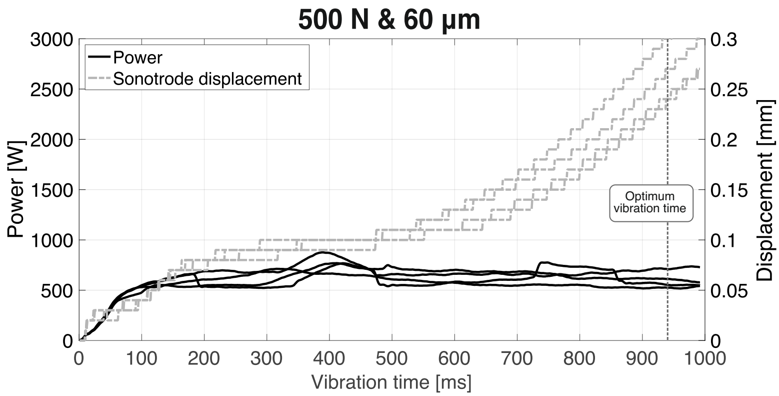

(c) (continued)

Figure 3.9 (continued): Power and vertical sonotrode displacement curves of the static ultrasonic welding process for the three combinations of force and vibrational amplitude.

3.3.3. Melt front analysis

Figure 3.10 shows representative fracture surfaces where the continuous welding process was prematurely stopped at 100 mm from the leftmost edge of the overlap for the three combinations of force and vibrational amplitude and optimum welding speeds. As shown in Figures 3.10a, 3.10b, and 3.10c, in all three cases the melt front was underneath the sonotrode, was relatively straight, parallel to the back and front edge of the sonotrode and closer to the latter. Behind the melt front (i.e. the welded area), rough resin-rich surface with occasional broken fibres (see Figures 3.10a, 3.10b, and 3.10c) could be observed. The whole energy director and presumably the resin on the outer surface of the adherends had been melted. Ahead of the melt front non-welded energy director was present. Figure 3.10d shows a close-up of a part of the non-welded energy director under and ahead of the sonotrode. It can be seen that close to the melt front the ED was significantly deformed and flattened, the degree of deformation and flattening decreased towards fully pristine ED far ahead of the sonotrode.

In Figure 3.10 the position of the melt front was dependent on the process parameters. Table 3.2 shows the position of the melt front relative to the front edge of the sonotrode (referred to as melt front distance) and the position of the melt front relative to the pristine ED at three different positions in the overlap for each combination of processing parameters (see Section 3.2.3). It can be seen that the melt front distance remained relatively constant during the welding process with the largest standard deviation found for the 500 N and 60 µm combination.

Figure 3.11 shows representative fracture surfaces of adherends statically welded under different vibration times for the three combinations of welding force and vibrational amplitude used in this study. It can be seen that for each combination of welding parameters the centre of the overlap melted the latest. The area of non-welded energy director material decreased for increased vibration times. The first vibration times for which the welds contained no non-welded energy director are 440 ms for 500 N and 80 μm, 335 ms for 1500 N and 80 μm, and 940 ms for 500 N and 60 μm. For most of the welds obtained under vibration times beyond those values fibre distortion could be observed at the edges of the overlap.

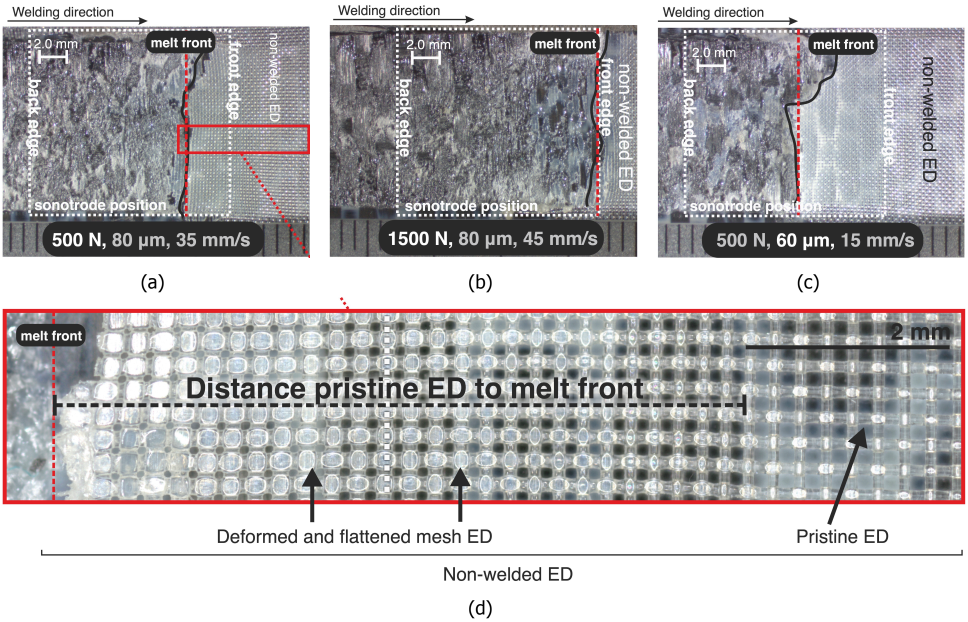

Figure 3.10: Representative fracture surfaces showing the melt front positions at optimum welding speeds after stopping the welding process at 100 mm from the leftmost edge of the overlap for (a) 500 N, 80 μm and 35 mm/s, (b) 1500 N, 80 μm, and 45 mm/s, (c) 500 N, 60 μm, and 15 mm/s. The white dashed rectangles mark the position of the sonotrode when the welding process was stopped. The front edge and the back edge of the sonotrode are also indicated. (d) Close-up from (a) of mainly the non-welded energy directing mesh ahead of sonotrode. The distance between the pristine ED and the melt front is shown.

Table 3.2: Average melt front distances with respect to the front edge of the sonotrode and position of melt front relative to the pristine ED for the three combinations of welding force (F) and vibrational amplitude (A) welded at the optimum welding speeds (S).

Parameters			**Avg. melt front distance**	**Avg. position melt front**
F [N]	**A [μm]**	**S [mm/s]**	**to front edge sonotrode [mm]**	**relative to pristine ED [mm]**
500	80	35	3.2 ± 0.6	6.2 ± 0.4
1500	80	45	0.5 ± 0.5	4.3 ± 0.7
500	60	15	6.0 ± 0.9	8.2 ± 1.7

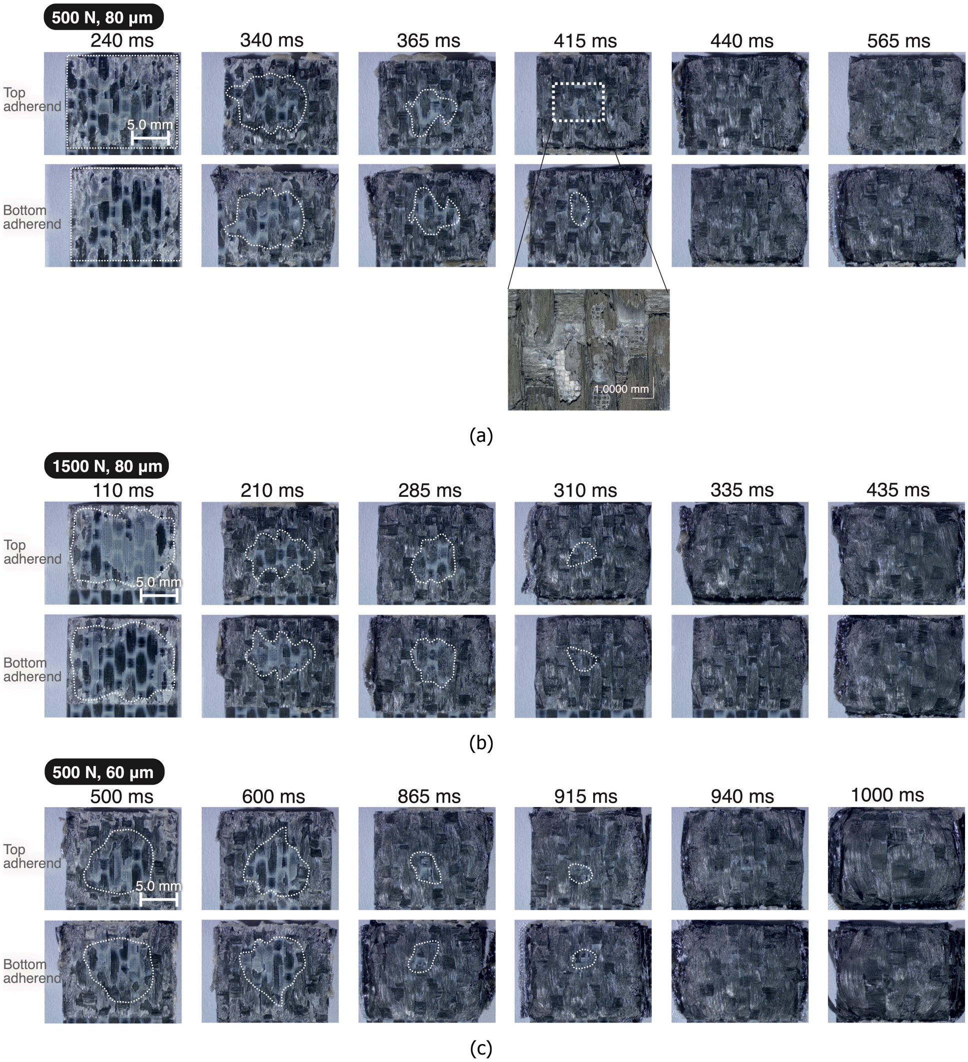

Figure 3.11: Representative fracture surfaces of statically welded adherends at multiple different vibration times for the three combinations of welding force and vibrational amplitude: 500 N and 80 µm, 1500 N and 80 µm, and 500 N and 60 µm. The white dashed areas indicate the presence of non-welded energy director.

3.3.4. Power, energy and temperature measurements

Table 3.3 shows the areal energy density and the average consumed power for both the static and continuous welding processes at the optimum vibration time and welding speed, respectively. It can be seen that energy and power were significantly higher for the continuous welding process. The difference was most pronounced for the 500 N and 80 µm parameter combination, where both the average power and the energy density in continuous ultrasonic welding were almost twice as high as those of the static welding process. The smallest difference occurred for the 1500 N and 80 µm parameter combination, with the power and energy being 1.4 times higher in continuous than in static welding.

Table 3.3: Average power and average areal energy density and corresponding standard deviation for the three combinations of force and vibrational amplitude welded at the optimum static vibration times and optimum continuous welding speeds.

combination	Technique	Optimum	Areal energy density [J/mm^2]	Average power [W]
500 N, 80 µm	Static	440 ms	1.9 ± 0.1	843 ± 41
	Continuous	35 mm/s	3.6 ± 0.3	1605 ± 131
1500 N, 80 µm	Static	335 ms	2.4 ± 0.1	1352 ± 60
	Continuous	45 mm/s	3.3 ± 0.2	1869 ± 135
500 N, 60 µm	Static	940 ms	2.9 ± 0.3	588 ± 54
	Continuous	15 mm/s	4.8 ± 0.4	916 ± 76

Figure 3.12 shows the temperatures measured during the continuous welding process at five different locations in the welding interface (see Section 3.2.5). The grey shaded areas indicate the time span during which a specific thermocouple was located under the sonotrode. It can be seen that the temperature measured by all the thermocouples increased almost instantly to values between 100 °C and 200 °C at the beginning of the welding process. Afterwards, the temperature started to increase more steeply well before the sonotrode reached the thermocouple until a maximum value was reached coinciding with the point where the sonotrode moved away from the thermocouple. The maximum temperatures were 474 °C ± 45 °C, 512 °C ± 41 °C, and 433 °C ± 17 °C for 500 N & 80 µm (Figure 3.12a), 1500 N & 80 µm (Figure 3.12b), and 500 N & 60 µm (Figure 3.12c), respectively.

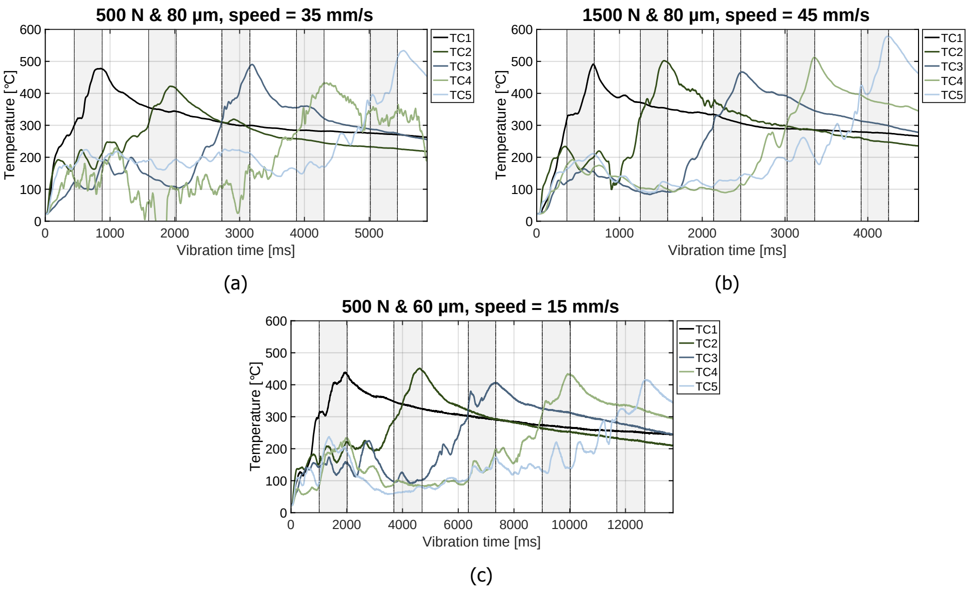

Figure 3.12: Representative temperature measurements for the continuous ultrasonic welding process at the optimum welding speeds for the three parameter combinations. The grey areas indicate the time span during which a specific thermocouple was located under the sonotrode.

Figure 3.13 shows representative temperature measurements at the welding interface for the static ultrasonic welding process. Temperature measurements both at the centre and at one of the edges of the overlap (see Section 3.2.5) are represented in this Figure. As seen in Figures 3.13a, 3.13b, and 3.13c, in all cases the temperature evolution showed a first stage in which it increased quickly from room temperature to over the melting temperature of PPS (280 °C [26]) within the first 50 to 100 ms of the process (50 ms for 1500 N & 80 µm and 100 ms for 500 N & 80 µm and 500 N & 60 µm). After that, a second stage could be observed in which the temperature increase rate slowed down significantly. The duration of this second stage was also between 50 and 100 ms. Temperatures at the centre and at the edge of the overlap were similar during these first and second stages. After that, the temperatures at both locations still showed increasing trends but tended to diverge from each other. While for the 1500 N & 80 µm (Figure 3.13b) and the 500 N & 60 µm (Figure 3.13c) combinations, the temperature at the edge of the overlap was generally higher than at the centre, for the 500 N & 80 µm combination (Figure 3.13a) the opposite behaviour was observed. For the 500 N & 80 µm combination the maximum temperature amounted to around 450 °C (centre of the overlap). For the 1500 N & 80 µm combination the maximum temperature was around 550 °C (edge of the overlap). Finally, for the 500 N & 60 µm combination the maximum temperature was around 500 °C (edge of the overlap).

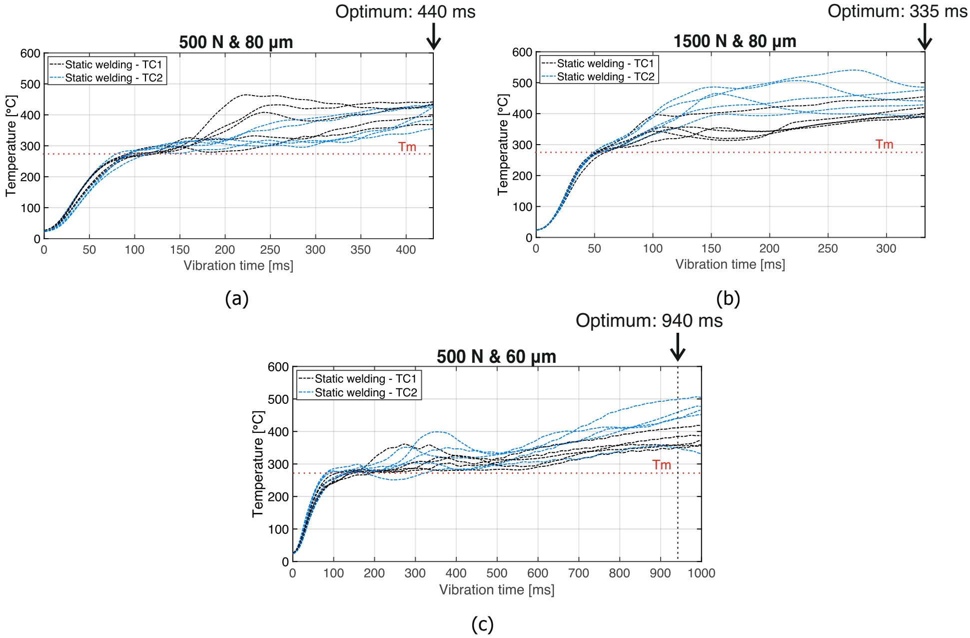

Figure 3.13: Representative temperature measurements for the static welding process until the optimum vibration time for the three parameter combinations. TC1 was located in the centre of the overlap and TC2 was located on the edge of the overlap as indicated in Figure 3.4b.

3.4. Discussion

The aim of this paper was to identify and understand differences and similarities between the static and continuous ultrasonic welding processes for thermoplastic composites. In particular, melting of the interface, consumed power and energy density, temperature evolution at the weld interface, and optimum welding conditions for both types of processes were investigated. This was done for three combinations of welding force and vibrational amplitude, parameters which are known to have a significant effect in both welding processes. Our interpretation of the results obtained in this study is provided in what follows.

Regarding melting of the interface, the fracture surfaces in Figures 3.10 and 3.11 show a fundamental difference between the continuous and the static welding process. While in the static process the amount of non-welded area gradually decreases until it becomes zero, in the continuous process the amount of non-welded area under the sonotrode remains constant. In other words, in static welding the condition of the material under the sonotrode gradually changes, as it sequentially undergoes all the stages in the welding process. Contrarily, an unchanging condition (a simultaneous combination of the different stages the material goes through during the welding process, as schematically represented in Figure 3.14) can be found under the sonotrode in the continuous welding process. The amount of non-welded area under the sonotrode in the continuous process is reduced when either

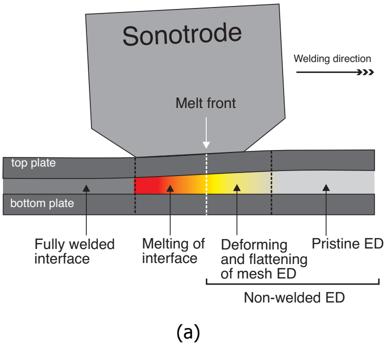

Figure 3.14: (a) Schematic exaggerated interpretation of the CUW process at the interface. (b) Schematic situation for the static welding process.

the welding force or amplitude increase (Figure 3.10). This is consistent with faster heat generation and hence a shorter time for the non-welded energy director to turn into a welded joint.

When it comes to the power dissipated during the welding process, the morphology of the power curves is similar in both processes (Figures 3.8 and 3.9). They feature an initial rapid increase followed by fluctuations around a certain value, which are believed to represent the different phases undergone by the material. However, the overall dissipated power as well as the energy density are significantly higher in the continuous process (see Table 3.3). We believe this is related to the differences in adherend size since, as widely acknowledged in literature, the power or energy in ultrasonic welding is not only invested in creating the weld but also dissipated in its surroundings. As a matter of fact, additional experiments in which a 15 mm-wide static weld was made at the centre of 220 mm-wide adherends (same adherend and energy director configuration as in continuous welding) showed power dissipation levels comparable to those observed in continuous welding (Figure 3.15).

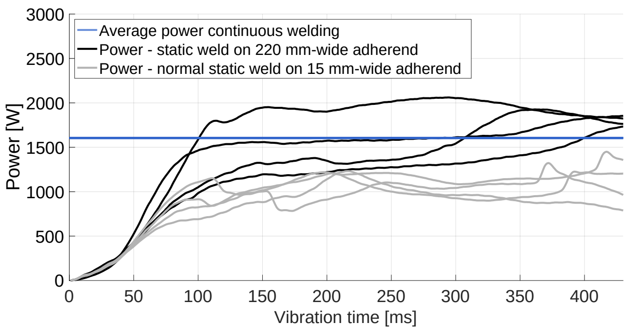

Figure 3.15: Power curves for the 500 N & 80 μm combination for a normal static weld on 15 mm-wide coupons as shown in Figure 3.3, and a static welds made in the middle of 220 mm-wide adherends normally used for continuous welding.

Higher power dissipation when the adherends are wider than the sonotrode (i.e. continuous versus static welding situations in this study) may be explained by two phenomena. Firstly, by the vibrations being transmitted beyond the material directly underneath the sonotrode. As shown in Figure 3.12, all the thermocouples registered a rather simultaneous temperature increase to a temperature level between 100 - 200 °C at the beginning of the continuous process. Such phenomenon can be interpreted as resulting from the occurrence of vibration and hence friction between the thermocouples and adherends all along the overlap and not only at the specific location of the sonotrode. Secondly, by the initial phases of the welding process occurring beyond the boundaries of the sonotrode. As seen in Figure 3.10, the mesh energy director experiences local melting and flattening ahead of the sonotrode in the continuous process. Additionally, the temperature at each thermocouple location starts the ramp-up associated with the welding process before the sonotrode arrives at that location (Figure 3.12). Therefore, owing to pressure distribution and amplitude transmission beyond the sonotrode, the effective area undergoing the different stages of the welding process can be said to be bigger than the actual imprint of the sonotrode, which results in higher power needs.

As mentioned earlier, in continuous welding the temperature starts ramping up beyond the pseudo-initial 100 - 200 °C level before the sonotrode reaches each location. This is obviously not the case in static welding. However the maximum temperatures reached in both types of process are roughly within the same 150 °C-wide range as seen in Figure 3.16. Despite the higher thermal energy input derived from longer exposure to high temperatures in continuous welding, both the continuous and static process show similar melting kinetics at the welding interface. Firstly, the time to transform pristine ED into melted ED connected to the adherends, represented by the distance between the melt front and pristine ED in continuous welding (Figure 3.10) and by the time until the end of the displacement plateau in static welding [17], are similar as shown in Table 3.4. Secondly, the optimum vibration times (static welding) and optimum welding speeds (continuous welding) are also similar (Table 3.4). This indicates that in the particular case studied here, results from the static process can be used to determine the optimum welding speed in the continuous process. This is an important result since it could lead to a considerable reduction of the effort needed to define optimum welding conditions in continuous ultrasonic welding by making use of the relatively simple and efficient methods available in literature to define the optimum vibration time in the static process [5, 8]. Nevertheless, the obvious differences in temperature evolution between the two processes and their potential impact on the validity of the relation between vibration time (static) and welding speed (continuous) need to be further understood. In particular, changing the thermal properties of the adherends and/or the melting behaviour of the energy director by, for instance, welding a different composite material, might challenge the aforementioned relation. On the contrary, introducing changes in the welding setup (ultrasonic welder, clamping jig) could likely result in different absolute values for both the vibration time and welding speed but not in the relation between them. This is supported by the fact that the three force and amplitude combinations used in this study showed a similar relation between vibration time and welding speed despite the very different absolute values in each combination.

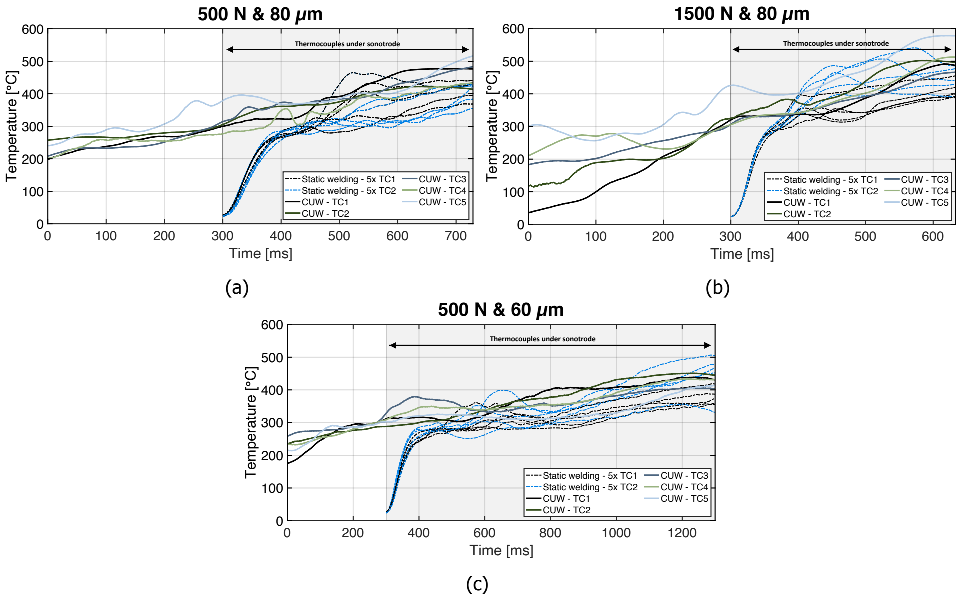

Figure 3.16: Representative temperature measurements for the continuous and the static welding process when the thermocouple is directly under the sonotrode (grey shaded area) and 300 ms before shown for the three parameter combinations at the optimum welding speed (continuous) and optimum vibration time (static) respectively.

Table 3.4: Time to transform pristine ED into melted ED for static (time values at the end of the displacement plateaus in Figure 3.9) and CUW (calculated by dividing the distance from the pristine ED to the melt front in Table 3.2 by the corresponding welding speeds). Translation of optimum welding speeds into vibration times for CUW (by dividing the sonotrode width of 15 mm by the optimum CUW speed), and optimum vibration times in static welding identified in Section 3.3.1.

		500 N and 80 μm	**1500 N and 80 μm**	**500 N and 60 μm**
Time to transform pristine ED into melted ED	Static	200 ms	100 ms	490 ms
	CUW	180 ms	100 ms	550 ms
Optimum	Time based on CUW speed	429 ms	333 ms	1000 ms
	Time static	440 ms	335 ms	940 ms

Finally, the maximum lap shear strength of continuous welded joints is significantly lower than that of statically welded joints. We believe this to be related to the presence of voids weakening the welding interface (main failure location as seen in Figure 3.6) and, potentially, the adjacent layers in the adherends (secondary failure location as also seen in Figure 3.6). These voids, which could be distinctly observed on the fracture surfaces of the continuous welds (Figure 3.6), are believed to be caused by lack of consolidation during the welding process, i.e. no pressure applied during cooling. Lack of consolidation could result from: (i) the continuous welding set-up missing a consolidation shoe which would enable the welded areas to cool down under pressure; (ii) uneven thickness and resulting uneven pressure caused by the presence of non-welded ED under the sonotrode (as indicated in Figure 3.14). Owing to the fact that welded joints obtained at 1500 N and 80 μm featured the same maximum LSS as the other welded joints despite the fact that the melt front was aligned with the front edge of the sonotrode (Figure 3.10) points at the absence of a consolidation shoe as the main cause in the LSS knock down. We therefore expect that adding a consolidation shoe to the continuous welding setup will decrease the amount of voids in the weld line and the adherends and will hence increase the strength of the continuous ultrasonic welds to values similar to those of static welds. We however do not expect the optimum welding speeds defined in the present study to be significantly affected by the addition of a compaction shoe to the welding setup. This is based on the fact that the fracture surfaces of samples welded at welding speeds below and above the optimum featured initial signs of overheating (fibre distortion, discoloured resin) and areas of not completely molten ED, respectively (see e.g. Figure 3.17). Both overheating and non-molten ED are majorly related to the heating phase of the welding process and, consequently, we do not expect them to be affected by whether consolidation pressure is applied or not during the cooling phase.

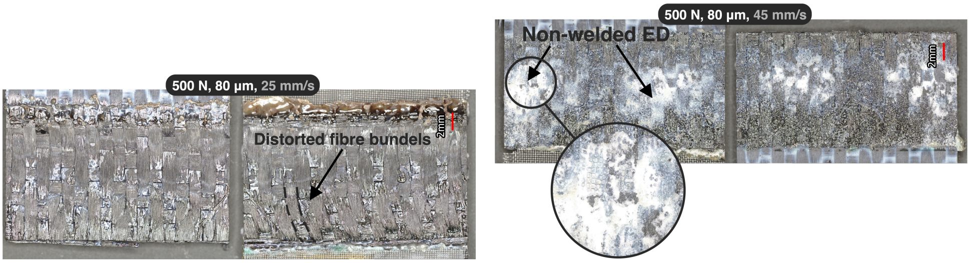

(a) (b)

Figure 3.17: Representative fracture surfaces of continuous welds for the 500 N and 80 μm parameter combination obtained at welding speed (a) below and (b) above the optimum welding speed. (a) displays distorted fibre bundles and discoloured resin at the edges of the overlap, (b) shows areas of non-welded ED. Top adherend is shown on the left and bottom adherend is shown on the right.

3.5. Conclusions

The objective of this paper was to investigate similarities and differences between the static and continuous ultrasonic welding process for thermoplastic composites in order to identify how we can benefit from the available knowledge in static welding to further develop and understand the continuous process. The two processes were compared experimentally with respect to the melting of the interface, the required areal energy density and consumed power, the temperature at the interface, and the effect of changes in welding parameters welding force and vibrational amplitude on the optimum welding conditions. The main conclusions from this study are the following:

- For the continuous process the amount of non-welded area under the sonotrode remains constant, while for the static process the amount of non-welded area gradually decreases until it becomes zero. In other words, for the continuous process there is a constant coexistence of different phases the material goes through. In the static process, on the other hand, the material sequentially undergoes all phases of the welding process.
- The morphology of the power curves is similar for both processes. Both featuring a rapid increase at the beginning followed by fluctuation around a certain value. However, the overall dissipated power for the continuous process is significantly higher. This is most likely caused by the larger adherend size in the continuous process.
- For the continuous welding process the temperature measured at each thermocouple location starts to ramp before the sonotrode arrives at that specific location. Therefore, the effective area undergoing the different stages of the welding process can be said to be bigger than the actual imprint of the sonotrode, which results in higher power needs. Despite the higher power needs for the continuous process both the static and continuous process resulted in maximum temperatures within the same range.
- The optimum vibration times and welding speeds in both processes are similar, indicating that the kinetics of the melting process were not sensitive to whether the process was performed in a static or continuous manner. This similarity has the potential to significantly reduce the labour and material effort invested in defining optimum welding conditions in continuous ultrasonic welding by making use of the relatively simple and efficient methods available in literature to define the optimum vibration time in the static process. Further work is however needed to identify the sensitivity of this conclusion to changes in, for instance, the nature of the composite material being welded.
- The maximum lap shear strength of the continuous welded joints is significantly lower than that of the statically welded joints. This is most likely related to the presence of voids at the continuous welded interface. The voids are believed to be caused by a lack of consolidation during cooling. Therefore, we expect the weld quality and the lap shear strength to increase once a consolidation shoe is implemented into the welding process.

References

[1] G. Gardiner, "Thermoplastic composites gain leading edge on the A380," *High-Performance Composites*, vol. 14(2), pp. 50–55, 2006.

[2] A. Offringa, "New thermoplastic composite design concepts and their automated manufacture," *JEC composites magazine*, vol. 58, pp. 45–49, 2010.

[3] H. Potente, "Ultrasonic welding - principles & theory," *Materials & Design*, vol. 5, no. 5, pp. 228 – 234, 1984.

3

[4] Zongbo Zhang, Xiaodong Wang, Yi Luo, Zhenqiang Zhang, and Liding Wang, "Study on Heating Process of Ultrasonic Welding for Thermoplastics," *Journal of Thermoplastic Composite Materials*, vol. 23, no. 5, pp. 647–664, 2010.

[5] I. Villegas, "In situ monitoring of ultrasonic welding of thermoplastic composites through power and displacement data," *Journal of Thermoplastic Composite Materials*, vol. 28, no. 1, pp. 66–85, 2015.

[6] G. Palardy and I. Villegas, "On the effect of flat energy directors thickness on heat generation during ultrasonic welding of thermoplastic composites," *Composite Interfaces*, vol. 24, no. 2, pp. 203–214, 2017.

[7] I. Villegas, B. Valle Grande, H. Bersee, and R. Benedictus, "A comparative evaluation between flat and traditional energy directors for ultrasonic welding of cf/pps thermoplastic composites," *Composite Interfaces*, vol. 22, no. 8, pp. 717–729, 2015.

[8] I. Villegas, "Strength development versus process data in ultrasonic welding of thermoplastic composites with flat energy directors and its application to the definition of optimum processing parameters," *Composites Part A: Applied Science and Manufacturing*, vol. 65, pp. 27–37, 2014.

[9] T. Zhao, G. Palardy, I. Villegas, C. Rans, M. Martinez, and R. Benedictus, "Mechanical behaviour of thermoplastic composites spot-welded and mechanically fastened joints: A preliminary comparison," *Composites Part B: Engineering*, vol. 112, pp. 224–234, 2017.

[10] I. Villegas and P. Rubio, "On avoiding thermal degradation during welding of high-performance thermoplastic composites to thermoset composites," *Composites Part A: Applied Science and Manufacturing*, vol. 77, no. Supplement C, pp. 172 – 180, 2015.

[11] A. Levy, S. Le Corre, and I. Villegas, "Modeling of the heating phenomena in ultrasonic welding of thermoplastic composites with flat energy directors," *Journal of Materials Processing Technology*, vol. 214, no. 7, pp. 1361–1371, 2014.

[12] I. Villegas and H. Bersee, "Ultrasonic welding of advanced thermoplastic composites: An investigation on energy-directing surfaces," *Advances in Polymer Technology*, vol. 29, no. 2, pp. 112–121, 2010.

[13] T. Zhao, C. Broek, G. Palardy, I. Villegas, and R. Benedictus, "Towards robust sequential ultrasonic spot welding of thermoplastic composites: Welding process control strategy for consistent weld quality," *Composites Part A: Applied Science and Manufacturing*, vol. 109, pp. 355–367, 2018.

[14] N. Koutras, J. Amirdine, N. Boyard, I. F. Villegas, and R. Benedictus, "Characterisation of crystallinity at the interface of ultrasonically welded carbon fibre pps joints," *Composites Part A: Applied Science and Manufacturing*, vol. 125, p. 105574, 2019.

[15] W. Tao, X. Su, H. Wang, Z. Zhang, H. Li, and J. Chen, "Influence mechanism of welding time and energy director to the thermoplastic composite joints by ultrasonic welding," *Journal of Manufacturing Processes*, vol. 37, pp. 196–202, 2019.

[16] F. Senders, M. van Beurden, G. Palardy, and I. Villegas, "Zero-flow: A novel approach to continuous ultrasonic welding of CF/PPS thermoplastic composite plates," *Advanced Manufacturing: Polymer & Composites Science*, vol. 0340, no. September 2017, pp. 1–10, 2016.

[17] B. Jongbloed, J. Teuwen, G. Palardy, I. F. Villegas, and R. Benedictus, "Continuous ultrasonic welding of thermoplastic composites: Enhancing the weld uniformity by changing the energy director," *Journal of Composite Materials*, vol. 54, no. 15, pp. 2023–2035, 2020.

[18] R. H. Rizzolo and D. F. Walczyk, "Ultrasonic consolidation of thermoplastic composite prepreg for automated fiber placement," *Journal of Thermoplastic Composite Materials*, pp. 1–18, 2015.

[19] Q. Chu, Y. Li, J. Xiao, D. Huan, X. Zhang, and X. Chen, "Processing and characterization of the thermoplastic composites manufactured by ultrasonic vibration–assisted automated fiber placement," *Journal of Thermoplastic Composite Materials*, vol. 31, no. 3, pp. 339–358, 2018.

[20] F. Lionetto, R. Dell'Anna, F. Montagna, and A. Maffezzoli, "Modeling of continuous ultrasonic impregnation and consolidation of thermoplastic matrix composites," *Composites Part A: Applied Science and Manufacturing*, vol. 82, pp. 119–129, 2016.

[21] R. Dell'Anna, F. Lionetto, F. Montagna, and A. Maffezzoli, "Lay-up and consolidation of a composite pipe by in situ ultrasonicwelding of a thermoplastic matrix composite tape," *Materials*, vol. 11, no. 5, 2018. cited By 15.

[22] I. Villegas and G. Palardy, "Ultrasonic welding of cf/pps composites with integrated triangular energy directors: melting, flow and weld strength development," *Composite Interfaces*, vol. 24, no. 5, pp. 515–528, 2017.

[23] I. F. Villegas, "Ultrasonic welding of thermoplastic composites," *Frontiers in Materials*, vol. 6, p. 291, 2019.

[24] G. Palardy, H. Shi, A. Levy, S. L. Corre, and I. F. Villegas, "A study on amplitude transmission in ultrasonic welding of thermoplastic composites," *Composites Part A: Applied Science and Manufacturing*, vol. 113, pp. 339 – 349, 2018.

[25] A. Benatar and T. Gutowski, "Ultrasonic welding of PEEK graphite APC-2 composites," *Polymer Engineering & Science*, vol. 29, no. 23, pp. 1705–1721, 1989.

[26] TenCate, *Product datasheet TenCate Cetex TC1100 PPS resin system, Nijverdal, The Netherlands*, 9 2016.

4

Improving the quality of continuous ultrasonically welded thermoplastic composite joints by adding a consolidator to the welding setup

This chapter is based on the journal article: B. Jongbloed, R. Vinod, J. Teuwen, R. Benedictus, and I.F. Villegas, *Improving the quality of continuous ultrasonically welded thermoplastic composite joints by adding a consolidator to the welding setup*, under peer review at Composites Part A: Applied Science and Manufacturing, (2021).

4.1. Introduction

The interest and the application of thermoplastic composites is increasing in the aerospace industry due to their advantages over the currently more common thermoset composites. The main advantages are that thermoplastics can be re-molten and reshaped upon heating, they are recyclable, and have a high material toughness. Especially, the first advantage can lead to major cost benefits, since it makes efficient forming and welding techniques possible. As a result, different welding techniques have been developed for joining thermoplastic composite structures. The most promising welding techniques are resistance, induction, and ultrasonic

Rahul Vinod significantly contributed to the experiments conducted in this chapter.

welding [1]. Ultrasonic welding is generally the fastest and most energy-efficient welding technique [2] among the three.

The ultrasonic welding process consists of a heating phase, known as vibration phase, during which the thermoplastic resin softens and melts, and a consolidation phase during which the weld cools down and solidifies. Heat is generated as follows: a metal horn, called a sonotrode, transversely exerts high-frequency low-amplitude vibrations to the weld interface, while at the same time applying a static pressure. Heat is generated at the weld interface due to surface and viscoelastic friction [3, 4]. To focus heat generation at the interface, an energy director is used [5]. This energy director is a layer of resin, i.e. a resin film or a mesh woven from thermoplastic resin filaments. Due to its lower stiffness and subsequent higher cyclic straining under the imposed vibrations, the viscoelastic heating undergone by the energy director is higher compared to that undergone by the fibre reinforced adherends [6–8].

Two ultrasonic welding processes can be distinguished, static (i.e. spot) and continuous welding [5]. During static welding both the sonotrode and adherends remain stationary during the welding process (which can be sequentially performed at different locations), while for the continuous process the sonotrode and the adherends move relative to each other during the welding process creating a continuous welded seam. The continuous ultrasonic welding process potentially has benefits over the static counterpart for certain applications. A generally larger welded area means a higher load carrying capability for the continuously welded joints. Continuous ultrasonic welding of thermoplastic composites is however a relatively new technology that still requires optimization. One of the important aspects to be optimized is the quality of the continuous welded joints [9–11]. Indeed, in a previous study [11] in which we compared the static and continuous ultrasonic welding processes for different welding parameters, we found a significantly lower maximum strength for the continuous welded joints. The lower strength was attributed to the presence of voids due to a lack of consolidation during cooling down. In the static process, the sonotrode itself provides the consolidation pressure during cooling. In the continuous process, on the other hand, the sonotrode cannot apply the consolidation pressure, because it continuously moves away from the area that was just heated up [11]. Up to now, most studies on ultrasonic welding of thermoplastic composites have focused on the vibration or heating phase of the static welding process [5, 7, 12–21], but not in the consolidation or cooling phase. Nevertheless, the consolidation is at least as important since it majorly impacts the void content, the autohesion process and ultimately the strength of the joint. Deconsolidation is a potential problem that can occur when processing thermoplastic composites and which significantly increases the void content reducing the quality of the material [22, 23]. It can occur when insufficient consolidation pressure is applied [23–25] or when the pressure is not applied for a long enough time during cooling. For amorphous matrices deconsolidation can occur when the temperature is sufficiently high above the glass transition temperature and for semi-crystalline matrices above the melting temperature [24, 26]. Deconsolidation typically is driven by either one of the following two factors: fibre decompaction due to the release of internal stresses [23–25, 27, 28] especially for fabrics; and the expansion of already existing voids and moisture [23, 24, 29].

The aim of this study is to investigate how the quality of continuous ultrasonically welded joints can be improved by adding a consolidation shoe (hereafter referred to as consolidator) to the welding setup. To determine the required consolidation pressure, the size of the consolidator, and its distance from the sonotrode the following steps were followed. Firstly, the effect of consolidation pressure on the weld quality was studied in the static ultrasonic welding process for a constant and sufficiently long consolidation time. Secondly, the effect of the consolidation time on the weld quality was studied on the static welding process by keeping the consolidation pressure constant and by using different consolidation times defined with the assistance of temperature measurements at the welding interface. Finally, those results were used to determine the consolidation pressure and the size of the consolidator in the continuous ultrasonic welding process. The effect of the distance between the consolidator and the sonotrode on the quality of the weld was lastly investigated. The weld quality was assessed through the presence of voids in the weld line and within the adherends, and through the single-lap shear strength and fractographic analysis of the welded joints.

4.2. Experimental procedures

4.2.1. Materials

The thermoplastic composite laminates used for the welding experiments in this study were made out of carbon fibre fabric (five harness satin weave) impregnated with polyphenylene sulphide powder (CF/PPS semipreg), CF 0286 127 Tef4 43% from Toray Advanced Composites, the Netherlands. The laminates were stacked according to a $[0/90]_{3s}$ sequence and subjected to a consolidation process in a hot platen press for 20 min at 320 °C and 1 MPa pressure, which, based on previous experience, results in void-free laminates. The consolidated laminates had a size of 580 mm by 580 mm and a thickness of approximately 1.85 mm. Rectangular adherends measuring 25.4 mm x 101.6 mm and 220 mm x 101.6 mm were cut from the consolidated laminates for the static and continuous welding experiments, respectively. For both adherend sizes the main apparent fibre orientation was in the 101.6 mm direction. A 0.20 mm-thick woven PPS mesh with 37% open area (PPS100, supplied by PVF GmbH, Germany) was used as energy director in all experiments to focus heat generation at the welding interface [10, 11].

4.2.2. Static ultrasonic welding

The ultrasonic welder (HiQ DIALOG 6200, Herrmann Ultrasonics) shown in Figure 4.1a was used for all static ultrasonic welding experiments. The operating frequency of the welder is 20 kHz. The welding train consists of a converter, booster and sonotrode. A rectangular sonotrode with a 15 mm x 27 mm contact area was used in these experiments. A custom-built fixture, shown in Figure 4.1b, was used to clamp the adherends in a single-lap configuration (Figure 4.1c) with an overlap area of 12.7 mm x 25.4 mm. In this fixture, the top adherend is kept in place by a sample holder resting on springs to minimize potential bending of the top adherend as the energy director melts and is squeezed out during the welding process. These springs apply a 18 N upward force (0.056 MPa) on the sample holder once fully pressed down by the sonotrode during the welding process.

For the vibration phase of the static process the following parameters were used: a peak-to-peak vibration amplitude of 80 µm, a welding force amounting to 500 N (1.6 MPa on the welding overlap), and a vertical sonotrode displacement of 0.07 mm defined according to the methodology described in [15, 19]. Note that the vertical displacement of the sonotrode was used to indirectly control the duration of the vibration phase and, hence, the onset of the subsequent consolidation phase. The consolidation pressure and consolidation time were varied independently of each other to understand their effect on the weld quality. Firstly, the effect of the consolidation pressure was studied by using different consolidation pressure values, while keeping the consolidation time fixed at 10 s to exclude influences of time on the results. Secondly, the effect of the consolidation time was studied by selecting different consolidation times based on exploratory temperature measurements at the weld interface while keeping the consolidation pressure constant at 1.6 MPa (500 N). An overview of the welding parameters used in this study is shown in Table 4.1.

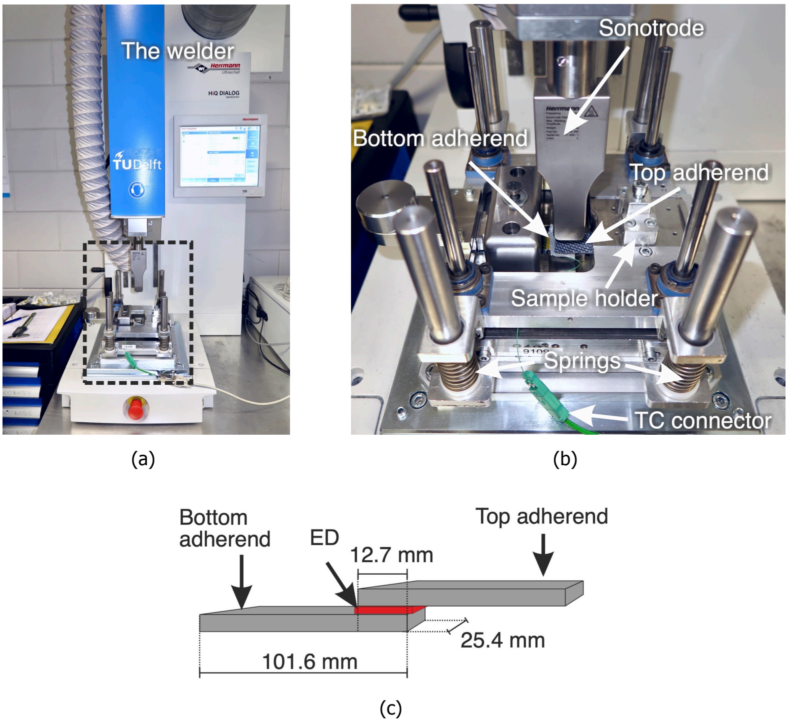

Figure 4.1: (a) Ultrasonic welder from Herrmann Ultrasonics. (b) Custom-built welding fixture with spring resting sample holder for top adherend. (c) Schematic of adherends and energy director (ED) in static process.

4.2.3. Continuous ultrasonic welding

The custom-built ultrasonic welding machine shown in Figure 4.2a was used for the continuous ultrasonic welding experiments. It consists of a stiff frame with a X-Y table on a guiding system, an off-the-shelf 20 kHz ultrasonic welder from Herrmann Ultrasonics (VE20 SLIMLINE DIALOG 6200), and a custom-built consolidation unit. Similar to the static ultrasonic welding process, a rectangular sonotrode with a 15 mm x 27 mm contact area was used in the welding setup. The consolidation unit (Figure 4.2b) consisted of a servo press kit YJKP of 1.5 kN from Festo, a stabilization guide unit to avoid sideways deflections, and a copper block (Figure 4.2c) in charge of applying the consolidation pressure on the material. The width of the copper block was 30 mm. The length of the copper block as well as the consolidation pressure were defined based on the results from the static tests. The placement of the consolidator with respect to the sonotrode could be changed via the adjustment wheel (Figure 4.2b). The consolidation distance was defined as the distance between the sonotrode and the consolidator, as indicated in Figure 4.2c. Three consolidation distances were considered in this study: 18.4 mm, 63 mm, and 86.4 mm. Additionally, a continuous weld obtained with the use of no consolidator was produced and used as a reference. An overview of the continuous welds made in this study is shown in Table 4.1.

During the welding process the X-Y table was translated by an servo motor underneath the sonotrode in X-direction (see Figure 4.2a). The resulting relative movement of adherends with respect to the sonotrode and consolidator is indicated in Figure 4.2b. The sonotrode was oriented with its 15 mm-wide side parallel to the direction of translation (Figure 4.2c). A welding force amounting to 500 N (2.6 MPa on the welding overlap), a peak-to-peak amplitude of 80 μm, and a constant welding speed of 35 mm/s were used based on the results of a previous study [11]. Note that the resulting pressure from the 500 N welding force in the continuous process was higher compared to the static process. The top and bottom adherends (Figure 4.3a) were kept in place by two aluminium bar clamps located at 130 mm from each other (Figure 4.3b). Note that the configuration used in this study, which we found to provide a more uniform temperature distribution across the overlap (Figure 4.4), differs slightly from the one used in our previous study [11] both in distance between bar clamps and in the position of the sonotrode relative to the overlap (Figure 4.4). Each clamp was secured with two M8 bolts tightened at a torque of 14 N/m.

4

4

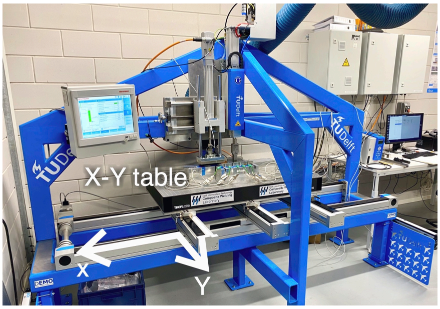

(a)

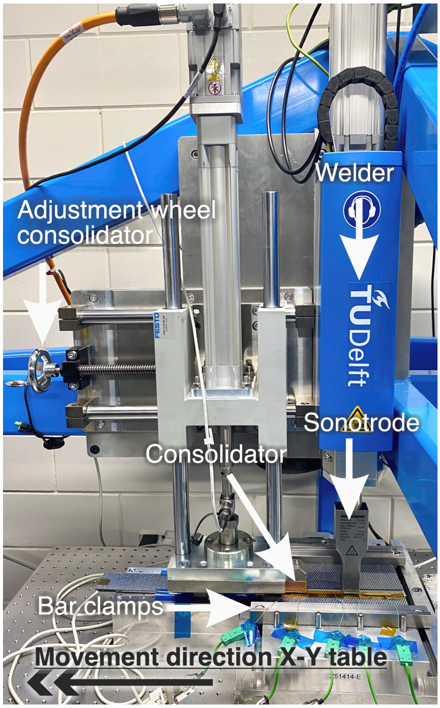

(b)

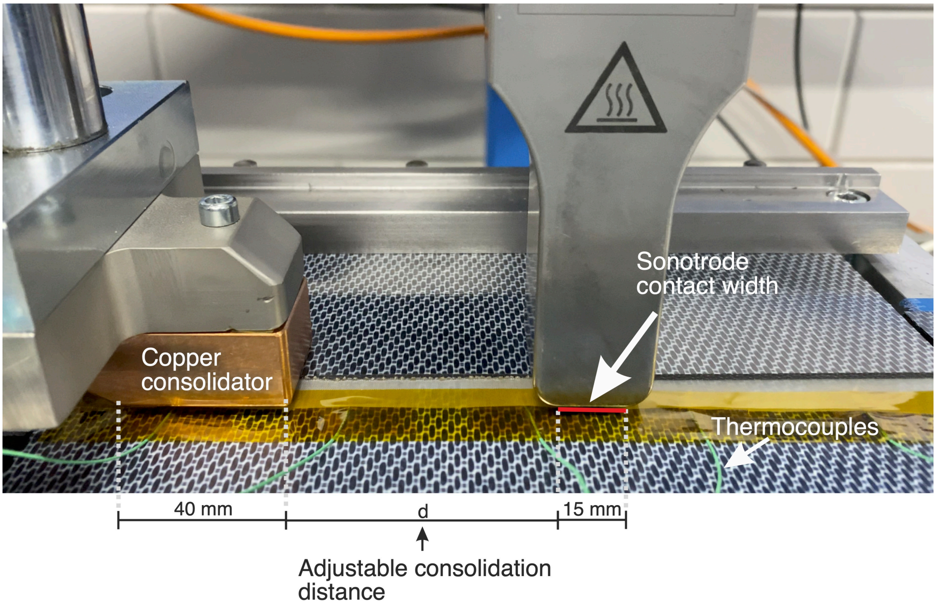

(c)

Figure 4.2: (a) In house developed continuous ultrasonic welding machine, (b) close-up of the consolidation device and the welder, (c) close-up of consolidator placement.

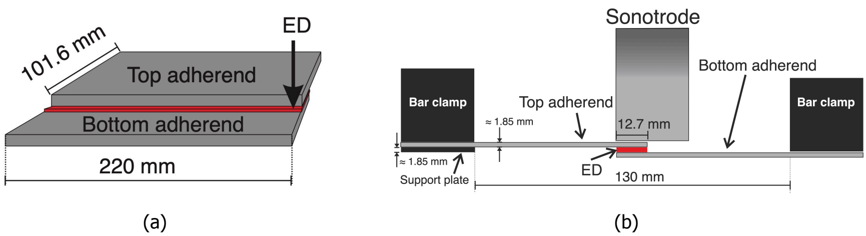

Figure 4.3: Schematic of (a) dimensions of the adherends, and (b) sonotrode and clamps placement for the continuous ultrasonic welding process.

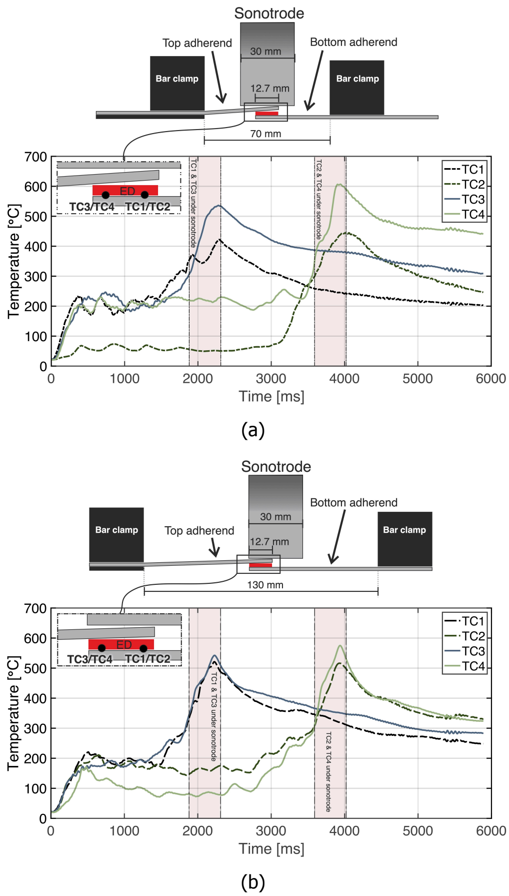

Figure 4.4: Temperature profiles during the continuous welding process for thermocouples placed at the weld interface approximately 2 mm from the edges for (a) 70 mm clamping distance as used in [10, 11], and (b) 130 mm as used in the current study as shown in Figure 4.3a. The angle between the top adherend and energy director has significantly been over-exaggerated. The red shaded areas indicate when a pair of thermocouples was located under the sonotrode. Welding force was 500 N, vibrational amplitude was 80 µm, welding speed was 35 mm/s, and without consolidator.

4.2.4. Temperature measurements

Temperatures were measured at the welding overlap using K-type thermocouples (GG220-2K-0, product number 2-2200-0004, Tempco B.V., Bodegraven, the Netherlands). The sleeved thermocouples had a total diameter of 0.70 mm, while the diameter of the thermocouple wires was 0.10 mm. An analog thermocouple output amplifier (Adafruit AD8495) was used to simultaneously sample temperature readings at 1 kHz from a maximum of five thermocouples. A moving average filter (10 points for the static process and 40 points for the continuous process) was applied in MATLAB to filter out high frequency fluctuations from the temperature data. Figure 4.5 shows where the thermocouples were placed for (a) the static and (b) the continuous process. Table 4.1 provides information about which temperature measurements were performed in which experiments.

4

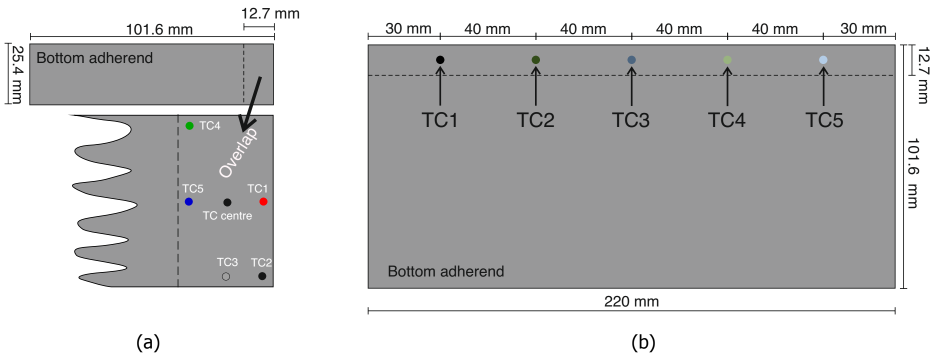

Figure 4.5: Bottom adherends for (a) the static and (b) the continuous ultrasonic welding setup together with the locations where thermocouples (TCs) were placed. The dotted lines indicates the end of the 12.7 mm overlap.

Table 4.1: Overview of static (SUW) and continuous (CUW) ultrasonic experiments. (Note that the amplitude values are peak-to-peak.)

Process	Parameters vibration phase (welding pressure (force), amplitude, displacement/ welding speed)	Consolidation pressure (and force)	Consolidation time / consolidator distance	Adherend size [mm]	Remarks
SUW	1.6 MPa (500 N), 80 µm, 0.07 mm	0 MPa (0 N) 0.4 MPa (130 N) 0.6 MPa (200 N) 1.6 MPa (500 N) 3.1 MPa (1000 N) 4.7 MPa (1500 N)	10000 ms	25.4 x 101.6	6 welds per pressure value of which 5 for LSS and 1 for cross-sectional microscopy
	1.6 MPa (500 N), 80 µm, 0.07 mm	1.6 MPa (500 N)	10000 ms	25.4 x 101.6	5 welds with TC2 (Figure 4.5a); 1 weld with TC1, TC2, TC3, TC4, and TC5; 1 weld with TC centre
	1.6 MPa (500 N), 80 µm, 0.07 mm	1.6 MPa (500 N)	0 ms, 100 ms, 600 ms, 1000 ms 2500 ms, 4000 ms, 5000 ms, 10000 ms	25.4 x 101.6	7 welds per consolidation time of which 5 for LSS, 1 for cross-sectional microscopy, and 1 for micro-CT. Note: no micro-CT performed for 0 ms, 100 ms, and 2500 ms
CUW	2.6 MPa (500 N), 80 µm, 35 mm/s	1.6 MPa (800 N)	No consolidator, 18.4 mm, 63 mm, 86.4 mm	220 x 101.6	1 weld per consolidation distance with all TCs shown in Figure 4.5b

4.2.5. Mechanical testing and fractography

The statically welded joints could directly be mechanically tested to obtain their single-lap shear strength (LSS). The continuously welded joints were cut into six 25.4 mm-wide single lap shear samples after discarding approximately 28.8 mm-wide bands of material at both edges of the joint. Five of these samples were used for mechanical testing, and one sample was used for cross-sectional microscopy. One of the five mechanically tested samples was used for micro-CT prior to mechanical testing. The welded single-lap shear samples from both the continuous and static welding processes were mechanically tested using a Zwick/Roell 250 kN universal testing machine under a cross-head speed of 1.3 mm/min. The grips were given the necessary offset to ensure parallelism between the load introduction and the weld line. The LSS was calculated by dividing the maximum load by the overlap area. After mechanical testing, a Keyence VR one-shot 3D (VR-5000) microscope was used to analyze the fracture surfaces.

4.2.6. Cross-sectional microscopy, and void content determination

To obtain cross-sectional views from the welded adherends, specimens were cut parallel to the longitudinal orientation of the welded samples and embedded in epoxy resin. They were ground and polished with a Struers Tegramin-20 polisher. A Keyence 3D laser scanning confocal (VK-X1000) microscope was used for obtaining the cross-sectional micrographs. A Phoenix Nanotom Micro-CT scanner (180 kV maximum voltage, and 15 W maximum power) was used to quantify the volumetric void content within the welded overlap with a resolution of 14 μm. Avizo CT software from ThermoFisher Scientific was used to determine the volumetic void content in the welded overlap.

4.3. Results

4.3.1. Effect of consolidation pressure for the static ultrasonic welding process

Figure 4.6 shows the lap shear strength values for static ultrasonic welds consolidated under different consolidation pressure values. The corresponding representative fracture surfaces obtained after mechanical testing are shown in Figure 4.7. Representative cross-sectional micrographs are shown in Figure 4.8.

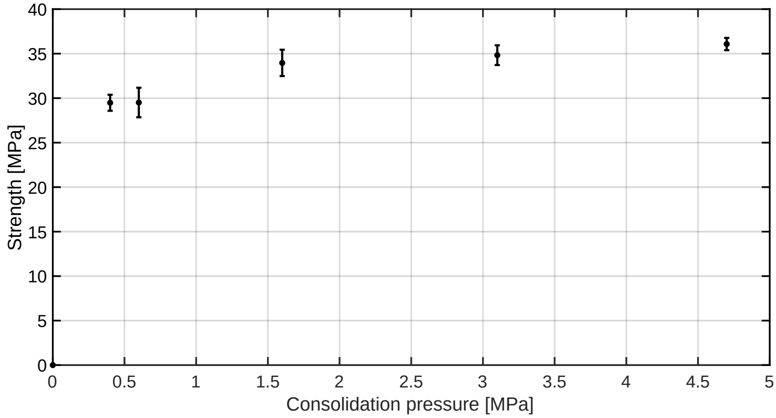

Figure 4.6: Average lap shear strength with standard deviation error bars (n=5) for static ultrasonic welds consolidated under different consolidation pressure values.

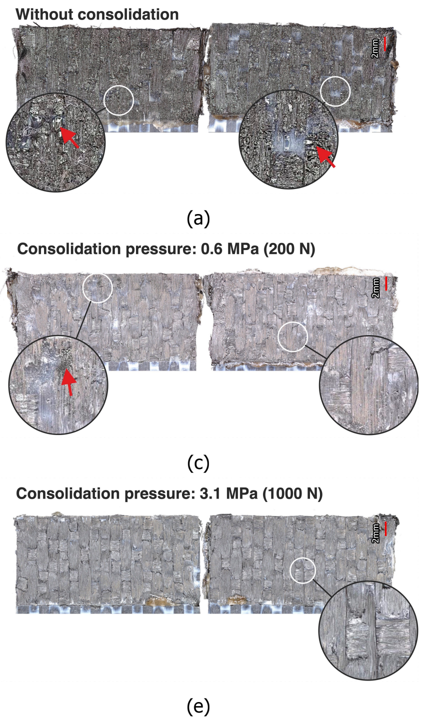

(a) (b) (c) (d) (e) (f)

Figure 4.7: Representative fracture surfaces of static ultrasonic welds consolidated under different pressure values. The top adherends are shown left, and the bottom adherends are shown right. Some white circled areas are enlarged to show representative details of the fracture surfaces. The red arrows indicate areas containing voids.

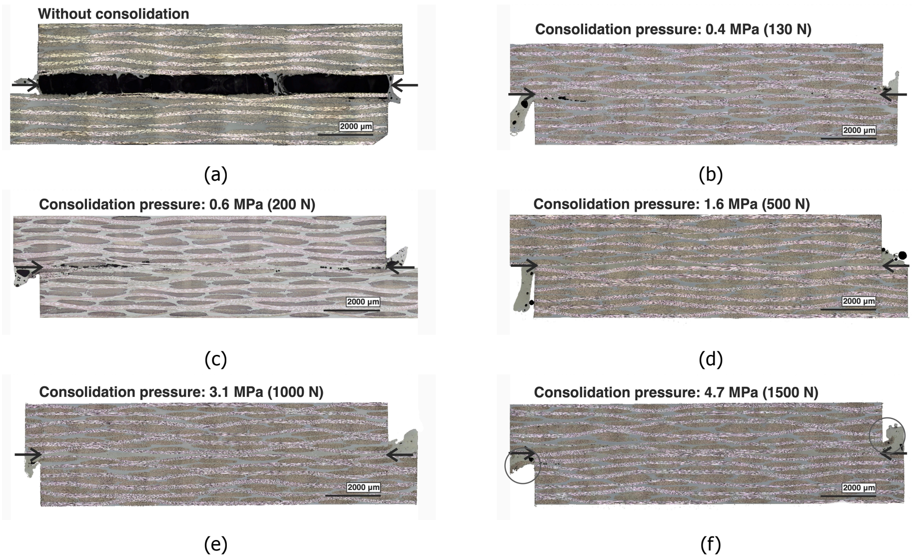

(a) (b) (c) (d) (e) (f)

Figure 4.8: Representative cross-sectional micrographs of static ultrasonic welds consolidated under different pressures. The black arrows indicate the weld lines. The grey circled areas indicate fibre squeeze-out.

4

4.3.2. Effect of consolidation time for the static ultrasonic welding process

Figure 4.9a shows a representative temperature profile of a static ultrasonic weld of both the vibration and consolidation phase. The temperature distribution at the weld interface during the consolidation phase is shown in Figure 4.9b together with the glass transition temperature (T_g, 97 °C) and the melting temperature (T_m, 280 °C) obtained from a DSC test. Figure 4.9c shows the temperature profiles at the hottest TC2 location (Figure 4.5a) for only the consolidation phase of five welds together with the average single-lap shear strength values of welds consolidated for the selected consolidation times. Table 4.2 summarizes the interface temperature until which the welds were consolidated, the average single-lap strength, and when available the volumetric void content for the selected consolidation times. Figure 4.10 and Figure 4.11 shows corresponding representative fracture surfaces and cross-sectional micrographs, respectively, of the welds obtained at different consolidation times.

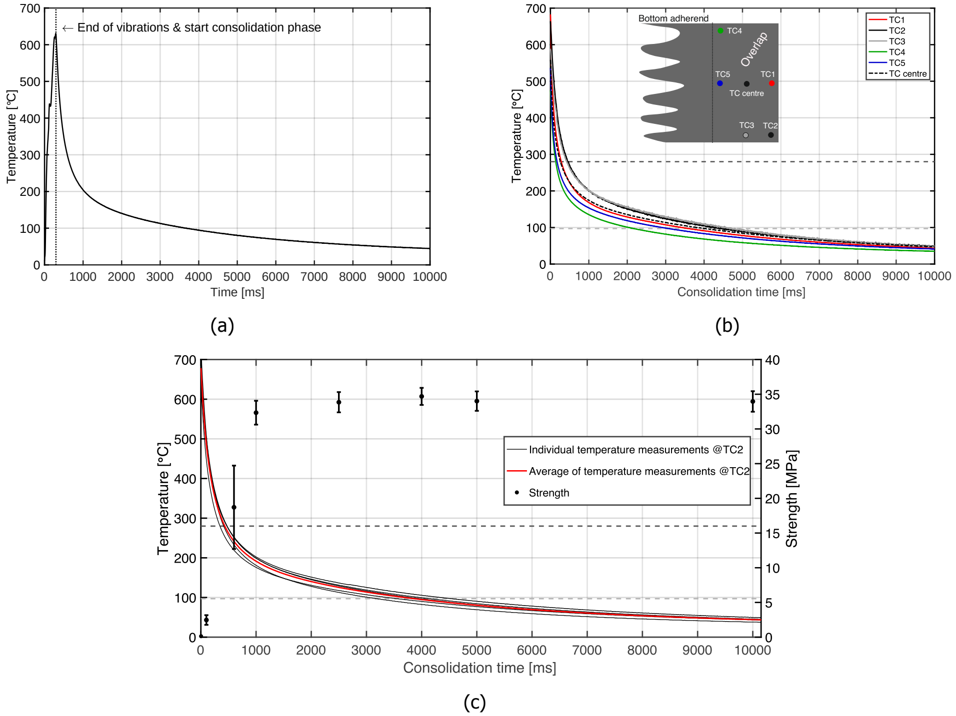

Figure 4.9: Temperature profile(s) for the static welding process for (a) both the vibration and the consolidation phase at TC2 location (Figure 4.5a), and only the consolidation phase (b) at multiple TC locations obtained from 2 welds and (c) at TC2 location for five welds together with their average temperature. Additionally in (c), average lap shear strength values with standard deviation error bars (n=5) are shown for welds consolidated for different consolidation times. Note that for 100 ms n=2 as some samples broke in the clamps before mechanical testing. The dark grey and light grey dashed lines indicate the T_m and T_g, respectively.

Table 4.2: Selected consolidation times, corresponding average interface temperature with standard deviation (n=5) (rounded to nearest integer 5), corresponding single lap shear strength (LSS) with standard deviation shown (n=5), and volumetric void content from static welds.

Consolidation time [ms]	Temperature [$^{\circ}C$]	Explanation	LSS [MPa]	Void content [%]
0	680 ± 45	No consolidation	0.0	NA
100	485 ± 25	Interface above T_m	2.5 ± 0.7	NA
600	240 ± 15	Interface just below T_m	18.7 ± 6.0	0.61
1000	190 ± 10	Interface in the middle of T_m and T_g	32.3 ± 1.7	0.05
2500	125 ± 10	Interface just above T_g	33.9 ± 1.5	NA
4000	95 ± 10	Interface approximately at T_g	34.7 ± 1.2	0.05
5000	80 ± 10	Interface just below T_g	34 ± 1.4	0.07
10000	45 ± 5	Interface well below T_g	34 ± 1.5	0.06

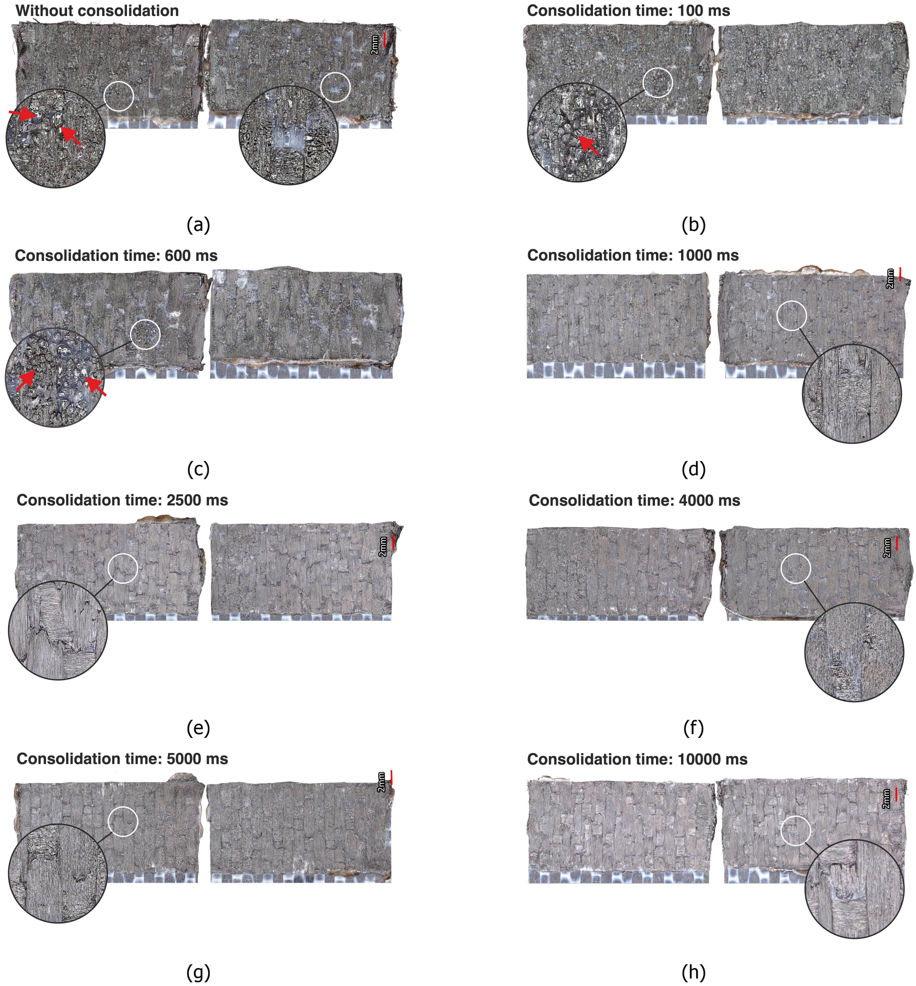

Figure 4.10: Fracture surfaces of mechanically tested static ultrasonic welds consolidated for different consolidation times. The top adherends is shown left, and the bottom adherends is shown right. The white circled areas are enlarged to show details of the fracture surfaces. The red arrows indicate areas containing voids.

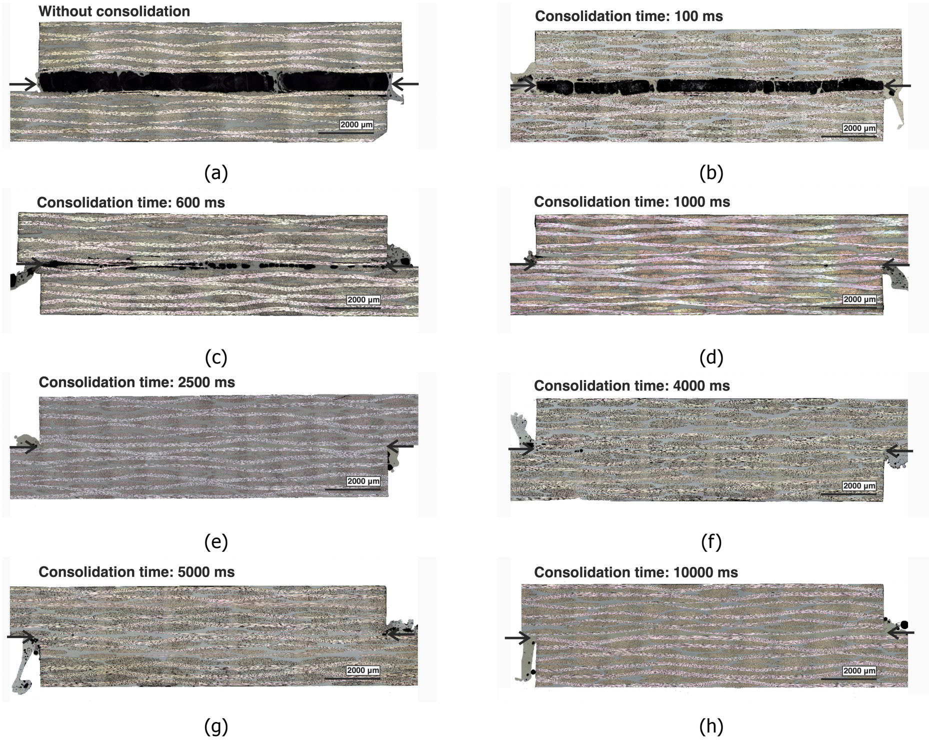

Figure 4.11: Cross-sectional micrographs of static ultrasonic welds consolidated for different consolidation times. The black arrows indicate the weld line.

4.3.3. Consolidation in continuous ultrasonic welding

Figure 4.12 shows the interface temperatures measured at five locations in the overlap during the continuous welding process without the use of the consolidator. The red shaded areas indicate the time span during which a specific thermocouple was located under the sonotrode. The moment the sonotrode completely passed a specific thermocouple was defined as the start of the consolidation phase for that specific thermocouple location. Figure 4.13 shows the superimposed temperature profiles of the consolidation phase for the continuous ultrasonic welding process (Figure 4.13a) without consolidator and (Figures 4.13b, 4.13c, and 4.13d) for consolidation distances 18.4 mm, 63 mm and 86.4 mm, respectively. The grey shaded area indicates the time span during which the consolidator applied the consolidation pressure. The obtained strength and the volumetric void content for these four cases is shown in Table 4.3 and representative fracture surfaces and cross-sectional micrographs are shown in Figure 4.14 and Figure 4.15, respectively.

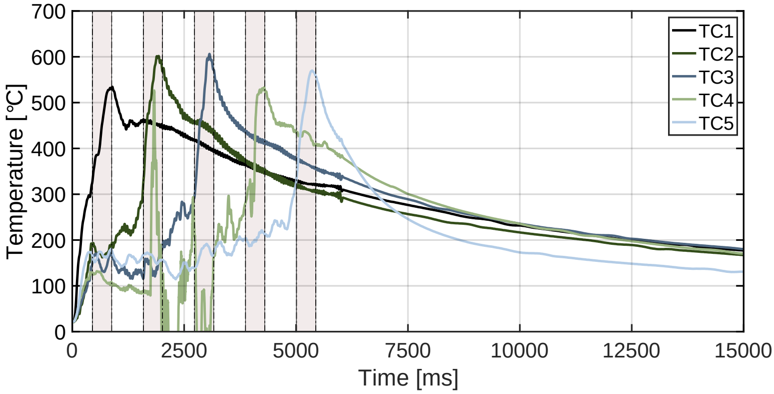

Figure 4.12: Temperature profiles measured by five thermocouples (TC) placed according to Figure 4.5b of a continuous ultrasonic weld without the use of a consolidator. The shaded areas indicate when a particular thermocouple was located under the sonotrode during the welding process.

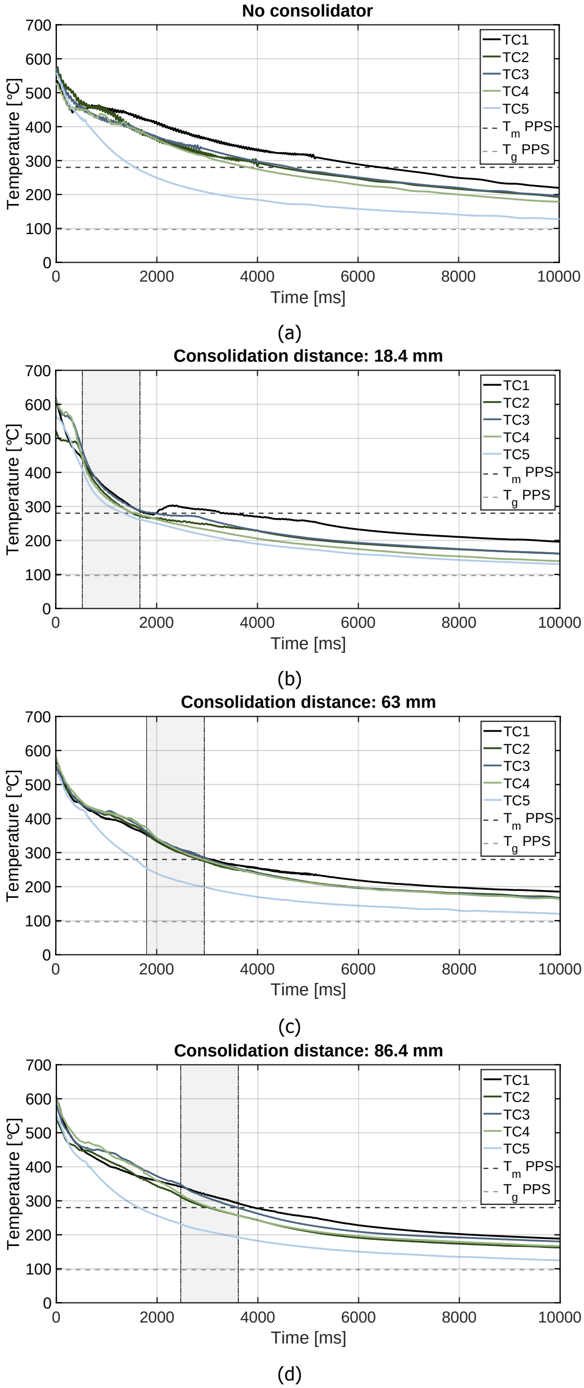

Figure 4.13: Superimposed temperature profiles of the consolidation phase of continuous ultrasonic welds displayed for each thermocouple from the moment the sonotrode passed the individual thermocouple for different consolidation cases: (a) no consolidator, (b, c, and d) with consolidator at a consolidation distance of 18.4 mm, 63.0 mm and 86.4 mm respectively. The grey shaded area indicates the time span during which the consolidator applied the consolidation pressure.

Table 4.3: Average lap shear strength (LSS) with the standard deviation (SD) (n=5), and volumetric void content of continuous welds for different consolidation distances.

Consolidation distance [mm]	**LSS [MPa]**	**Void content [%]**
No consolidator	15.1 ± 2.6	7.80
18.4 mm	9.5 ± 2.9	8.32
63.0 mm	38.6 ± 2.7	N/A
86.4 mm	39.6 ± 2.3	1.01

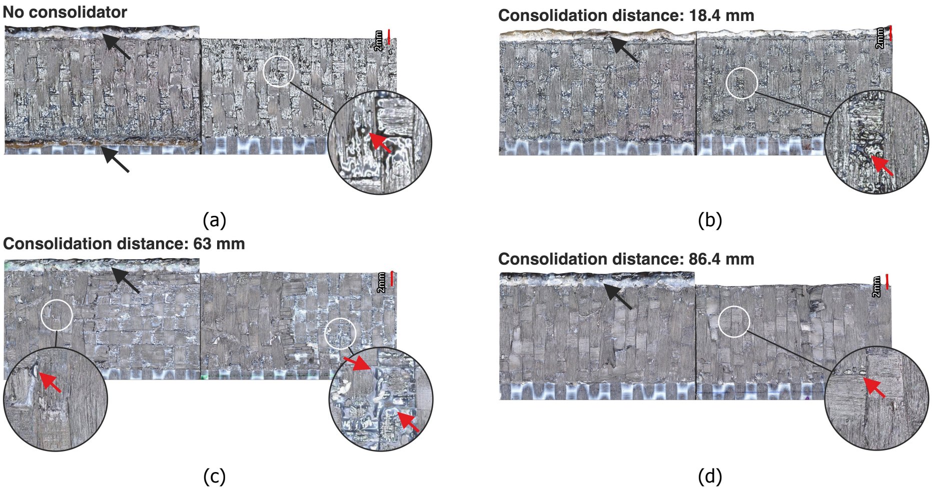

Figure 4.14: Representative fracture surfaces of mechanically tested samples of continuous ultrasonic welds consolidated: (a) without consolidator, and (b, c, and d) for consolidation distances of 18.4 mm, 63 mm and 86.4 mm, respectively. The left samples show the top adherends, and right samples show the bottom adherend. White circled areas are enlarged to show details of the fracture surfaces. The black arrows indicate excessive fibre and resin squeeze out. The red arrows indicate areas with voids.

4.4. Discussion

The aim of this study was to improve the quality of continuous ultrasonically welded joints by adding a consolidator to the welding setup. The lack of a consolidator behind the sonotrode does not allow the continuous joint to cool down under pressure, resulting in a relatively low weld quality characterized by porosity within the weld line and adherends (Figure 4.14a, and 4.15a, and Table 4.3) and low strength (Table 4.3). To determine the required consolidation pressure, the size of the consolidator, and its distance from the sonotrode a stepwise approach was followed. Firstly, the effect of the consolidation pressure on the quality of welds obtained through a static ultrasonic welding process was studied. This was followed by a study on the effect of the consolidation time on the quality of static welds. Finally, the obtained results were used to design a consolidation unit which was further tested in the continuous ultrasonic welding process in order to define the required distance between consolidator and sonotrode.

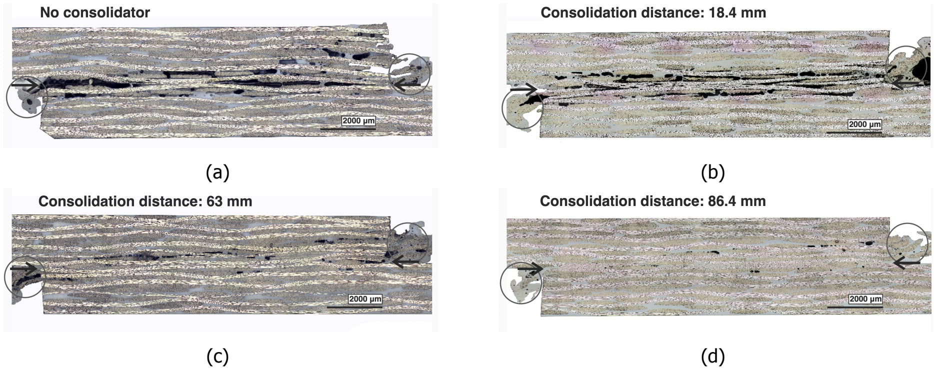

Figure 4.15: Representative cross-sectional micrographs of continuous ultrasonic welds consolidated: (a) without consolidator, and (b, c, and d) for consolidation distances of 18.4 mm, 63 mm and 86.4 mm, respectively. The black arrows indicate the weld line. The grey circles indicate fibre and resin squeeze-out.

Low consolidation pressure values (0.4 MPa and 0.6 MPa) during the static welding process resulted in the presence of voids at the weld line as observed on the fracture surfaces (Figures 4.7b, and 4.7c) and cross sections (Figures 4.8b, and 4.8c). The pressure was most likely not sufficient to eliminate the initial air present within the open areas of the energy director. The resulting voids contributed to the observed reduction in strength at low consolidation pressures (Figure 4.6). For the higher consolidation pressure values (1.6 MPa, 3.1 MPa, and 4.7 MPa), on the other hand, the pressure was sufficient to minimize the number of voids (Figures 4.7d, 4.7e, 4.7f, 4.8d, 4.8e, and 4.8f). Consequently, a higher strength, similar for all these high consolidation pressure values (Figure 4.6), was obtained.

For consolidation times of 1000 ms or longer in the static process a similar high weld quality was obtained in terms of practical absence of voids (Figures 4.10d to 4.10h, 4.11d to 4.11h, and Table 4.2) and high strength (Figure 4.9c). Regarding the temperature evolution within the welding overlap (Figure 4.9b), at 1000 ms consolidation time the temperature was found to be within 200°C and 135°C, with the highest temperatures measured at the longitudinal edge, TC2 location. Temperatures at all locations were found to drop below Tg of the PPS resin only after 5000 ms consolidation time. It is interesting to note that the maximum rate of crystallization of PPS falls within the temperature range measured at 1000 ms consolidation time. Indeed, Chung and Cebe [30] and Furushima et al. [31] reported it to be between 170°C to 190°C and at 160°C, respectively. Consequently, the crystallization of the polymer in the weld line is believed to play an important role in the development of weld strength during consolidation. Note that, despite the high cooling rates in ultrasonic welding, non-negligible crystallinity within the weldline was measured by Koutras et al. [20] when using the same material and similar welding parameters as the present study.

Based on the minimum consolidation pressure and time necessary for high weld quality in the static welding process, the consolidation pressure and length of the consolidator in the continuous process were set at 1.6 MPa and 40 mm, respectively, which corresponds to approximately 1100 ms of consolidation at a welding speed of 35 mm/s. High-quality continuously welded joints with virtually no porosity, and high strength were obtained under such consolidation conditions and the longest distance (86.4 mm) between consolidator and sonotrode (Figure 4.15d and Table 4.3), however some fundamental differences with the static process could be identified. Firstly, the cooling rates were overall lower and hence the temperatures measured at the welding interface just behind the consolidator were around 280°C for all three considered consolidator-sonotrode distances (Figure 4.13). These were well above the 200°C-135°C critical temperature range defined by the static process. The fact that continuous welds with virtually no porosity could be obtained despite the high interface temperatures may be related to the compressive force applied on the welding interface by the clamping jig in the continuous process as opposed to the tensile force caused by the clamping jig in the static process. Secondly, the shortest consolidator-sonotrode distance in the continuous welding process, which among all the cases studied is the one that best approximates the consolidation conditions during the static process, resulted however in the lowest overall weld quality (Figure 4.15b and Table 4.3). Analysis of the state of the material in the area between sonotrode and consolidator with only some voids present (see II in Figure 4.16) suggests that, in that case, the observed porosity (see I in Figure 4.16) was caused by the passing of the consolidator. In particular, the pressure applied by the consolidator caused significant matrix squeeze-out in the areas of the adherends adjacent to the welding interface which, due to the incompressibility of the fibre reinforcement, resulted in the observed porosity (Figure 4.15b). Significant squeeze-out was also observed when the consolidator was located further away from the sonotrode (Figures 4.15c and 4.15d). This, however, caused little (Figure 4.15c) to no porosity (Figure 4.15d) most likely because in those cases the reinforcement fibres were locally squeezed out together with the matrix, and hence the limitation imposed by their incompressibility was removed. Such combined squeeze flow resulted from the lower temperature and hence higher viscosity of the matrix encountered by the consolidator (Figure 4.13). It is interesting to note that none of the static welds investigated in this work displayed the severe porosity in the adherends observed in Figures 4.15a and 4.15b, which suggests that the continuous ultrasonic welding process causes more bulk heating in the adherends than the static process. The significantly slower cooling measured at the welding interface in the continuous process is also consistent with such hypothesis (less efficient heat transfer owing to warmer surroundings). Further research out of the scope of this paper is necessary to understand what causes those important differences.

The strength values measured in the continuous welded joints in the cases in which the consolidator was located 63 mm and 86.4 mm away from the sonotrode were even higher than the strength values measured in the static welded joints. We believe this difference is caused by the reduction of peel stresses at the edges because of both the taper and fillet associated with the matrix and fibre squeeze-out (Figures 4.15c and 4.15d). Additionally, it should be noted that the strength measured in the continuous welds obtained in the absence of consolidator (Table

4.3) was significantly lower than that reported in our previous studies [10, 11]. This difference is attributed to the differences in clamping distance (130 mm vs. 70 mm in previous studies) and the indirect pressure applied by the clamps on the welded overlap.

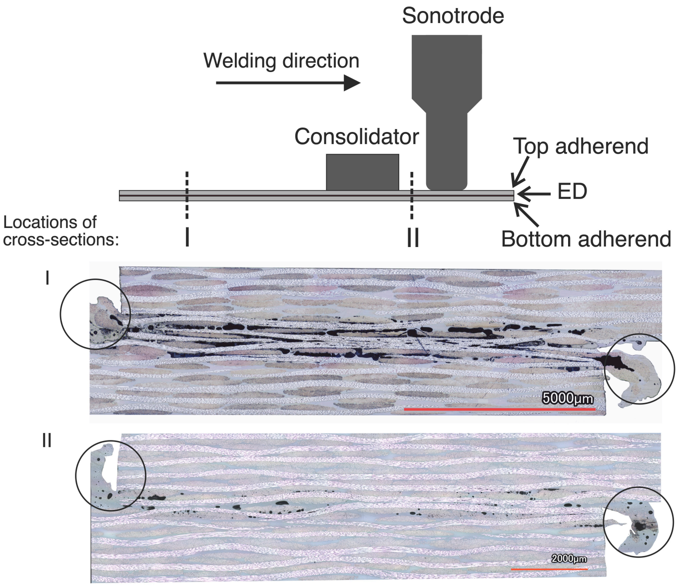

Figure 4.16: Schematic of sonotrode and consolidator placed 18.4 mm from the sonotrode together with indicated locations from where cross-sectional micrographs were taken after the process was stopped in the shown position: after consolidator passed (I) (taken from Figure 4.15b), and in between the sonotrode and consolidator (II). The consolidator was kept on the overlap for 60 s after stopping the welding process.

4.5. Conclusions

The aim of this study was to improve the quality of continuous ultrasonically welded joints by adding a consolidator to the welding setup. To determine the required consolidation pressure, the size of the consolidator, and its distance from the sonotrode a stepwise approach was taken based on the static process. Firstly, the effect of the consolidation pressure on the quality of welds obtained through a static ultrasonic welding process was studied. Low consolidation pressure values (0.4 MPa and 0.6 MPa) resulted in voids and a reduced strength. For pressure values of 1.6 MPa and above a similar high weld quality in terms of reduced presence of voids and strength increase was observed. Secondly, the effect of the consolidation time on the quality of static welds was studied. For consolidation times of 1000 ms or longer a similar high weld quality was observed, which is believed to be related crystallization of the polymer in the weld line. Finally, based on the minimum consolidation pressure and time necessary for high weld quality in the static welding process, the consolidation pressure and length of the consolidator in the continuous process were set at 1.6

MPa and 40 mm, respectively. High-quality continuously welded joints with virtually no porosity and high strength were obtained under such consolidation conditions and the longest distance between consolidator and sonotrode. The closest consolidation distance, best representing the static welding conditions, did not improve the weld quality as porosity was most likely caused by squeeze flow of molten matrix in the adherends by the consolidator. The continuous welding process was found to generate more bulk heating in the adherends than the static process for reasons that are currently unknown and should be investigated in further research.

References

[1] C. Ageorges, L. Ye, and M. Hou, "Advances in fusion bonding techniques for joining thermoplastic matrix composites: A review," *Composites - Part A: Applied Science and Manufacturing*, vol. 32, no. 6, pp. 839–857, 2001.

[2] I. F. Villegas, L. Moser, A. Yousefpour, P. Mitschang, and H. E. Bersee, "Process and performance evaluation of ultrasonic, induction and resistance welding of advanced thermoplastic composites," *Journal of Thermoplastic Composite Materials*, vol. 26, no. 8, pp. 1007–1024, 2013.

[3] H. Potente, "Ultrasonic welding - principles & theory," *Materials & Design*, vol. 5, no. 5, pp. 228 – 234, 1984.

[4] Zongbo Zhang, Xiaodong Wang, Yi Luo, Zhenqiang Zhang, and Liding Wang, "Study on Heating Process of Ultrasonic Welding for Thermoplastics," *Journal of Thermoplastic Composite Materials*, vol. 23, no. 5, pp. 647–664, 2010.

[5] I. F. Villegas, "Ultrasonic welding of thermoplastic composites," *Frontiers in Materials*, vol. 6, p. 291, 2019.

[6] A. Benatar, R. V. Eswaran, and S. K. Nayar, "Ultrasonic welding of thermoplastics in the near-field," *Polymer Engineering & Science*, vol. 29, no. 23, pp. 1689–1698, 1989.

[7] A. Levy, S. Le Corre, and I. Villegas, "Modeling of the heating phenomena in ultrasonic welding of thermoplastic composites with flat energy directors," *Journal of Materials Processing Technology*, vol. 214, no. 7, pp. 1361–1371, 2014.

[8] D. Grewell, A. Benatar, and J. Park, *Plastics and Composites Welding Handbook*. No. 10 in Plastics and composites welding handbook, Hanser Gardener, 2003.

[9] F. Senders, M. van Beurden, G. Palardy, and I. Villegas, "Zero-flow: A novel approach to continuous ultrasonic welding of CF/PPS thermoplastic composite plates," *Advanced Manufacturing: Polymer & Composites Science*, vol. 0340, no. September 2017, pp. 1–10, 2016.

[10] B. Jongbloed, J. Teuwen, G. Palardy, I. F. Villegas, and R. Benedictus, "Continuous ultrasonic welding of thermoplastic composites: Enhancing the weld uniformity by changing the energy director," *Journal of Composite Materials*, vol. 54, no. 15, pp. 2023–2035, 2020.

[11] B. Jongbloed, J. Teuwen, R. Benedictus, and I. F. Villegas, "On differences and similarities between static and continuous ultrasonic welding of thermoplastic composites," *Composites Part B: Engineering*, vol. 203, p. 108466, 2020.

[12] I. Villegas, "In situ monitoring of ultrasonic welding of thermoplastic composites through power and displacement data," *Journal of Thermoplastic Composite Materials*, vol. 28, no. 1, pp. 66–85, 2015.

[13] G. Palardy and I. Villegas, "On the effect of flat energy directors thickness on heat generation during ultrasonic welding of thermoplastic composites," *Composite Interfaces*, vol. 24, no. 2, pp. 203–214, 2017.

[14] I. Villegas, B. Valle Grande, H. Bersee, and R. Benedictus, "A comparative evaluation between flat and traditional energy directors for ultrasonic welding of cf/pps thermoplastic composites," *Composite Interfaces*, vol. 22, no. 8, pp. 717–729, 2015.

[15] I. Villegas, "Strength development versus process data in ultrasonic welding of thermoplastic composites with flat energy directors and its application to the definition of optimum processing parameters," *Composites Part A: Applied Science and Manufacturing*, vol. 65, pp. 27–37, 2014.

[16] T. Zhao, G. Palardy, I. Villegas, C. Rans, M. Martinez, and R. Benedictus, "Mechanical behaviour of thermoplastic composites spot-welded and mechanically fastened joints: A preliminary comparison," *Composites Part B: Engineering*, vol. 112, pp. 224–234, 2017.

[17] I. Villegas and P. Rubio, "On avoiding thermal degradation during welding of high-performance thermoplastic composites to thermoset composites," *Composites Part A: Applied Science and Manufacturing*, vol. 77, no. Supplement C, pp. 172 – 180, 2015.

[18] I. Villegas and H. Bersee, "Ultrasonic welding of advanced thermoplastic composites: An investigation on energy-directing surfaces," *Advances in Polymer Technology*, vol. 29, no. 2, pp. 112–121, 2010.

[19] T. Zhao, C. Broek, G. Palardy, I. Villegas, and R. Benedictus, "Towards robust sequential ultrasonic spot welding of thermoplastic composites: Welding process control strategy for consistent weld quality," *Composites Part A: Applied Science and Manufacturing*, vol. 109, pp. 355–367, 2018.

[20] N. Koutras, J. Amirdine, N. Boyard, I. F. Villegas, and R. Benedictus, "Characterisation of crystallinity at the interface of ultrasonically welded carbon fibre pps joints," *Composites Part A: Applied Science and Manufacturing*, vol. 125, p. 105574, 2019.

[21] W. Tao, X. Su, H. Wang, Z. Zhang, H. Li, and J. Chen, "Influence mechanism of welding time and energy director to the thermoplastic composite joints by ultrasonic welding," *Journal of Manufacturing Processes*, vol. 37, pp. 196–202, 2019.

[22] T. Slange, L. Warnet, W. Grouve, and R. Akkerman, "Deconsolidation of c/peek blanks: on the role of prepreg, blank manufacturing method and conditioning," *Composites Part A: Applied Science and Manufacturing*, vol. 113, pp. 189 – 199, 2018.

[23] H. Shi, I. F. Villegas, and H. E. Bersee, "Analysis of void formation in thermoplastic composites during resistance welding," *Journal of Thermoplastic Composite Materials*, vol. 30, no. 12, pp. 1654–1674, 2017.

[24] L. Ye, M. Lu, and Y.-W. Mai, "Thermal de-consolidation of thermoplastic matrix composites - i. growth of voids," *Composites Science and Technology*, vol. 62, no. 16, pp. 2121 – 2130, 2002.

[25] L. Ye, Z.-R. Chen, M. Lu, and M. Hou, "De-consolidation and re-consolidation in cf/pps thermoplastic matrix composites," *Composites Part A: Applied Science and Manufacturing*, vol. 36, no. 7, pp. 915 – 922, 2005.

[26] R. M. Ogorkiewicz and l. P. D. Imperial Chemical Industries, *Thermoplastics: properties and design.* London: Wiley, 1974.

[27] J. Wolfrath, V. Michaud, and J.-A. Månson, "Deconsolidation in glass mat thermoplastic composites: Analysis of the mechanisms," *Composites Part A: Applied Science and Manufacturing*, vol. 36, no. 12, pp. 1608 – 1616, 2005.

[28] M. Lu, L. Ye, and Y.-W. Mai, "Thermal de-consolidation of thermoplastic matrix composites - ii. "migration" of voids and "re-consolidation"," *Composites Science and Technology*, vol. 64, no. 2, pp. 191 – 202, 2004.

[29] S. Roychowdhury, J. J. W. Gillespie, and S. G. Advani, "Volatile-induced void formation in amorphous thermoplastic polymeric materials: I. modeling and parametric studies," *Journal of Composite Materials*, vol. 35, no. 4, pp. 340–366, 2001.

[30] J. S. Chung and P. Cebe, "Crystallization and melting of cold-crystallized poly(phenylene sulfide)," *Journal of Polymer Science Part B: Polymer Physics*, vol. 30, no. 2, pp. 163–176, 1992.

[31] Y. Furushima, M. Nakada, Y. Yoshida, and K. Okada, "Crystallization/melting kinetics and morphological analysis of polyphenylene sulfide," *Macromolecular Chemistry and Physics*, vol. 219, no. 2, p. 1700481, 2018.

5

A study on through-the-thickness heating in continuous ultrasonic welding of thermoplastic composites

This chapter is based on the journal article: B. Jongbloed, J. Teuwen, R. Benedictus, and I.F. Villegas, *A study on through-the-thickness heating in continuous ultrasonic welding of thermoplastic composites*, Materials **14**, 21 (2021).

5.1. Introduction

Because of their high specific mechanical properties, fibre-reinforced polymer composite materials are interesting for industries in which weight is of utmost importance, such as the aerospace industry. The polymers used as matrix in these composite materials are typically thermoset or thermoplastic. Thermoplastics, in contrast to thermosets, do not form a cross-linked network and they rely on the entanglement of linear polymer chains to form a solid structure. These thermoplastic polymer chains become mobile when heated sufficiently above the melting temperature for semi-crystalline polymers or above the glass transition temperature for amorphous polymers. This allows the use of cost-effective manufacturing and joining processes such as press forming and welding for thermoplastic composite parts and structures.

Ultrasonic welding is a fast and low energy consuming joining technique for thermoplastic composites [1]. During the ultrasonic welding process, a static force and high frequency/low amplitude mechanical vibrations are applied on the parts to be welded by means of a sonotrode (vibration phase of the process). Subsequently, the welded joint is allowed to cool down under pressure (consolidation phase). The vibrations generate heat through surface and viscoelastic friction [2–4]. Heat generation is focused at the weld interface by means of an energy director (ED) placed in between the adherends [3, 5]. This ED consists of either one or more resin protrusions moulded on the surface of one of the adherends [6–8] or a loose resin rich layer such as a film (also referred to as flat ED) [5, 9] or a woven mesh [10, 11] made from the same polymer material as that in the adherends. Due to the lower compressive stiffness of the ED compared to that of the fibre reinforced adherends, the ED undergoes higher cyclic strains and it therefore generates more heat than the adherends [8, 12].

Ultrasonic welding of thermoplastic composites can be performed in either a static or a continuous fashion. During static ultrasonic welding, e.g. spot welding, a relatively small area is welded while both the welder and the adherends remain stationary during the vibration and consolidation phase. Sequential application of this static process allows obtaining multi-spot welded joints [13]. In continuous ultrasonic welding, on the other hand, a relatively large area is welded by continuously translating the welder with respect to the adherends or vice versa while exerting the ultrasonic vibrations and welding pressure [10, 11]. While in static welding the consolidation pressure is applied by the sonotrode itself, an additional consolidation shoe needs to be placed behind the sonotrode in continuous ultrasonic welding [14]. The continuous process has some benefits over the static process, i.e., a higher load can be transferred, and the joint is air and liquid tight, its maturity level is however lower. One of the main lessons learned so far in the development of continuous ultrasonic welding of thermoplastic composites is that the compliance of the energy director plays a more prominent role on ensuring weld uniformity than in the static process [10]. Likewise, heating and melting of the energy director extends beyond the footprint of the sonotrode in the continuous welding process and the temperatures at the welding interface are overall higher [11]. Finally, higher through-the-thickness or bulk heating occurs in continuous ultrasonic welding, especially in the adherend in direct contact with the sonotrode. As shown in Figure 5.1 [14], this leads to significant fibre and resin squeeze out, as well as accompanying porosity, upon application of the consolidation pressure.

Excessive resin and fibre squeeze out is undesirable since it may compromise the structural integrity of the adherends and, hence, of the welded assembly. Consequently, the focus of the present study is gaining a better insight into what causes higher through-the-thickness heating in continuous ultrasonic welding of thermoplastic composites as compared to the static process. To this end, thermocouples were used to measure the temperature evolution within the adherends and at the weld interface for different welding configurations and combinations of welding parameters. The results were compared to temperature measurements from an equivalent static welding process and to the predictions from a simplified numerical heat transfer model. To further understand the through-the-thickness heating, also the total energy input was reduced by either increasing the welding speed or decreasing the vibration amplitude. Additionally, to understand heating ahead of the sonotrode a damping unit was introduced to dampen vibrations travelling downstream. Finally, the effect of the adherend size, i.e. large adherends for the continuous process versus small coupon sized adherends for the static process, on the temperature evolution was studied by means of static welds on different sized adherends.

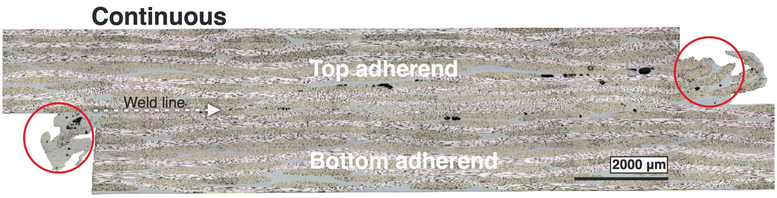

(a)

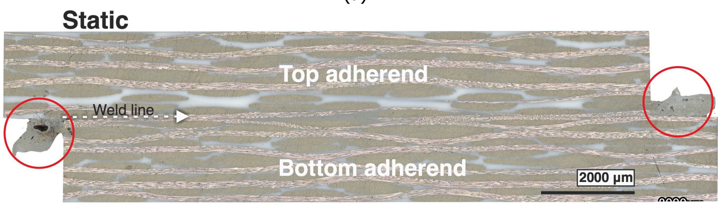

(b)

Figure 5.1: Cross-sectional micrographs of a (a) continuous (adapted from [14]) and a (b) static ultrasonic weld. Welding force 500 N, vibration amplitude 80 µm, welding speed 35 mm/s (a), equivalent vibration time 430 ms (b) [11]. Same clamping jig and clamping configuration in both cases. The red circles indicate squeeze out of fibres and/or resin.

5.2. Experimental procedures

5.2.1. Materials

The thermoplastic composite laminates used for the welding experiments in this study were made out of carbon fibre fabric (five harness satin weave) impregnated with polyphenylene sulphide powder, CF/PPS semipreg (CF 0286 127 Tef4 43% from Toray Advanced Composites, the Netherlands). The laminates were stacked according to a $[0/90]_{3s}$ sequence and subjected to a consolidation process in a hot platen press for 20 min at 320 °C and 1 MPa pressure, which, based on previous experience, results in void-free laminates. The consolidated laminates had a size of 580 mm by 580 mm and a thickness of approximately 1.85 mm. Different size adherends measuring 220 mm x 101.6 mm and 15 mm x 101.6 mm were cut from the consolidated laminates using a water jet cutter. For both adherend sizes the main apparent fibre orientation was in the 101.6 mm direction. A 0.20 mm-thick woven PPS mesh energy director with 37% open area (PPS100, supplied by PVF GmbH, Germany) was used in all experiments to focus heat generation at the welding interface [10, 11].

5.2.2. Continuous ultrasonic welding

The custom-built ultrasonic welding machine shown in Figure 5.2a was used for the continuous ultrasonic welding experiments. It consists of a stiff frame with a X-Y table on a guiding system, an off-the-shelf 20 kHz ultrasonic welder (VE20 SLIMLINE DIALOG 6200, Herrmann Ultrasonics, Germany), and a custom-built consolidation unit. Both the welder and consolidation unit are connected to the stiff frame. A rectangular sonotrode with a 15 mm x 27 mm contact area and a maximum peak-to-peak operational amplitude of 80 μm was used in the welding setup. The consolidation unit consisted of a 1.5 kN servo press kit (YJKP, Festo, The Netherlands), a stabilization guide unit to avoid sideways deflections, and a 40 mm x 30 mm copper block (Figure 5.2b). The consolidation force could be adjusted to a maximum of 1500 N. The distance between the consolidator and the sonotrode was set to 86.4 mm, based on the results of our previous study [14]. During the welding process the adherends were translated with respect to the sonotrode generally following the welding direction I (Figure 5.2b). For some experiments the consolidation unit was used as a damping unit for which it was placed 18.4 mm ahead of the sonotrode (Figure 5.2b) and welding took place in the opposite direction (II). An aluminium base with bar clamps was used to clamp the adherends during the welding process (Figure 5.2b). Figure 5.2c shows the positioning of the bar clamps and of the sonotrode relative to the overlap. Note that this configuration, which we found to provide a more uniform temperature distribution across the overlap [14], differs slightly from the one used in [11]. The different sets of welding parameters used in this study are shown in Table 5.1.

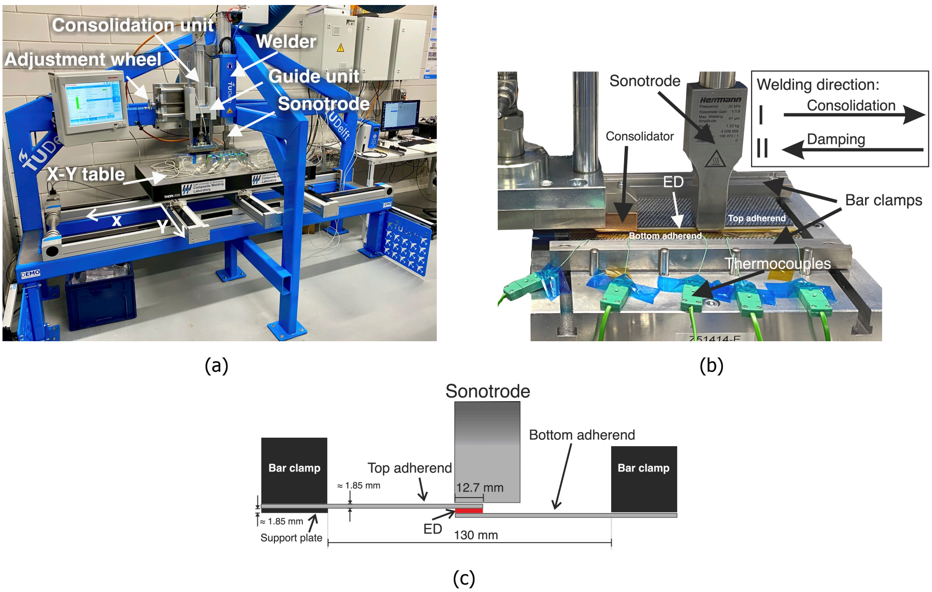

Figure 5.2: (a) Custom-built welding machine for static and continuous ultrasonic welding, (b) close-up of the continuous welding set-up visualising relative sonotrode and consolidator placement, and (c) schematic side-view of clamping distance and sonotrode placement.

Table 5.1: Overview of continuous (CUW) and static (SUW) ultrasonic welding experiments. (Note: the amplitude (amp) values are peak-to-peak.)

Process	Welding parameters (Speed/time, force, amp)	Consolidation parameters	Number of welds	Adherend size [mm]	Config (Figure 5.3)	Remarks
CUW	35 mm/s, 500 N, 80 µm	800 N (1.6 MPa)	1	220 x 101.6	B	Setup with consolidation unit (Figure 5.2b). Reference case.
	35 mm/s, 500 N, 80 µm	800 N (1.6 MPa)	1	220 x 101.6	C	Setup with consolidation unit (Figure 5.2b).
	35 mm/s, 500 N, 80 µm	800 N (1.6 MPa)	3	220 x 101.6	D	Setup with consolidation unit (Figure 5.2b).
	35 mm/s, 500 N, 80 µm	800 N (1.6 MPa)	1	220 x 101.6	B	Setup with consolidation unit as damping unit (Figure 5.2b). Thermocouples were connected in reverse order shown in config B.
	65 mm/s, 500 N, 80 µm	800 N (1.6 MPa)	1	220 x 101.6	B	Setup with consolidation unit (Figure 5.2b). Higher speed case.
	35 mm/s, 500 N, 70 µm	800 N (1.6 MPa)	1	220 x 101.6	B	Setup with consolidation unit (Figure 5.2b). Lower amp case.
SUW	430 ms, 500 N, 80 µm	300 N (1.6 MPa) for 4 s	6	15 x 101.6	E	-
	430 ms, 500 N, 80 µm	300 N (1.6 MPa) for 4 s	3	15 x 101.6	F	-
	430 ms, 500 N, 80 µm	300 N (1.6 MPa) for 4 s	2	220 x 101.6	A	Static weld at TC location

5.2.3. Static ultrasonic welding

The same experimental setup as described in the previous subsection was used for the static welding process (Figure 5.2). In this case, however, the adherends remained stationary and the consolidation unit was not used. The welding parameters used in the static process are shown in Table 5.1. Note that the vibration time used for the static process, 430 ms, is equivalent to 35 mm/s welding speed in a continuous welding process with a 15 mm wide sonotrode. Static welds on the 15 mm-wide adherends covered the entire overlap, whereas in the case of 220 mm-wide adherends, a single 15 mm-wide static weld was created in the middle of the 220 mm-wide overlap. During the static welding process, the vertical position of the sonotrode was monitored at 1 kHz sampling frequency.

5.2.4. Temperature measurements

Temperatures were measured at the welding overlap and within the adherends using K-type thermocouples (GG220-2K-0, product number 2-2200-0004, Tempco B.V., Bodegraven, the Netherlands). The sleeved thermocouples had a total diameter of 0.70 mm, while the diameter of the thermocouple wires was 0.10 mm. An analog thermocouple output amplifier (Adafruit AD8495) was used to simultaneously sample temperature readings at 1 kHz from a maximum of five thermocouples. A moving average filter (10 points for the static process and 25 or 60 points for the continuous process) was applied in MATLAB to filter out high frequency fluctuations from the temperature data. For the temperature measurements at the weld interface, the thermocouples were placed in the middle of the overlap, sandwiched between the bottom adherend and the energy director. For the measurements within the adherends, the thermocouples were inserted into 0.7 mm-diameter holes drilled up to a depth of approximately 7 mm. The placement and depth of each hole ensured that the tip of the thermocouple was located approximately in the middle of the overlap width (directly above or below the thermocouple at the weld interface) and approximately midway through the thickness of the adherend. Note that the diameter of the hole and of the sleeved thermocouple were the same to ensure a press fit. To measure the temperature at the weld interface and through the thickness in the top or bottom adherends different thermocouple configurations shown in Figure 5.3 were used for the static (configurations A, E, and F) and continuous welding process (configurations B, C and D). Table 5.1 shows which of these thermocouple configurations were used in the different experiments.

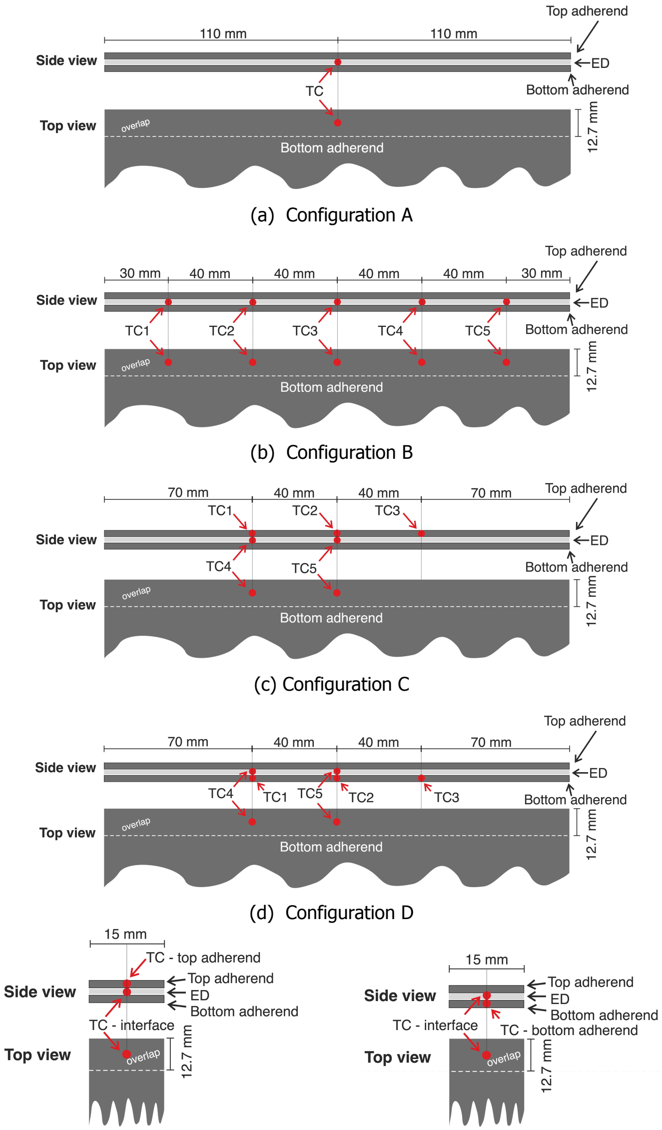

Figure 5.3: Schematic side and top view of the temperature measurement configurations used in this study on 220 mm-wide and 15 mm-wide adherends.

5

5.2.5. Testing and analysis techniques

Whenever necessary, the continuously welded adherends were cut into six 25.4 mm-wide single lap shear samples with a diamond saw of which five were used for mechanical testing. The remaining sample was used for cross-sectional microscopy. The 28.8 mm-wide edges at the start and at the end of the continuous welds were discarded. The single-lap shear samples were mechanically tested with a Zwick/Roell 250 kN universal testing machine with a cross-head speed of 1.3 mm/min. The grips were given the necessary offset to minimize secondary bending. The apparent lap shear strength (LSS) was calculated by dividing the maximum load by the overlap area. After mechanical testing, a non-contact roughness measurement/profiler system (Keyence VR-5000) was used for the analysis of fracture surfaces. To obtain cross-sectional views from the welded adherends, specimens were cut and embedded in epoxy resin. They were ground and polished with a Struers Tegramin-20 polisher. A 3D laser scanning confocal microscope (Keyence VK-X1000) was used for inspecting the cross-sections.

5.2.6. Heat transfer model

A 2D transient heat transfer model representing the static welding process was created in COMSOL Multiphysics 5.5 to estimate the temperature increase in the adherends resulting from only heat conduction from the weld interface in both the static and the continuous process. Since the energy director is very thin compared to the adherends, it was not included in the model. The heat transfer model is based on the following heat transfer equation:

$$\rho C_p \frac{\partial T}{\partial t} = k\nabla^2 T \qquad (5.1)$$

in which T is temperature, t is time, and ρ, C_p, and k are the density, specific heat and thermal conductivity of CF/PPS, respectively.

Figure 5.4 shows the geometry and boundary conditions and Table 5.2 lists the material properties used in the model. The outer boundaries were thermally insulated and the initial temperature of the sonotrode and base was 20°C. The experimental temperature data obtained from measurements at the welding interface was applied as an input to the entire welding interface in the model. The resulting temperature evolution predicted by the model was evaluated midway through the thickness of the top and of the bottom adherends. It should be noted that due to the conservative nature of the boundary conditions (i.e. no heat dissipation to the environment) as well as the room-temperature material properties used for the CF/PPS material, the model most likely provides an overestimation of the heat transferred from the weld interface to the adherends when used to predict the temperature evolution in the static process. When used for the continuous process, however, the following simplifications in the model: (i) the sonotrode is in contact with the top adherend during the entire cooling phase, and (ii) there is no heat flux from downstream and upstream of the sonotrode into the studied area, can be expected to somewhat offset this overestimation.

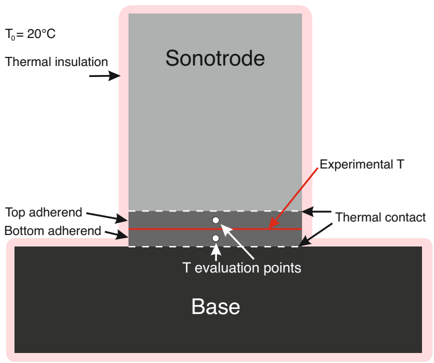

Figure 5.4: Schematic model with boundary conditions for heat transfer model of static welding setup.

Table 5.2: Material properties used for model.

CF/PPS adherends		
Property	**Value**	**Remarks**
Density (ρ)	1540 kg/m^3	Calculated based on weight measurements
Specific heat (C_p)	681 $J/(kg{\cdot}°C)$	Value taken at 20°C [15]
Thermal conductivity (k)	0.34 $W/(m{\cdot}°C)$	Value taken at 20°C [15]
Aluminum base		
Property	**Value**	**Remarks**
Density (ρ)	2665 kg/m^3	From COMSOL material library of aluminum 5083
Specific heat (C_p)	955 $J/(kg{\cdot}°C)$	From COMSOL material library of aluminum 5083 Value shown at 20°C
Thermal conductivity (k)	120 $W/(m{\cdot}°C)$	From COMSOL material library of aluminum 5083 Value shown at 20°C
Steel sonotrode		
Property	**Value**	**Remarks**
Density (ρ)	7860 kg/m^3	From COMSOL material library of steel 1040
Specific heat (C_p)	480 $J/(kg{\cdot}°C)$	From COMSOL material library of steel 1040 Value shown at 20°C
Thermal conductivity (k)	52 $W/(m{\cdot}°C)$	From COMSOL material library of steel 1040 Value shown at 20°C

5

5.3. Results

The temperature evolution at the weld interface for the continuous process is shown in Figure 5.5 for the reference case, higher welding speed case, lower amplitude case, and consolidator as damping case (Figures 5.5a, 5.5b, 5.5c, and 5.5d, respectively). Figure 5.6 shows temperature and vertical sonotrode displacement curves for static welds on (a) 15 mm-wide and (b) 220 mm-wide adherends. Figure 5.7 and Figure 5.8 show the temperature evolution at the weld interface and through the thickness for the (a) top and (b) bottom adherends in the continuous and static process, respectively. It should be noted that some thermocouples malfunctioned during the continuous process (Figures 5.3c and 5.3d): TC2 for all welds and multiple thermocouples in one weld for configuration D (Table 5.1). Therefore, these results have been omitted. The measurements within the top adherend (Figure 5.7a) might be less trustworthy as severe overheating was observed of this adherend at the thermocouple locations and thermocouples TC3 and TC4 partially malfunctioned (as seen by the temperature spikes in Figure 5.7a). Figure 5.9 shows the modelled temperature prediction due to heat transfer to the middle of the adherends for the static welding setup (indicated in Figure 5.4) based on the experimental temperature input at the weld interface from (a) the continuous and (b) the static welding process. It should be noted that for the top adherend in the continuous process no experimental value is shown because, as mentioned before, the top adherend was severely overheated at the thermocouple locations making the results less trustworthy. Figure 5.10 shows cross-sectional micrographs from continuous ultrasonic welds for (a) the higher speed case and (b) the lower amplitude case. Note that for the reference case the cross-section was shown in Figure 5.1a. Representative fracture surfaces from the reference, higher speed, and lower amplitude cases are shown in Figures 5.11a, 5.11b, and 5.11c, respectively. The single lap shear strength values for the continuous and static welds are shown in Table 5.3.

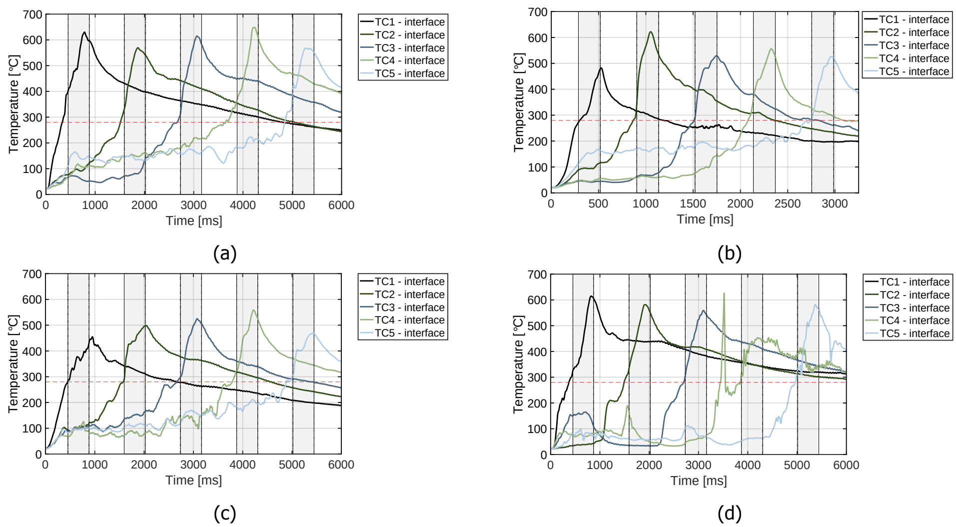

Figure 5.5: Temperature evolution for the continuous welding process at the weld interface for: (a) reference case, (b) higher welding speed case (65 mm/s), (c) lower amplitude case (70 µm), and (d) damping case. TC1 to TC5 were respectively located under the sonotrode during the five grey areas. The red dashed line indicates the melting temperature of PPS (T_m, 280 °C) as experimentally determined by DSC analysis.

Table 5.3: Average lap shear strength (LSS) values with standard deviation for different continuous and static welds.

Process	**Parameters (Speed/time, force, amplitude)**	**LSS [MPa]**	**Remarks**
CUW	35 mm/s, 500 N, 80 µm	39.6 ± 2.3 (n=5)	Reference case. Samples tested from configuration B with consolidation unit (Figure 5.2b).
CUW	35 mm/s, 500 N, 70 µm	37.2 ± 2.5 (n=5)	Lower amplitude case. Samples tested from configuration B with consolidation unit (Figure 5.2b).
CUW	65 mm/s, 500 N, 80 µm	25.0 ± 3.9 (n=5)	Higher speed case. Samples tested from configuration B with consolidation unit (Figure 5.2b).
SUW	440 ms, 500 N, 80 µm	34.3 ± 1.2 (n=4)	Value taken from [11].

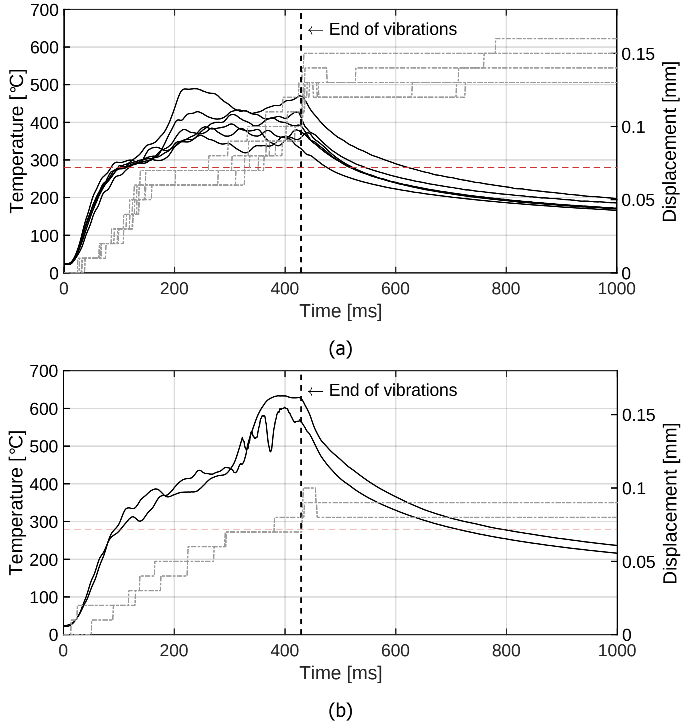

Figure 5.6: Interface temperature (black curves) and measured downward vertical displacement (grey curves) of the sonotrode for static welds on (a) 15 mm-wide and (b) 220 mm-wide adherends. It should be noted that one of the two welds in (b) was made 40 mm to the left from the intended location in Figure 5.3a. The red dashed line indicates the melting temperature of PPS (T_m, 280 °C) as experimentally determined by DSC analysis.

5

5.4. Discussion

The aim of this study was gaining further insight into what causes higher through-the-thickness heating in continuous than in static ultrasonic welding. Through-the-thickness heating combined with the application of the welding/consolidation pressure may cause matrix and fibre squeeze flow as well as porosity in the adherends [14] and hence may affect their structural integrity. Firstly, the heating mechanisms responsible for through-the-thickness heating were investigated by comparing temperature measurements from the static and continuous process to heat transfer model predictions. Secondly, it was studied what causes the temperature differences between the static and continuous process. Finally, the quality of the welds was discussed in view of the temperature evolution.

A plausible cause of higher through-the-thickness heating is the higher overall temperatures at the welding interface (Figure 5.12) resulting in increased thermal conduction to the adherends. The predictions of the heat transfer model (Figure 5.9) show indeed that the higher interface temperatures in the continuous process do result in higher temperature increase caused by conduction in the middle of the

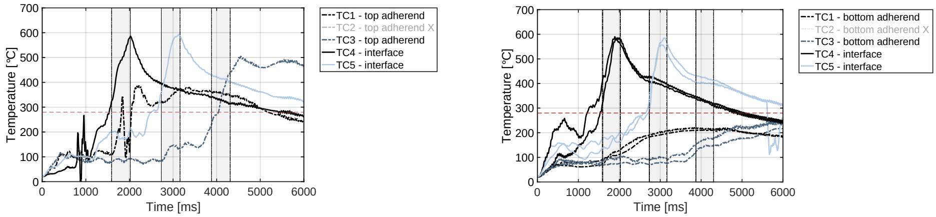

(a) (b)

Figure 5.7: Temperature evolution for the continuous welding process at the weld interface and through the thickness for (a) the top adherend and (b) the bottom adherend. The grey areas indicate the time span during which a specific thermocouple was located under the sonotrode. The red dashed line indicates the melting temperature of PPS (T_m, 280 °C) as experimentally determined by DSC analysis.

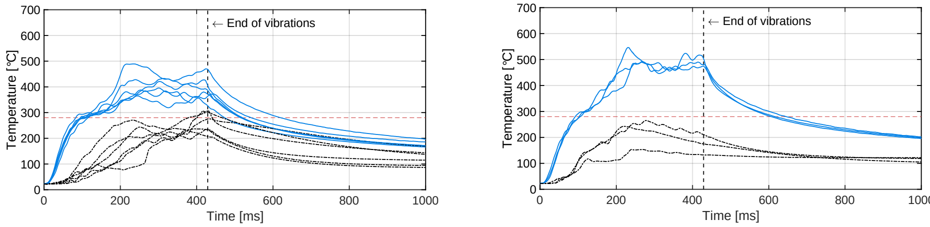

(a) (b)

Figure 5.8: Temperature evolution for the static welding process at the weld interface (blue curves) and through the thickness (black curves) for (a) the top adherend and (b) the bottom adherend. The temperature evolution at the weld interface in (a) is the same as Figure 5.6a. The red dashed line indicates the melting temperature of PPS (T_m, 280 °C) as experimentally determined by DSC analysis.

adherends. However, there are notorious differences between measured and predicted temperature evolutions for the adherends in the static process (Figure 5.9b) and presumably for the top adherend in the continuous process (Figures 5.7a and 5.9a). These differences indicate the existence of an extra heating mechanism responsible for the steep temperature increase of the adherends during the heating phase of the welding process (Figures 5.7a and 5.8) in addition to the relatively gentle temperature increase caused by thermal conduction observed in the model predictions (Figure 5.9), which peaks during the cooling phase. This extra mechanism is bulk viscoelastic heating and its prevalent role in the temperature evolution in the adherends is not surprising since, once compressed, the energy director is very thin ($\approx$ 0.10 mm) and hence it has a low compliance [10] and low ability to concentrate viscoelastic heat generation at the interface only [9].

Contrarily, temperature measurements in the bottom adherend during the continuous process (Figure 5.7b) show trends that are closer to what one could expect from thermal conduction from the interface (Figure 5.9a). This observation, together with the overheating observed at the locations of the thermocouples within the top adherend (Figure 5.7a), prompts us to think that in the continuous process the top adherend absorbs significantly more vibration energy than the bottom adherend. This is contrary to a more balanced energy distribution in the static

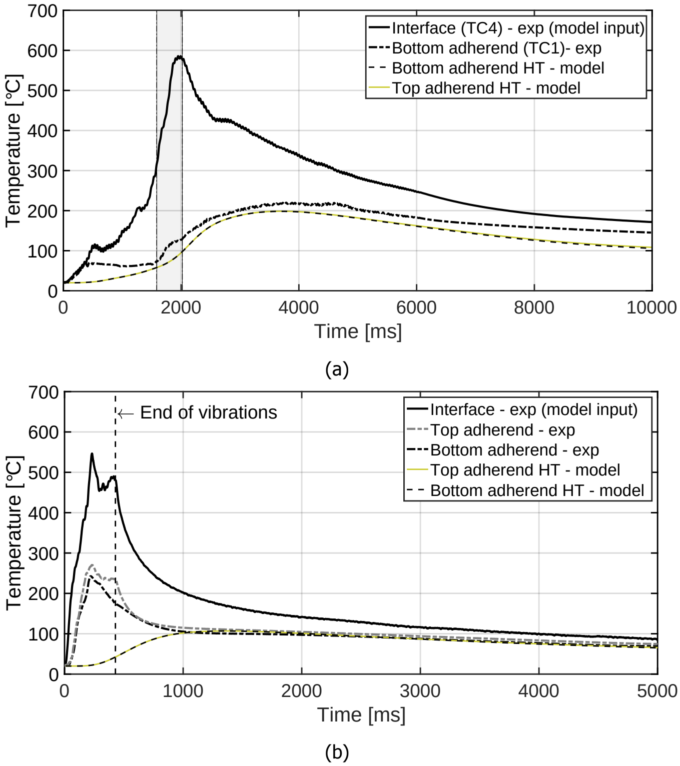

Figure 5.9: Modelled through-the-thickness temperature evolution due to heat transfer (HT) as a result from experimental (exp) temperature input at the weld interface for (a) the continuous and (b) static temperature evolution together with a representative experimental temperature evolution as a reference. The grey area (a) and the vertical line (b) indicate the time span during which the thermocouples were located under the sonotrode. Note that in (a) no experimental temperature evolution for the top adherend is shown as it was deemed less trustworthy due to severe overheating.

process (Figure 5.8). This is consistent with the top adherend experiencing more severe heating than the bottom adherend and than any of the adherends in the static process under equivalent process parameters (Figure 5.1). Reducing the total vibration energy associated to the process, by either increasing the welding speed or decreasing the vibration amplitude, has indeed a substantial effect on reducing through-the-thickness heating and the corresponding matrix and fibre squeeze flow in the top adherend (Figure 5.10) supporting our hypothesis. The cause of uneven distribution of vibration energy between top and bottom adherend in the continuous process is yet unknown. We believe that the translation of the vibrating sonotrode on the surface of the top adherend might cause an extra component of cyclic strains parallel to the welding interface resulting in a superposition of viscoelastic heating sources in that adherend. Further research should however be performed to test this hypothesis.

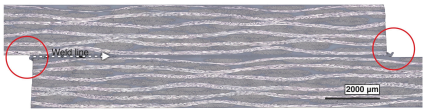

(a) (b)

Figure 5.10: Representative cross-sectional micrographs of continuous ultrasonic welds for (a) higher speed case (65 mm/s), and (b) lower amplitude case (70 µm). Red circles indicate squeeze-out location.

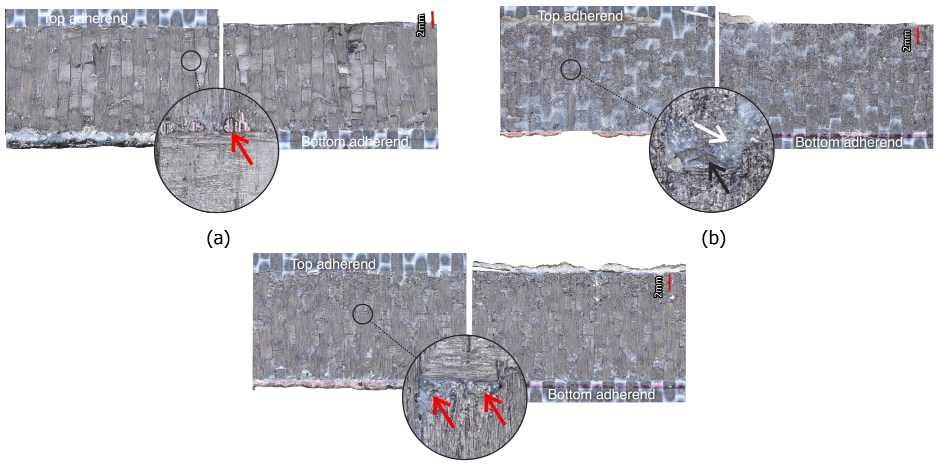

(a) (b)

(c)

Figure 5.11: Representative fracture surfaces from continuous welds for (a) the reference case, (b) higher welding speed case (65 mm/s), and (c) the lower amplitude case. Red arrows indicate voids, white arrow indicates unwelded area together with voids, and black arrow indicates area without connection between top and bottom adherends.

Additionally, given the importance of the temperature evolution at the welding interface in quality of the welded joints, it is important to understand what causes the temperature differences between the continuous and the static process (Figure 5.12) and their relevance in the outcome of the welding process. It should be noted that the temperature differences between the two processes shown in Figure 5.12 are much higher than those reported in our previous work [11]. We believe such seeming inconsistency stems from the different clamping schemes in both studies; in particular differences in the clamping distance, which is known to affect the cycling strains and, hence, heat generation in the energy director [16].

Firstly, the pre-heating experienced by the energy director, which is consistent with previous observation of thermal effects in the energy director downstream of the sonotrode [11], is believed to result from the ultrasonic vibration being transmitted downstream of the sonotrode. Far from the sonotrode, surface friction between thermocouples, energy director and adherends most likely causes the temperature to almost instantaneously increase to around 100°C at the onset of the welding process. Once the sonotrode is close enough for the stiff adherends to exert sufficient

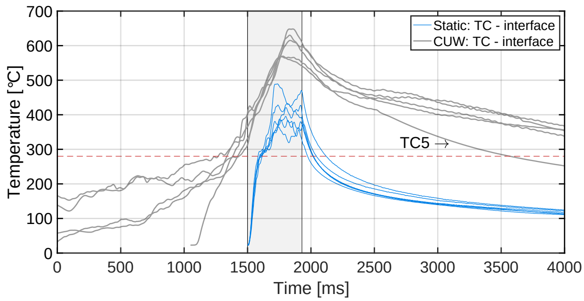

Figure 5.12: Combined interface temperature evolutions of continuous (reference case) (Figure 5.5a) and static (Figure 5.8a) processes superimposed for time that thermocouple experiences vibrations directly under sonotrode. The red dashed line indicates the melting temperature of PPS as experimentally determined by DSC analysis.

5

pressure and, hence, sufficient cyclic strain in the energy director, viscoelastic heating accounts for a faster temperature increase. Indeed, damping of the vibrations beyond the sonotrode effectively minimizes pre-heating far from the sonotrode (Figure 5.13). It does, however, not remove pre-heating as the sonotrode gets closer to the measuring location owing to limitations in the experimental setup (i.e., minimum practical distance between the damping unit and the sonotrode).

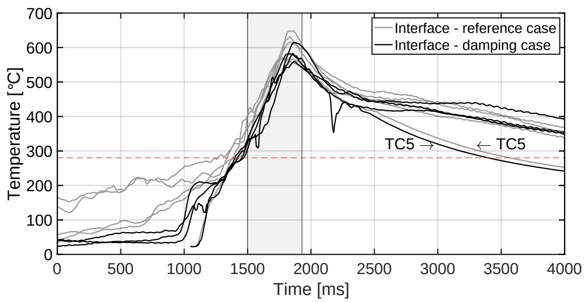

Figure 5.13: Combined interface temperature evolutions of the continuous ultrasonic welding process for reference case (Figure 5.5a) and damping case with the consolidator as damping unit (Figure 5.5d without TC4) superimposed for time that thermocouple experiences vibrations directly under sonotrode (grey area). The red dashed line indicates the melting temperature of PPS as experimentally determined by DSC analysis.

Secondly, the temperature at the interface experiences a continuous increase during the time the sonotrode is moving above a certain location which results in higher maximum temperatures as compared to the static process (Figure 5.12). Based on the results of the static welds on the same adherend size used for the continuous process (Figure 5.6), this continuous temperature increase can be attributed to the limitations imposed by the adherends to the squeeze flow of the energy director (as seen in a lower total displacement) and, consequently, limitations to the associated cooling effect (as seen in the continuous temperature increase) [9].

Thirdly, longer times needed to cool down the interface below T_m are associated to the heat flux originated downstream as the welding process progresses, as indicated by the consistently faster cooling measured by the last thermocouple (TC5) in the weld line (i.e., the one with the lowest influence by downstream heating, Figures 5.12 and 5.13). It is worth noticing that before this effect becomes relevant (i.e., beyond divergence point between thermocouple measurements in Figures 5.12 and 5.13), there is an initial faster cooling stage most likely influenced by the temperature in the composite layers in close proximity to the interface. In fact the process that results in the lowest matrix and fibre squeeze out from the top adherend, i.e., higher speed case, is the one showing a significantly higher cooling rate in that initial stage (Figure 5.14a).

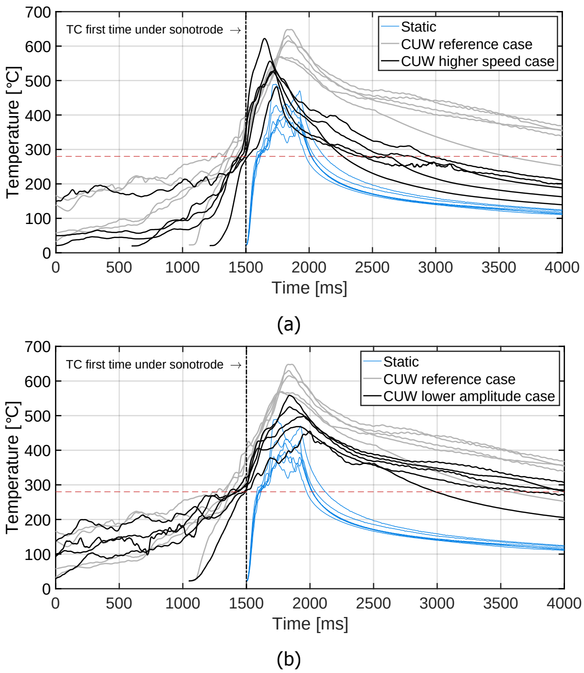

Figure 5.14: Combined interface temperature evolutions of the reference case (Figure 5.5a) of the continuous process, the static process (Figure 5.8a), and the temperature evolutions for (a) the higher welding speed case (65 mm/s) (Figure 5.5b), and (b) the lower amplitude case (70 µm) (Figure 5.5c). The temperature evolutions were superimposed at the moment they were under the sonotrode for the first time. The red dashed line indicates the melting temperature of PPS as experimentally determined by DSC analysis.

Finally, regarding the quality of the welds, it is interesting to note that in those cases in which the strength of continuously welded joints is comparable (or higher) to that of the static welds (i.e., reference and lower amplitude case, see Table 5.3), the average area delimited by the temperature curves and the melting temperature of PPS (presumably related to the actual thermal energy invested in the creation of the welded joints) is much higher than that in the static process (Figures 5.12 and

5.14b). Interestingly, in the case in which both areas are closer to each other (i.e., higher speed case, Figure 5.14a) the strength of continuous joints is significantly lower in accordance with the presence of unwelded areas on the fracture surfaces (Figure 5.11b). These observations, which indicate that in the continuous process the thermal energy input required to create a weld is higher than in the static process, relate to the lower temperature in the bottom adherend (as discussed previously) hindering the creation of the welded joint.

5.5. Conclusions

The aim of this study was to gain further insight into what causes higher through-the-thickness heating in continuous ultrasonic welding of thermoplastic composites as compared to the static process. In the continuous process, temperatures at the welding interface were indeed found to be significantly higher than in the static process. This was attributed to a combination of pre-heating of the energy director due to the vibrations being transmitted downstream of the sonotrode, reduced squeeze-flow of energy director due to the larger adherend size, and heat flux originating downstream as the welding process continues. Thermal conduction from the hotter interface was however found to not be the main cause of higher through-the-thickness heating in the top adherend, which was in turn attributed to viscoelastic bulk heat generation. The top adherend seemed to indeed absorb most of the vibrational energy in the continuous process as opposed to a more balanced energy share between top and bottom adherend in the static process. On the contrary, the bottom adherend showed a temperature evolution similar to what could be expected from predominant thermal conduction from the welding interface. Consequently, reducing the total vibration energy introduced in the material in the continuous welding process proved to have a substantial effect on reducing through-the-thickness heating leading to continuous ultrasonic welds with no matrix and fibre squeeze flow in the top adherend.

5

References

[1] I. F. Villegas, L. Moser, A. Yousefpour, P. Mitschang, and H. E. Bersee, "Process and performance evaluation of ultrasonic, induction and resistance welding of advanced thermoplastic composites," *Journal of Thermoplastic Composite Materials*, vol. 26, no. 8, pp. 1007–1024, 2013.

[2] Zongbo Zhang, Xiaodong Wang, Yi Luo, Zhenqiang Zhang, and Liding Wang, "Study on Heating Process of Ultrasonic Welding for Thermoplastics," *Journal of Thermoplastic Composite Materials*, vol. 23, no. 5, pp. 647–664, 2010.

[3] A. Benatar and T. Gutowski, "Ultrasonic welding of PEEK graphite APC-2 composites," *Polymer Engineering & Science*, vol. 29, no. 23, pp. 1705–1721, 1989.

[4] M. Tolunay, P. Dawson, and K. Wang, "Heating and bonding mechanisms in

ultrasonic welding of thermoplastics," *Polymer Engineering & Science*, vol. 23, no. 13, pp. 726–733, 1983.

[5] I. F. Villegas, "In situ monitoring of ultrasonic welding of thermoplastic composites through power and displacement data," *Journal of Thermoplastic Composite Materials*, vol. 28, no. 1, pp. 66–85, 2015.

[6] I. Villegas, B. Valle Grande, H. Bersee, and R. Benedictus, "A comparative evaluation between flat and traditional energy directors for ultrasonic welding of cf/pps thermoplastic composites," *Composite Interfaces*, vol. 22, no. 8, pp. 717–729, 2015.

[7] I. Villegas and G. Palardy, "Ultrasonic welding of cf/pps composites with integrated triangular energy directors: melting, flow and weld strength development," *Composite Interfaces*, vol. 24, no. 5, pp. 515–528, 2017.

[8] A. Benatar, R. V. Eswaran, and S. K. Nayar, "Ultrasonic welding of thermoplastics in the near-field," *Polymer Engineering & Science*, vol. 29, no. 23, pp. 1689–1698, 1989.

[9] G. Palardy and I. Villegas, "On the effect of flat energy directors thickness on heat generation during ultrasonic welding of thermoplastic composites," *Composite Interfaces*, vol. 24, no. 2, pp. 203–214, 2017.

[10] B. Jongbloed, J. Teuwen, G. Palardy, I. F. Villegas, and R. Benedictus, "Continuous ultrasonic welding of thermoplastic composites: Enhancing the weld uniformity by changing the energy director," *Journal of Composite Materials*, 2019.

[11] B. Jongbloed, J. Teuwen, R. Benedictus, and I. F. Villegas, "On differences and similarities between static and continuous ultrasonic welding of thermoplastic composites," *Composites Part B: Engineering*, vol. 203, p. 108466, 2020.

[12] A. Levy, S. Le Corre, and I. Villegas, "Modeling of the heating phenomena in ultrasonic welding of thermoplastic composites with flat energy directors," *Journal of Materials Processing Technology*, vol. 214, no. 7, pp. 1361–1371, 2014.

[13] T. Zhao, C. Broek, G. Palardy, I. Villegas, and R. Benedictus, "Towards robust sequential ultrasonic spot welding of thermoplastic composites: Welding process control strategy for consistent weld quality," *Composites Part A: Applied Science and Manufacturing*, vol. 109, pp. 355–367, 2018.

[14] B. C. P. Jongbloed, R. Vinod, J. J. E. Teuwen, R. Benedictus, and I. F. Villegas, "(de)consolidation in ultrasonic welding of thermoplastic composites," *Under peer review at Composites Part A: Applied Science and Manufacturing*, 2021.

[15] I. F. Villegas and J. V. Bramon, *World Class Composite Solutions, TUDelft Work Package 3 Technical Report*. Aerospace Structures and Materials, faculty of

aerospace engineering, Delft University of Technology: Delft, the Netherlands, May 2018.

[16] C. B. G. Brito, J. Teuwen, C. A. Dransfeld, and I. F. Villegas, "The effects of misaligned adherends on static ultrasonic welding of thermoplastic composites," *Under peer review at Composites Part A: Applied Science and Manufacturing*, 2021.

6

Conclusions and recommendation

6.1. Overview of research

As stated in Chapter 1, the main objective of this research was to acquire a deeper understanding of the continuous ultrasonic welding process of thermoplastic composites to promote its development for future industrial applications. As mentioned in Section 1.4, the weld quality of the state-of-the-art continuous welds [1] was significantly lower than the weld quality obtained for the static process [2, 3]. Therefore, to meet the objective the following research question was proposed: How can high-quality continuous ultrasonic welds be obtained for thermoplastic composites? 'High-quality' in this research was defined as follows: an uniformly welded interface (e.g. no unwelded or overwelded areas), single-lap shear strength values similar to that of joints obtained with the static ultrasonic welding process for optimum welding parameters for the same material (i.e. approximately 37 MPa [2, 3]), and the lowest possible porosity. To find an answer to the aforementioned research question the following research areas were defined and studied:

- Investigate whether increasing the energy director compliance would improve the weld uniformity.
- Identifying and understanding differences and similarities between the static and the continuous welding processes to identify how to benefit from the existing knowledge in static welding to boost the development of the continuous process.
- Investigate how the quality of continuous ultrasonically welded joints can be improved by adding a consolidation shoe (referred to as consolidator) to the welding setup.

- Gaining insight into what causes higher through-the-thickness heating in continuous ultrasonic welding as compared to the static process.

To address these research areas, a mostly experimental approach was taken throughout different investigations. Continuous and static ultrasonic welding experiments were conducted for various welding parameters and configurations. The quality of the welded joints was mostly evaluated by means of single-lap shear testing, observations of the welded adherends and fracture surfaces, and microscopy of the fracture surfaces and cross-sections. To better understand the heating and cooling phase, temperature measurements were performed by means of thermocouples at the welding interface and within the adherends. Additionally, results from a simplified heat transfer model were compared to temperature measurements (Chapter 5) to understand the role of heat transfer on the heating of the adherends.

To conclude the work performed in this dissertation, Section 6.2 addresses the main research question based on the above-mentioned research areas and summarises and discusses the main findings. The final conclusion of this dissertation is presented in Section 6.3. Finally, recommendations are given in Section 6.4 to further boost the development of continuous ultrasonic welding for future industrial applications.

6.2. Summary of conclusions

The investigation on whether increasing the energy director compliance would improve the weld uniformity in continuous ultrasonic welding was presented in Chapter 2. The previously used thin film energy director resulted in a continuous seam characterized by many unwelded areas and numerous voids could be identified on the welding interface. The presence of unwelded areas is an indication of insufficient heat generation at those locations to melt the energy director. It was expected that a more compliant energy director would heat up more efficiently and as such result in a more uniform weld. Considering that the same material will be used for the energy director as was used for the matrix of the composite, the compliance of the energy director can be increased significantly by simultaneously increasing the thickness and creating open areas. Consequently, a woven polymer mesh energy director was introduced and compared to the current state-of-the-art thin film energy director. It was found that the mesh energy director significantly improved the weld uniformity and single-lap shear strength compared to the thin film energy director. An average lap shear strength of 33.7 ± 2.4 MPa was obtained for the mesh energy director, compared to 18.8 ± 6.2 MPa for the thin film energy director. However, the joint still contained a significant number of voids and the strength was still lower compared to what was observed in literature [2, 3] for static welds. To understand how the behaviour of the mesh improved the weld quality during the welding process compared to the thin film energy director, the static welding process was utilized. This made it possible to evaluate the welding process for both energy directors at different welding stages. The filament crossings of the mesh energy director, uniformly present all over the joint, directly come in contact with the adherends from the start of the welding process. The filaments flatten early in the process and the contact between the mesh and the adherends gradually improves during the welding process by deforming the filaments and filling up the open areas within the mesh. This resulted in full contact between the energy director and the adherends, ensuring a more uniform heat generation and the wetting of the welding interface. For the thin film energy director, on the other hand, no flattening takes place during the welding process, the absence of downward sonotrode displacement prevents improvement in contact and wetting during the vibration phase. Since the mesh energy director improved the quality of continuous ultrasonically welded joints significantly, it is expected that energy directors in the form of polymer meshes will play an important role in the future for continuous ultrasonic welding of thermoplastic composites.

In Chapter 3, differences and similarities between the static and continuous welding processes were identified to understand whether the continuous process can benefit from the available knowledge on the static process. The two processes were experimentally compared for three combinations of welding force and vibration amplitude (500 N & 80 μm, 1500 N & 80 μm, and 500 N & 60 μm) with respect to the melting of the interface, the required areal energy density and consumed power, the temperature at the welding interface, the optimum welding conditions and the corresponding single-lap shear strength values. For the continuous process there was a constant simultaneous existence of different phases the material goes through at the welding interface. In the static process, on the other hand, the material sequentially underwent all phases of the welding process. The morphology of the power curves was similar for both static and continuous processes. Both featuring a rapid increase at the beginning followed by fluctuation around a certain value. However, the overall dissipated power for the continuous process was significantly higher. This was most likely caused by the larger adherend size in the continuous process as it is known that the ultrasonic power or energy is not only invested in creating the weld but also dissipates to the surroundings. The dissipation of energy to the surroundings during the continuous process was substantiated by the temperatures measured at each thermocouple location: the temperature started to ramp up before the sonotrode arrived at that specific location. Therefore, the effective area undergoing the different stages of the welding process can be said to be bigger than the actual imprint of the sonotrode, which results in higher power needs. An interesting finding is that the optimum vibration times and welding speeds (i.e. conditions that result in the highest singe-lap shear strength) in both processes were similar for the three combinations of welding force and vibration amplitude, indicating that the kinetics of the melting process are not sensitive to whether the process was performed in a static or continuous manner. This similarity has the potential to significantly reduce the labour and material effort invested in defining optimum welding conditions in continuous ultrasonic welding by making use of the relatively simple and efficient methods available in literature to define the optimum vibration time in the static process. Further work is however needed to identify the sensitivity of this conclusion to changes in, for instance, the nature of the composite material being welded and the clamping conditions. Despite the observed similar-

6

ity between the optimum vibrations times and welding speeds for both processes, the weld quality of the continuous welded joints was significantly lower than the weld quality of the statically welded joints. For the continuous welded joints significantly lower single-lap shear strength values were measured. This was attributed to the presence of voids at the continuously welded interface caused by a lack of consolidation during cooling.

To improve the weld quality of the continuous ultrasonically welded joints a consolidator was introduced to the welding setup in Chapter 4. The results in this chapter confirmed that without a consolidator behind the sonotrode a relatively low weld quality is observed characterized by porosity and a lower strength. To determine the required consolidation pressure, the size of the consolidator, and its distance from the sonotrode a stepwise approach was taken based on the static process. Firstly, the effect of the consolidation pressure on the quality of static welds was studied. Low consolidation pressure values (0.4 MPa and 0.6 MPa) resulted in voids at the welding interface and a reduced strength. The pressure was most likely not sufficient to eliminate the initial air present within the mesh. For pressure values of 1.6 MPa, 3.1 MPa and 4.7 MPa a similar high weld quality in terms of reduced presence of voids and strength increase was observed. Afterwards, the effect of the consolidation time on the quality of static welds was studied. For consolidation times of 1000 ms or longer a similar high weld quality was observed. At 1000 ms consolidation time the temperature distribution over the welding overlap was found to be between 200°C and 135°C, which is the temperature range in which the maximum rate of crystallization was observed in literature [4, 5]. Consequently, crystallization of the polymer in the weld line is believed to play an important role in the development of weld strength during consolidation. Finally, based on the minimum consolidation pressure and time necessary for high weld quality in the static welding process, the consolidation pressure and length of the consolidator in the continuous process were set at 1.6 MPa and 40 mm, respectively. High-quality continuously welded joints with virtually no porosity and high strength were obtained under such consolidation conditions and the longest distance (86.4 mm) between consolidator and sonotrode. The closest consolidation distance, best representing the static welding conditions, did however not improve the weld quality as porosity seems to be caused by squeeze flow of molten matrix in the adherends by the consolidator. For all consolidation distances (18.4 mm, 63 mm, and 86.4 mm), the cooling rates were overall lower compared to the static welding process, and after the passing of the consolidator the interface temperatures were above the defined critical temperature range (200°C and 135°C). The fact that still high-quality continuous joints were obtained for the longest consolidation distance (86.4 mm) despite the high interface temperatures may be related to the compressive force applied on the welding interface by the clamping jig in the continuous process. The squeeze-out of the matrix and the reinforcement fibres under the pressure from the consolidator indicate that in the continuous process more bulk heating in the adherends takes place compared to the static process. This squeeze out reduces the quality of the welds as it affects the structural integrity of the adherends and should therefore be avoided.

The aim of the study performed in Chapter 5 was to gain insight into what causes higher through-the-thickness heating in the top adherend in continuous ultrasonic welding as described in the previous paragraph. Thermocouples were used to measure the temperature evolution within the adherends and at the weld interface for different welding configurations and combinations of welding parameters. The results were compared to temperature measurements from an equivalent static welding process and to the predictions from a simplified numerical heat transfer model. The observed higher temperatures at the welding interface in continuous ultrasonic welding were attributed to pre-heating of the energy director due to the vibrations being transmitted downstream of the sonotrode, to reduced squeeze-flow of energy director due to the larger adherend size, and to and to heat flux originating downstream as the welding process continues. The predictions from the heat transfer model showed that the higher interface temperatures observed for the continuous process result in higher temperatures through the thickness of the adherends. The comparison of the temperature measurements and the model predictions in the static process indicates that viscoelastic heating plays a prevalent role in the steep increase of the temperatures measured within the top and bottom adherends. The temperature measurements in the bottom adherend during the continuous process show trends closer to what could be expected from heat conduction from the interface. This observation together with overheating/malfunctioning of the thermocouples within the top adherend, makes it highly plausible that in the continuous process the top adherend absorbs significantly more vibration energy compared to the bottom adherend. Consequently, the top adherend experiences more severe heating than the bottom adherend due to viscoelastic bulk heat generation. Finally, the integrity of the adherends could be significantly improved with regard to preventing fibre and resin squeeze-out by reducing the total vibration energy by either increasing the welding speed or decreasing the vibration amplitude. Especially, when decreasing the vibration amplitude a high strength weld (37.2 MPa) was obtained with almost no fibre reinforcement or matrix squeezed out from the adherends.

6.3. Final conclusion

At the starting point of the research conducted in this dissertation the knowledge available on continuous ultrasonic welding of thermoplastic composites was very limited and the weld quality of the continuous joints was much lower compared to the static counterpart. Therefore the main objective was to acquire a deeper understanding of the continuous ultrasonic welding process of thermoplastic composites to promote its development for future industrial applications, and the encompassing question to be answered was: how can high-quality continuous ultrasonic welds be obtained for thermoplastic composites?

The findings in this dissertation showed that it is possible to obtain a high weld quality for the continuous welding process. Firstly, it was found that focusing the heat generation at the weld interface during the heating phase is key in obtaining a uniform weld. This can be done by utilizing a compliant energy director, e.g. a woven polymer mesh, that heats up efficiently. A thin film energy director with a relatively low compliance, on the other hand, results in unwelded areas and thus a non-uniform weld. Secondly, a combination of welding force, vibration amplitude, and welding speed needs to be chosen so that a fully welded overlap is reached without unwelded or overwelded areas at the weld interface. Thirdly, the weld needs to be consolidated after the heating phase. This is done by placing a consolidator behind the sonotrode that applies a consolidation pressure. Without the use this additional consolidation step, voids remain at the weld interface and within the adherends, and a significantly lower strength is obtained. By implementing this consolidation step, the number of voids is minimized and the single-lap shear strength becomes similar to statically welded joints as observed in literature [2, 3]. Finally, it is important to prevent the negative effects associated with through-the-thickness heating, i.e. resin and fibre squeeze out and the related porosity, in especially the top adherend. The top adherend absorbs a larger portion of the vibration energy compared to the bottom adherend and thus more viscoelastic heat generation takes place in the top adherend that potentially leads to fibre and resin squeeze out. This resin and fibre squeeze out can be mitigated by either increasing the welding speed or reducing the vibration amplitude.

6.4. Recommendations

Before continuous ultrasonic welding of thermoplastic composites can be be applied for the aerospace industry still some important steps need to be taken. This section envisions some topics that require a deeper understanding before the process can be applied industrially.

6.4.1. Effect of materials on the welding process

For the research conducted in this dissertation, laminates made from CF/PPS fabric plies were used for all experiments. It can, however, be expected that the fibre type (e.g. carbon or glass), fibre architecture and orientation have a significant effect on the welding process. These fibre related features influence not only the stiffness of the adherends and through this also the viscoelastic heat generation, but also the heat transfer characteristics of the adherends. In Chapter 5 it has been shown that viscoelastic heating plays a dominant role in the heating of the top adherend, while heat transfer is prevalent for the bottom adherend. It has been shown by Köhler et al. [6] that the fibre orientation of the unidirectional plies at the weld interface significantly influences the weld quality in terms of weld uniformity for the static welding process. They stated that the fibre orientation has a significant influence on heat conduction outside the weld zone. For the continuous process the influence of the fibre orientation might be magnified compared to the static process as the larger adhered size also allows upstream and downstream heat transfer. To utilize the continuous ultrasonic welding process for many different thermoplastic composite materials, it is important to understand the effect of fibre and matrix type, fibre architecture and fibre orientation on the welding process in terms of heat generation and heat transfer. A potential method could be to make an extensive multi-physics model that can be adjusted and validated for different fibre/matrix types, fibre architectures and orientations.

As seen in Chapter 2 the energy director type has a significant influence on the weld quality. From Chapter 3 onwards the same mesh energy director was used for all experiments, however a thick energy director might also result in high-quality welds, and the added benefit would be that a thick film is significantly less costly compared to a woven polymer mesh. Therefore, it is worthwhile to investigate the use of a thick film in continuous ultrasonic welding and potentially perform an optimization study for its thickness. Additionally, it might be interesting to investigate continuous ultrasonic welding with integrated energy directors, i.e. ridges moulded on top of the adherends. This might be beneficial for industrial processes as no additional step of placing the energy director would be required anymore. Besides, the integrated energy director might serve as an alignment guide for the adherends.

6.4.2. Effect of a robotic system on the welding process

For large scale industrial continuous ultrasonic welding, it will be necessary to automate the welding process and use either gantry systems or multi-axis robotic systems. These systems will not be as stiff compared to the experimental laboratory setup used in Chapters 2 to 5, as a result the more flexible gantry or robotic system might deflect under the static and dynamic loading during the welding process. These deflections might cause the sonotrode to deviate from its perpendicular orientation with respect to the adherends, which might result in non-uniformly welded areas. Brito et al. [7] demonstrated that the misalignment of the top adherend with the respect to the sonotrode negatively impacts the weld uniformity. It should be investigated how to mitigate the effect of these potential deflections by for instance actively controlling the orientation of the sonotrode and potentially designing the joint as such that it would be less sensitive to small sonotrode misalignments by perhaps using a more compliant energy director.

6

6.4.3. In situ monitoring of the process

From the results presented in Chapter 3 it becomes clear that it is not possible to use the in situ measured vertical sonotrode displacement or consumed power to monitor the weld quality or even control the continuous ultrasonic welding process. Where for the static process the weld quality could be linked to the vertical sonotrode displacement [8], for the continuous process this measured displacement only occurs once at the start of the welding process and afterwards changes based on material thickness variations and the alignment of the base with respect to the sonotrode. Additionally, in the continuous process the power fluctuates around a certain value, considering that all phases are simultaneously present under the sonotrode, the shape of the power curve cannot aid in identifying a certain phase to aim for to reach optimum welding conditions demonstrated for the static welding process by Villegas et al. [8, 9]. Thus, it will be needed to deploy external sensors to in situ monitor alternative parameters that can be linked to the weld quality. The in situ measurements could then potentially be used to control the welding process by in situ changing welding parameters like the vibration amplitude. Potentially the weld line thickness could be measured by measuring the total thickness of the adherends plus energy director ahead and after the sonotrode and linking this to the weld quality. All in all, it should be noted that it is important to investigate the development of an in situ monitoring system that eventually can be used to control the welding process.

6.4.4. Welding of single-curved components

The rectangular sonotrode design used in the research conducted for this dissertation limits the application of the continuous ultrasonic welding process to flat adherends. However, many large structures in the aviation industry are single-curved, e.g. the fuselage panels. With preliminary experiments for a patent application [10] it was shown that it is possible to utilize a round sonotrode to obtain high-quality welds with flat panels. It can be expected that the same round sonotrode can be used for welding of single-curved panels, which would allow joining of omega stiffeners to single-curved fuselage panels. Utilizing a round sonotrode seems to have extra benefits compared to using a rectangular sonotrode, like significantly lower interface and adherend temperatures, and almost no vibrations transmitted ahead of the sonotrode. However, utilizing a round sonotrode in continuous ultrasonic welding is not fully understood and the cause for the previously described benefits are currently unknown and should be understood before applying it in an industrial setting. Additionally, it should be investigated how to increase the welding speeds when utilizing a round sonotrode as currently the speeds seem to be approximately a factor 3 to 5 lower compared to the rectangular sonotrode. Additionally, for curved panels it will be required to understand how to best consolidate the welds. Most likely a consolidation roller or an array of rollers should be used behind the sonotrode.

6

References

[1] F. Senders, M. van Beurden, G. Palardy, and I. Villegas, "Zero-flow: A novel approach to continuous ultrasonic welding of CF/PPS thermoplastic composite plates," *Advanced Manufacturing: Polymer & Composites Science*, vol. 0340, no. September 2017, pp. 1–10, 2016.

[2] I. Villegas, B. Valle Grande, H. Bersee, and R. Benedictus, "A comparative evaluation between flat and traditional energy directors for ultrasonic welding of cf/pps thermoplastic composites," *Composite Interfaces*, vol. 22, no. 8, pp. 717–729, 2015.

[3] N. Koutras, R. Benedictus, and I. F. Villegas, "Thermal effects on the performance of ultrasonically welded cf/pps joints and its correlation to the degree of crystallinity at the weldline," *Composites Part C: Open Access*, vol. 4, p. 100093, 2021.

[4] J. S. Chung and P. Cebe, "Crystallization and melting of cold-crystallized poly(phenylene sulfide)," *Journal of Polymer Science Part B: Polymer Physics*, vol. 30, no. 2, pp. 163–176, 1992.

[5] Y. Furushima, M. Nakada, Y. Yoshida, and K. Okada, "Crystallization/melting kinetics and morphological analysis of polyphenylene sulfide," *Macromolecular Chemistry and Physics*, vol. 219, no. 2, p. 1700481, 2018.

[6] F. Köhler, I. Villegas, C. Dransfeld, and A. Herrmann, "Static ultrasonic welding of carbon fibre unidirectional thermoplastic materials and the influence of heat generation and heat transfer," *Journal of Composite Materials*, vol. 55, no. 15, pp. 2087–2102, 2021.

[7] C. B. G. Brito, J. Teuwen, C. A. Dransfeld, and I. F. Villegas, "The effects of misaligned adherends on static ultrasonic welding of thermoplastic composites," *Under peer review at Composites Part A: Applied Science and Manufacturing*, 2021.

[8] I. Villegas, "In situ monitoring of ultrasonic welding of thermoplastic composites through power and displacement data," *Journal of Thermoplastic Composite Materials*, vol. 28, no. 1, pp. 66–85, 2015.

[9] I. Villegas, "Strength development versus process data in ultrasonic welding of thermoplastic composites with flat energy directors and its application to the definition of optimum processing parameters," *Composites Part A: Applied Science and Manufacturing*, vol. 65, pp. 27–37, 2014.

[10] B. C. P. Jongbloed, I. F. Villegas, and J. J. E. Teuwen, "Round tool (sonotrode) for ultrasonic welding of thermoplastic composites." European Patent Office. European patent. PCT application number: PCT/NL2021/050397. Filed June 24, 2020, PCT filed June 23, 2021, and publication December 24, 2021.

Acknowledgements

The PhD journey arguably is solitary. However, along the way you get support and guidance from great people who made the journey enjoyable, and without whom the journey would not have been successful. Therefore, I like to take a moment to thank those that supported me on along the way.

First of all, Irene Fernandez Villegas, my daily supervisor and promotor, and Julie Teuwen, my copromotor and daily supervisor. Under both your guidance I learned how to perform research independently and in a structured way. You were true mentors to me. Irene, thank you for giving me the opportunity to pursue a PhD and for all the support you gave me. Thank you for your passion and enthusiasm towards ultrasonic welding, it is truly inspiring. You transferred your enthusiasm on the topic to me. I will always be an ambassador for ultrasonic welding! I'm convinced we will see continuous ultrasonic welding being applied for the assembly of aircraft structures. Julie, thank you for all your support and for our discussions and for reviewing my papers. It helped me a lot to see how structured you approach research design. Finally, Rinze Benedictus, thank you for having me as a PhD candidate within the department and for your support.

I had the pleasure to get to know and work together with three amazing secretaries from the ASM department. Thank you Gemma, Marianne, and Laura for all your help on ordering tools/materials, organizing events, shipping parcels, and much more. Our discussions in the hallways and around the coffee table were always very enjoyable.

I would like to especially thank Rein van den Oever, Perry Posthoorn, Jan Graafland, and Stephan van 't Hof from the Electronic and Mechanical Support Division for all their help on the development of the continuous ultrasonic welding machine. It was absolutely a pleasure to work with you. Rein, thank you so much for thinking along with me, for your incredible help, and for your support even on short notice when there was a problem to be fixed. I sincerely enjoyed our talks and discussions both during meetings and in the lab. Additionally, I like to thank Marco Sebastian from Herrmann Ultrasonics for his help to integrate the off-the-shelf welder into our continuous ultrasonic welding machine, for trouble shooting problems, and for his continuous support and interest in the welding of thermoplastic composites. It was always a pleasure when you came by.

Performing experiments is not possible without a lab and the support from the people working there. Therefore, I like to thank the technicians for all their help. Firstly, Gertjan Mulder, thank you for your help and thank you for making work in the lab even more enjoyable. Our discussions, laughs, jokes, and coffees are much appreciated. Thank you, Berthil, Dave, Alexander, Johan, Victor, Fred, Misja, Durga, Marlies, and Cees for your help in the lab. And thank you, Ed, Peter and Rob from demo for your specialist work on making samples and equipment for my projects.

Please accept my appreciation to everyone from the welding group: Genevieve, Irene, Michiel, Tiago, Nikos, Eirini, Tian, Yannos, Camila, Eva, Abhas, Filipp, and Erdem. It was fun working together with you! And great to be part of such a lively welding community. I enjoyed our meetings, fun activities, dinners and virtual lunches a lot. Thanks a lot for all the nice discussions, talks, and for creating a pleasant working environment!

A special thanks to my (former) office mates. Fabricio, Megan, Julian, Aydin, Tian, Xi, Agnes, and Satya. Thank you for the great atmosphere in the office, the nice talks and discussions. I would like to also send a particular thanks to each and everybody from SI&C and AMT. Additionally, I like to thank Pedro for the discussions on ultrasonic welding.

Over a period of 3.5 years I also had a great time in the PhD council of the aerospace engineering faculty. I appreciated the opportunity to meet bright people from other departments and together organize academic and social events, and discuss many topics related to the PhD journey and graduate school. Thank you! Additionally, I like to thank Stefan, Nancy and Colette for their support and making it fun to be part of the PhD council.

I also like to thank Jesse and Daniël for the laughs and politically correct discussions at the coffee table at 15.00h while enjoying a cup of tea. This was always something to look forward to. Great that we found a way to have tea once a week online, and of course at 15.00h.

I'm also grateful to the project partners from the ecoTECH project for such a pleasant cooperation. It was truly a pleasure meeting you all! I really enjoyed visiting the different factories and research centres, and of course the taste of the local cuisine during the ecoTECH dinner.

Finally, I am very grateful to my partner Hao for her backing me up in the past years. Without her I would not have made it this far. And the last thanks goes to my family for their unconditional support.

Curriculum Vitæ

Bram Cornelius Petrus JONGBLOED

The author was born in 1992 in Breda, the Netherlands. June 2011 he graduated from high school 'Stedelijk Gymnasium Breda'. He obtained his bachelor (July 2014) and master (October 2016) of science degrees in aerospace engineering from the Delft University of Technology. During his bachelor studies he took part in the minor technology-based entrepreneurship. During his master studies he specialised in aerospace structures and materials and focused on aerospace manufacturing technologies. In February 2017 he started working on his PhD on the topic continuous ultrasonic welding of thermoplastic composites under the supervision of dr. Irene Fernandez Villegas and dr.ir. Julie Teuwen.

List of Publications

Journal articles

4. **B. Jongbloed**, J. Teuwen, R. Benedictus, and I.F. Villegas, *A study on through-the-thickness heating in continuous ultrasonic welding of thermoplastic composites*, Materials **14**, 21 (2021).

3. **B. Jongbloed**, R. Vinod, J. Teuwen, R. Benedictus, and I.F. Villegas, *Improving the quality of continuous ultrasonically welded thermoplastic composite joints by adding a consolidator to the welding setup*, under peer review at Composites Part A: Applied Science and Manufacturing, (2021).

2. **B. Jongbloed**, J. Teuwen, R. Benedictus, and I.F. Villegas, *On differences and similarities between static and continuous ultrasonic welding of thermoplastic composites*, Composites Part B: Engineering **203**, (2020).

1. **B. Jongbloed**, J. Teuwen, G. Palardy, I.F. Villegas, and R. Benedictus, *Continuous ultrasonic welding of thermoplastic composites: Enhancing the weld uniformity by changing the energy director*, Journal of Composite Materials **54**, 14 (2020).

Conference articles

3. **B. Jongbloed**, J. Teuwen, I.F. Villegas, and R. Benedictus, *Investigation on the melting of the weld interface in continuous ultrasonic welding of thermoplastic composites*, 22nd International Conference on Composite Materials (ICCM22) - Melbourne, Australia (2019). [oral presentation]

2. F. Köhler, **B. Jongbloed**, T.M. Morgado Martins Filipe, A. Herrmann, I.F. Villegas, and R. Benedictus, *A Roadmap for developing an Industrial Continuous Ultrasonic Welding Process for Thermoplastic Composites*, 4th International Conference and Exhibition on Thermoplastic Composites (ITHEC) - Bremen, Germany (2018). [oral presentation]

1. **B. Jongbloed**, J. Teuwen, G. Palardy, I.F. Villegas, and R. Benedictus, *Improving weld uniformity in continuous ultrasonic welding of thermoplastic composites*, 18th European Conference on Composite Materials (ECCM18) - Athens, Greece (2018). [oral presentation]

Patent applications

- *Round tool (sonotrode) for ultrasonic welding of thermoplastic composites*. Inventors: **B.C.P. Jongbloed**, I.F. Villegas, J.J.E. Teuwen. PCT application number: PCT/NL2021/050397. PCT filed June 23, 2021.